

# Mars Sample Return precise point rendezvous in Mars orbit

Literature Study

S.D. Petrovic



# PREFACE

Back in December 2013 Warren Gebbett gave a presentation on his work at the Jet Propulsion Laboratory ([JPL](#)) in Pasadena, California, USA and the opportunity for a new student to go and perform research at [JPL](#). At this point I sent in my application together with eight other students. Then at the end of December I was invited for an interview in the first week of January 2014. In this interview it was concluded that I met all the requirements and that I was the perfect candidate to follow Warren up as the next student at [JPL](#) with financial backing of Dutch Space (now Airbus Defence and Space, the Netherlands). Financial backing was also going to be provided by the Stichting Prof.dr.ir. H.J. van der Maas Fonds (Aerospace engineering faculty, TU Delft) and the Stichting Universitetsfonds Delft (TU Delft). Communication with [JPL](#) was thus started and in March 2015 it was clear that I would be working for the Mars Program Formulation Office under the supervision of Roby Wilson (inner solar system group, NASA [JPL](#)). He told me to focus on subjects that dealt with Mars missions. At that point I was doing my internship at DLR Bremen on Lunar rocket ascent and descent, which lasted till June 2015. When I came back to Delft me and my supervisors Erwin Mooij (rockets, trajectories, entry and descent, TU Delft) and Ron Noomen (mission design and orbit analysis, TU Delft) agreed that it would be best to perform a study on these Mars subjects in order to prepare for my visit to [JPL](#) and to formulate final proposition thesis topics. The first week at [JPL](#) I presented these initial thesis topics to both people from the inner solar system group and the Mars program formulation office. The next few weeks were spent choosing and refining one of these topics. This document is the result of the two month literature study on that topic in order to prepare for the thesis project.

*S.D. Petrovic  
Pasadena, California, January 2016*

# CONTENTS

<b>List of Figures</b>	<b>vi</b>
<b>List of Tables</b>	<b>viii</b>
<b>Nomenclature</b>	<b>ix</b>
<b>Abbreviations</b>	<b>xiii</b>
<b>1 Introduction</b>	<b>1</b>
<b>2 Overview of the subject</b>	<b>2</b>
2.1 Searching for subjects . . . . .	2
2.2 Initial proposal . . . . .	2
2.2.1 Research objective . . . . .	2
2.2.2 Research perspective . . . . .	3
2.2.3 Research framework . . . . .	3
2.2.4 Research questions . . . . .	3
2.2.5 Research strategy . . . . .	4
2.2.6 Research Method . . . . .	5
<b>3 Mission heritage</b>	<b>6</b>
3.1 Mars atmospheric ascent reference missions . . . . .	6
3.1.1 Martian ascent reference research . . . . .	6
3.1.2 Reference flown Lunar sample return missions . . . . .	8
3.1.3 Lunar ascent reference research . . . . .	9
3.2 Low-thrust orbital transfer reference missions . . . . .	10
3.2.1 Earth system low-thrust applications . . . . .	10
3.2.2 Low-thrust (Martian) planetary system reference research . . . . .	11
3.3 Ascent vehicle and orbiter direct rendezvous references . . . . .	12
3.3.1 Flown missions . . . . .	12
3.3.2 Direct rendezvous reference research . . . . .	13
3.4 MAV design . . . . .	13
3.4.1 Previous investigations . . . . .	14
3.4.2 Current MAV baseline design . . . . .	14
3.4.3 Current design restrictions . . . . .	16
<b>4 Optimisation</b>	<b>17</b>
4.1 Different local optimisation methods . . . . .	17
4.2 Different global optimisation methods . . . . .	17
4.2.1 Sampling methods . . . . .	17
4.2.2 Metaheuristics . . . . .	18
4.3 Technique comparison . . . . .	18
4.4 Chosen methods . . . . .	19
4.4.1 Frequently used methods . . . . .	19
4.4.2 TU Delft optimisation heritage . . . . .	19
4.4.3 Chosen candidate methods . . . . .	19
4.5 Implementation of Differential Evolution . . . . .	20
4.5.1 The workings of DE . . . . .	20
4.5.2 Variations of DE method . . . . .	22
4.6 Implementation of Monotonic Basin Hopping . . . . .	23
4.6.1 The workings of MBH . . . . .	23
4.6.2 Variations of the MBH method . . . . .	25

<b>5 Integrators</b>	<b>29</b>
5.1 Different integrators . . . . .	29
5.1.1 Single-step . . . . .	30
5.1.2 Multi-step . . . . .	30
5.2 Technique comparison . . . . .	30
5.3 Chosen methods . . . . .	31
5.3.1 Frequently used methods in related space problems . . . . .	31
5.3.2 TU Delft integration heritage . . . . .	32
5.3.3 Chosen methods . . . . .	32
5.4 Implementation of Taylor Series integration . . . . .	33
5.4.1 The workings of TSI . . . . .	33
5.4.2 Variations of TSI method . . . . .	35
5.5 Implementation of RK4 . . . . .	36
5.5.1 The workings of RK4 . . . . .	36
5.5.2 Methods based on RK4 . . . . .	37
<b>6 Atmospheric (Martian) launch</b>	<b>38</b>
6.1 Previous research . . . . .	38
6.2 Dynamic model and Equations of Motion . . . . .	39
6.2.1 Dynamic model and initial assumptions . . . . .	39
6.2.2 Corresponding EoM and initial assumptions . . . . .	41
6.3 Required launch trajectory . . . . .	43
6.3.1 Vertical rise . . . . .	43
6.3.2 First thruster control phase . . . . .	43
6.3.3 Gravity turn and second thruster control phase . . . . .	44
6.3.4 Coasting and orbit burn . . . . .	45
6.4 Mars 2020 landing site conditions . . . . .	45
<b>7 Transfer orbits</b>	<b>48</b>
7.1 High-thrust . . . . .	48
7.2 Low-thrust . . . . .	49
7.2.1 Low-thrust electrical propulsion transfer . . . . .	50
7.2.2 Reference missions . . . . .	50
7.3 Dynamic model and Equations of Motion . . . . .	51
7.3.1 Dynamic model and initial assumptions . . . . .	51
7.3.2 Corresponding EoM and initial assumptions . . . . .	51
7.4 Q-law . . . . .	54
7.5 Mars 2022 orbiter initial conditions . . . . .	57
<b>8 Reference systems and transformations</b>	<b>59</b>
8.1 Required reference systems . . . . .	59
8.1.1 Mars-centred inertial (MCI) RF (I-frame) . . . . .	59
8.1.2 Mars-centred Mars-fixed (MCMF) RF (R-frame) . . . . .	60
8.1.3 Vertical RF (V-frame) . . . . .	60
8.1.4 Body-fixed (BF) RF (B-frame) . . . . .	60
8.1.5 Propulsion RF (P-frame) . . . . .	61
8.2 Transformation between reference frames . . . . .	62
8.3 Transformation between different coordinate systems . . . . .	65
8.3.1 Spherical and Cartesian . . . . .	66
8.3.2 Keplerian and Cartesian . . . . .	67
8.3.3 Spherical and Keplerian . . . . .	70
8.3.4 Non-singular Kepler elements (MEE) . . . . .	71
<b>9 Mars atmospheric model</b>	<b>72</b>
9.1 Reference atmospheric models . . . . .	72
9.2 Chosen atmospheric model . . . . .	73

<b>10 Proposed software</b>	<b>74</b>
10.1 Existing software packages . . . . .	74
10.2 Adjustments to the software . . . . .	74
<b>11 Final subject definition and thesis proposal</b>	<b>76</b>
11.1 Final refined thesis topic and research questions . . . . .	76
11.1.1 Research objective . . . . .	76
11.1.2 Research perspective . . . . .	76
11.1.3 Research framework . . . . .	76
11.1.4 Research questions . . . . .	76
11.1.5 Research strategy . . . . .	78
11.1.6 Research Method . . . . .	78
11.2 Proposed time schedule . . . . .	79
<b>Bibliography</b>	<b>81</b>

# LIST OF FIGURES

2.1 Research framework for the literature study (a) and the thesis work (b, c & d) . . . . .	3
3.1 Left: Lunar Ascent Module, Right: Apollo Command and Service Module . . . . .	9
3.2 A number of rocket concepts visualized. a) Two stage solid rocket by Lockheed Martin [1], b) Single stage mono-liquid rocket by Firestar Technologies [2], c) Two stage gel rocket by Thompson Ramo Wooldridge inc. (TRW) [1] and d) Two stage bi-liquid rocket by Boeing and Northrop Grumman [3] . . . . .	14
3.3 Two stage bi-liquid baseline MAV with descriptions of different components [3] . . . . .	15
4.1 Construction of the mutation vector in a two-dimensional case [4] . . . . .	21
4.2 Construction of the trial vector in a 7-dimensional case [4] . . . . .	22
4.3 The first step of MBH where (a) first a random initial point $x$ (red dot) is generated after which (b) the local minimum $x^*$ (dark yellow point) is found through the use of a local optimiser. The local optimisation is visualized by a solid arrow. $x^*$ becomes $x_{current}$ if the local optimum is feasible. . . . .	24
4.4 The second step of MBH where (a) $x_{current}$ is perturbed within a uniform probability distribution creating (b) a new initial point $x'$ (purple dot). The perturbation is visualized by a dashed arrow. . . . .	25
4.5 The third step of MBH where (a) the new local minimum $x^*$ (orange dot) is compared to the current local minimum $x_{current}$ and is set as $x_{current}$ if it is better. Then (b) the second step repeats from the new $x_{current}$ creating a new perturbed point $x'$ (dark blue dot). . . . .	26
4.6 (a) A new local optimum is found (magenta dot), but (b) it is not better than the current optimum (orange dot), which is why it is disregarded visualized by the dotted arrow. . . . .	27
4.7 The process is repeated for another initial guess (yellow dot). In this case, the current funnel contains the global minimum, however the process is still repeated until one of the cut-off criteria has been met. . . . .	28
5.1 Comparison of single-step (left) and multi-step (right) methods for an eccentricity of 0.1 [5] . .	32
5.2 Principle of RK4 for a single parameter [6] . . . . .	36
6.1 (Left) Graphical definition of the spherical coordinate system. The angles are all defined positive in the direction of the arrow[7] (Right) Graphical definition of the force model [8] . . . . .	40
6.2 Drag coefficient as a function of Mach number [9] . . . . .	41
6.3 Constrained landing area on Mars between the 30°N and 30°S line. In that area, black land has an elevation above +0.5 km w.r.t. the MOLA geoid and the grey areas are lower thermal inertial constrained areas . . . . .	46
6.4 Locations of the eight potential landing sites within the constrained area . . . . .	47
7.1 Graphical representation for Earth-Mars Hohmann transfer burns . . . . .	49
7.2 Graphical representation of the four different high energy transfer orbit possibilities based on an arbitrary ellipse crossing both orbits[10] . . . . .	49
7.3 Example of continuous low-thrust trajectory[11] . . . . .	50
7.4 Example of a segmented low-thrust interplanetary trajectory: the Dawn spacecraft[10] . . . . .	50
7.5 Definition of the Kepler elements in 2D (left) and 3D (right) [12, 13] . . . . .	52
7.6 Definition of the perturbing accelerations [10] . . . . .	53
8.1 Graphical definition of the Mars-centred inertial reference frame [14] . . . . .	60
8.2 Graphical definition of the Mars-centred Mars-fixed reference frame [14] . . . . .	61
8.3 Graphical definition of the Vertical reference frame compared to the Mars-centred inertial frame [14] . . . . .	61

8.4 Graphical example of a Body-fixed reference frame used on the Apollo Command and Service module . . . . .	62
8.5 Propulsion frame relative to the body frame [7] . . . . .	62
8.6 General rotation around the x-axis [15] . . . . .	63
8.7 Relation between the MCI and the Gaussian body frame [10] . . . . .	65
8.8 Relation between spherical position coordinates and Cartesian position coordinates [12] . . . . .	66
8.9 atan2 function evaluation conditions adapted from . . . . .	67
8.10 Definition of the Kepler elements in 2D (left) and 3D (right) [12, 13] . . . . .	68
11.1 Research framework for the literature study (a) and the thesis work (b, c & d) . . . . .	77

# LIST OF TABLES

3.1 Previous and current Mars ascent trajectory research . . . . .	7
3.2 Previous Lunar Sample Return Missions . . . . .	8
3.3 Previous and current Lunar ascent trajectory research . . . . .	9
3.4 Previous Low-thrust Earth Missions . . . . .	10
3.5 Previous and current Mars low-thrust trajectory research . . . . .	11
3.6 Previous (nearly) direct rendezvous Missions . . . . .	12
3.7 Direct rendezvous reference research . . . . .	13
3.8 Previous MAV studies . . . . .	14
3.9 MAV baseline design characteristics . . . . .	15
4.1 optimisation method comparison . . . . .	18
4.2 Previous methods used for trajectory and orbit transfer optimisation problems . . . . .	20
5.1 Integration method comparison . . . . .	30
5.2 Previous integration methods used for trajectory and orbit (transfer) problems . . . . .	33
6.1 Reference characteristics from Mars Ascent research . . . . .	38
6.2 Current candidate landing sites (source:JPL) . . . . .	46
7.1 Flown low-thrust missions using Xenon engines and their characteristics (provided per thruster)	51
7.2 The two different engines currently under consideration for use on the Mars 2022 orbiter . . . . .	58
9.1 Mars atmospheric models used in reference research . . . . .	73
9.2 Atmospheric model trade-off table . . . . .	73
10.1 Required existing software . . . . .	74
11.1 Proposed time schedule thesis project . . . . .	79

# NOMENCLATURE

$\alpha$	Angle of attack	rad or deg
$\alpha$	In-plane thrust angle	rad or deg
$\beta$	Out-of-plane thrust angle	rad or deg
$\chi$	Azimuth (or heading angle)	rad or deg
$\chi$	Heading angle	rad or deg
$\Delta m_b$	Required propellant mass for orbit insertion	kg
$\Delta V$	Velocity increment	m/s
$\delta$	Latitude	rad or deg
$\dot{\Omega}_M$	Rotational velocity of Mars	rad/s or deg/s
$\dot{m}$	Mass flow rate	kg/s
$\epsilon_T$	Thrust elevation gimbal angle	rad or deg
$\eta$	Numerical approximation	-
$\eta$	Step multiplication factor	-
$\eta_a$	Absolute effectivity	-
$\eta_{cut}$	Cut effectivity	-
$\eta_r$	Relative effectivity	-
$\gamma$	Flight-path angle	rad or deg
$\gamma$	Flight-path angle	rad or deg
$\gamma_{\mathcal{A}}$	Adiabatic index	-
$\mathbb{T}$	General transformation matrix	-
$\mathbb{T}_x$	x-axis transformation matrix	-
$\mathbf{r}$	State vector containing coordinate values	-
$\mathbf{x}_{i+1}$	Next data point	-
$\mathbf{x}_i$	Current data point	-
$\mathcal{A}$	Local speed of sound	m/s
$\mathcal{M}$	Mach number	-
$\mu$	Standard gravitational parameter	$\text{m}^3/\text{s}^2$
$\mu_M$	Standard gravitational parameter of Mars	$\text{m}^3/\text{s}^2$
$\mu_S$	Standard gravitational parameter of the Sun	$\text{m}^3/\text{s}^2$
$\omega$	Orbital element	m,-,deg or rad

$\Omega$	Right ascension of the ascending node	rad or deg
$\omega$	Argument of periapsis	rad or deg
$\Omega_P$	Prime meridian offset at inertial reference frame definition	rad or deg
$\bar{X}$	State vector	-
$\Phi$	Increment function	-
$\phi$	General rotation angle	rad or deg
$\psi_T$	Thrust elevation gimbal angle	rad or deg
$\rho$	Air density	$\text{kg}/\text{m}^3$
$\rho_0$	Atmospheric density at zero elevation	$\text{kg}/\text{m}^3$
$\sigma$	Standard deviation	-
$\tau$	Local error tolerance	-
$\tau$	Longitude	rad or deg
$\theta$	True anomaly	rad or deg
$\xi$	Non-singular orbital elements	$\text{m}, \text{-}, \text{deg}$ or $\text{rad}$
$a$	Acceleration	$\text{m}/\text{s}^2$
$a$	Semi-major axis	m
$A_e$	Exit surface area of the nozzle	$\text{m}^2$
$c$	Expulsion velocity	$\text{m}/\text{s}$
$C_D$	Drag coefficient	-
$c_{eff}$	Effective expulsion velocity	$\text{m}/\text{s}$
$C_L$	Lift coefficient	-
$D$	Drag	N
$E$	Eccentric anomaly	rad or deg
$e$	Eccentricity	-
$e_{max}$	Estimate of maximum truncation error	-
$f_N$	Perturbing acceleration perpendicular to the radius vector	$\text{m}/\text{s}^2$
$f_s$	Radial perturbing acceleration	$\text{m}/\text{s}^2$
$f_{Thrust}$	Total thrust acceleration	$\text{m}/\text{s}^2$
$f_w$	Perturbing acceleration perpendicular to the orbital plane	$\text{m}/\text{s}^2$
$G$	Gravitational constant	$\text{m}^3/(\text{kg}\cdot\text{s}^2)$
$g$	Local gravitational acceleration	$\text{m}/\text{s}^2$
$g_0$	Gravitational acceleration at Earth sea-level	$\text{m}/\text{s}^2$
$h$	Altitude	m
$h$	Current step-size	s

$h$	Specific relative angular momentum	$\text{m}^2/\text{s}$
$h$	Step-size	s
$H_s$	Scale-height	m
$I$	Retrograde factor	-
$i$	Inclination	rad or deg
$I_{sp}$	Specific impulse	s
$k$	Penalty function adjustable scalar	-
$L$	Lift	N
$L$	True longitude	rad or deg
$M$	Mean anomaly	rad or deg
$M$	Order of the maximum truncation error estimate	-
$m$	Mass	kg
$m_{2,f}$	Final second stage mass	kg
$m_2$	Second stage mass after burn-out	kg
$M_{\mathcal{A}}$	Molar mass of the Martian atmosphere	$\text{kg/mol}$
$m_{MAV}$	MAV mass	kg
$M_M$	Mass of Mars	kg
$Max_{n,i}$	Maximum number of not improved iterations	-
$N_{n,i}$	Number of not improved iterations	-
$p$	Semi-latus rectum	m
$p_0$	Atmospheric pressure at zero elevation	Pa
$p_0$	Pressure of the surrounding air	Pa
$p_e$	Exit pressure	Pa
$Q$	Q-law function in Kepler elements	$\text{s}^2$
$Q_{MEE}$	Non-singular Q-law	$\text{s}^2$
$r$	Radial distance	m
$r_1$	Orbital radius of the inner planet	m
$r_2$	Orbital radius of the outer planet	m
$R_{\mathcal{A}}$	Molar gas constant	$\text{J}/(\text{mol}\cdot\text{K})$
$r_a$	Apocentre	m
$r_{MS}$	Distance between Mars and the Sun	m
$R_M$	(Local) radius of Mars	m
$r_p$	Pericentre	m
$S$	Surface area	$\text{m}^2$

$S_G$	Travelled ground distance	m
$T$	Thrust	N
$T$	Truncation error	-
$t_0$	Current time	s
$t_1$	First stage burn-time	s
$t_2$	Second stage burn-time	s
$T_{\mathcal{A}}$	Absolute temperature	K
$t_{c1}$	First-second stage coast time	s
$T_{MS}$	Orbital period of Mars around the Sun	s
$t_O$	Time from inertial reference frame definition	s
$t_{T2}$	Second thruster control phase start time	s
$ToF$	Time of Flight	s or days
$u_{i,G+1}$	Trial vector	-
$V$	Velocity	m/s
$v_1$	Velocity increment required at inner planet (Hohmann)	m/s
$v_2$	Velocity increment required at outer planet (Hohmann)	m/s
$v_{i,G+1}$	Mutation vector	-
$W_{\alpha e}$	Orbital element weight	-
$W_P$	Penalty function weight	-
$x_{i,G}$	Original, target, individual vector	-
$x_n$	n <sup>th</sup> variable	m, m/s and kg
CR	Crossover constant	-
D	Number of variables	-
F	Amplification factor	-
G	Generation	-
NP	Population size	-
$x_I$	x-axis of the Mars-centred inertial frame	-
$x_R$	x-axis of the Mars-centred Mars-fixed frame	-
$x_V$	x-axis of the Vehicle-carried normal Mars frame	-
$y_I$	y-axis of the Mars-centred inertial frame	-
$y_R$	y-axis of the Mars-centred Mars-fixed frame	-
$y_V$	y-axis of the Vehicle-carried normal Mars frame	-
$z_I$	z-axis of the Mars-centred inertial frame	-
$z_R$	z-axis of the Mars-centred Mars-fixed frame	-
$z_V$	z-axis of the Vehicle-carried normal Mars frame	-

# ABBREVIATIONS

<b>AB4</b>	Adams-Bashforth 4	<b>MEE</b>	Modified Equinoctial Elements
<b>AB6</b>	Adams-Bashforth 6	<b>MPFO</b>	Mars Program Formulation Office
<b>ABM4</b>	Low-order Predictor-Corrector	<b>MSL</b>	Mars Science Laboratory
<b>ABM12</b>	High-order Predictor-Corrector	<b>MSR</b>	Mars Sample Return
<b>ACS</b>	Attitude Control System	<b>N/A</b>	Not Available
<b>BF</b>	Body-fixed	<b>NAIF</b>	Navigation and Ancillary Information Facility
<b>CNES</b>	Centre National d'Études Spatiales	<b>OS</b>	Orbiting Sample
<b>CNRS</b>	Centre National de la Recherche Scientifique	<b>OTIS</b>	Optimal Trajectories by Implicit Simulation
<b>CSM</b>	Command and Service Module	<b>POST</b>	Program to Optimize Simulated Trajectories
<b>DE</b>	Differential Evolution	<b>RCS</b>	Reaction control system
<b>DLR</b>	German Aerospace Center (Deutsches Zentrum für Luft- und Raumfahrt)	<b>RF</b>	Frame of Reference
<b>EP</b>	Electric propulsion	<b>R.H.R.</b>	Right-hand-rule
<b>ESA</b>	European Space Agency	<b>RKF45</b>	Runge-Kutta-Fehlberg
<b>EoM</b>	Equations of Motion	<b>RK4</b>	Runge-Kutta 4
<b>GEO</b>	Geostationary Earth Orbit	<b>RKN12</b>	High-order Runge-Kutta-Nyström
<b>GLOM</b>	Gross Lift-Off Mass	<b>s/c</b>	Spacecraft
<b>GMT</b>	Greenwich Mean Time	<b>SC14</b>	Störmer-Cowell
<b>GRAM</b>	Global Reference Atmospheric Model	<b>SEP</b>	Solar Electric Propulsion
<b>GTO</b>	Geostationary Transfer Orbit	<b>SG</b>	Shampine-Gordon
<b>ITAR</b>	International Traffic in Arms Regulations	<b>SNOPT</b>	Sparse Nonlinear Optimizer
<b>ISS</b>	International Space Station	<b>SPICE</b>	Spacecraft Planet Instrument C-Matrix Events
<b>JPL</b>	Jet Propulsion Laboratory	<b>ToF</b>	Time of Flight
<b>JVSRP</b>	JPL Visitor Student Research Program	<b>TOSCA</b>	Trajectory Optimisation and Simulation of Conventional and Advanced space transportation system
<b>LAM</b>	Lunar Ascent Module	<b>TRW</b>	Thompson Ramo Wooldridge inc.
<b>LEO</b>	Low Earth Orbit	<b>TSI</b>	Taylor Series integration
<b>MAV</b>	Mars Ascent Vehicle	<b>TVC</b>	Thrust Vector Control
<b>MBH</b>	Monotonic Basin Hopping	<b>VCNM</b>	Vehicle-carried normal Mars
<b>MCI</b>	Mars-centred inertial		
<b>MCMF</b>	Mars-centred Mars-fixed		

# 1

## INTRODUCTION

What is the optimal trajectory solution for the combined trajectory problem of a high-thrust [MAV](#) and a low-thrust Mars orbiter single-revolution rendezvous in Mars orbit? This document has been written to provide back-ground information and an improved understanding of this preliminary thesis topic and the involved subjects that apply to the thesis work which will be performed at NASA [JPL](#). All the information gathered and provided in this report is used to finalise the thesis topic and formulate a final thesis proposal. The thesis work at [JPL](#) is made possible through the JPL Visitor Student Research Program ([JVSRP](#)), which has provided the opportunity to perform research at [JPL](#) over a period of 1 year. During this period, the [JPL](#) staff and resources are available to use for the research as long as it does not involve any restricted information or software. This literature study was performed during the first few months at [JPL](#), and the last few months will be used to carry out the thesis research. At the start of the research period it was known that the topic would involve a Mars mission. Because of restrictions and regulations it was decided that the thesis topic would include trajectory analysis and optimisation and the Mars Sample Return ([MSR](#)) mission. Eventually, the initial topic was set on combined [MSR MAV](#) ascent trajectory and Mars 2022 orbiter trajectory optimisation in order to rendezvous in Mars orbit. The road-map towards, and a comprehensive explanation of, the thesis topic will be explained in Chapter 2. In Chapter 3 different reference missions and research for each aspect of the thesis topic are presented to provide a perspective of what has already been done and which missions and what research could be used as reference and validation data. It is also important to gain a general understanding of different mathematical concepts that are necessary for the thesis work. Therefore Chapter 4 on optimisation and Chapter 5 on integrators were written and form the basic understanding that is required. In the optimisation chapter, different optimisation methods are described and a selection is made of the optimisation methods that will be used. The same is done for the different integrators. The thesis problem will need to be described using mathematical models to simulate the ascent and orbital conditions of the [MAV](#) and Mars 2022 orbiter respectively. Chapter 6 describes the used model, the assumptions and the corresponding equations for the ascent phase. In turn Chapter 7 describes the model, assumptions and equations for the orbiter. In these equations, many different reference frames and reference systems are used. This is why Chapter 8 describes the different required reference frames and systems and the transformation between them. All the required transformations, which follow from Chapters 6 and 7, are written out as well. One important aspect of the [MAV](#) ascent, which sets it apart from other sample return missions, is that Mars has an atmosphere which cannot be neglected. Accordingly Chapter 9 describes the different models and the trade-off that was performed in order to decide which model to use in this thesis problem. For some of the aspects that will be treated in the thesis problem, certain software is already available. A summary of this software is provided in Chapter 10. Finally, all the information gathered is used to write a final thesis topic proposal and corresponding proposed schedule which can be presented in Chapter 11. This literature study will be used during the thesis project and will serve as a guideline and provide background information for the final thesis report.

# 2

## OVERVIEW OF THE SUBJECT

In Chapter 1 the thesis topic was introduced. This chapter will explain where the idea for this topic originated from in Section 2.1. In Section 2.2 the proposal is presented which was written at the start of this literature study and will be updated to the final thesis proposal in Chapter 11.

### 2.1. SEARCHING FOR SUBJECTS

Since the thesis research is performed at NASA JPL under their supervision it made sense to look at the different missions that they have planned for the near future. An overview is provided on the JPL website <sup>1</sup>. Two of the future and proposed missions to Mars were MSR and Mars 2020. The MSR mission is described as a mission that would return samples to Earth using a MAV to launch from the Martian surface. The MAV would contain rock, soil and atmospheric samples to be analysed back on Earth. The Mars 2020 mission (also sometimes referred to as the Mars Science Laboratory (MSL) 2 mission) will be the next rover mission to Mars. Its prime goal will be to investigate the (past) habitability of Mars, and assess natural resources and possible hazards in order to help in the preparation of future human expeditions <sup>1</sup>. It is in its concept similar to the current Curiosity mission.

Given these two missions, it was then decided to formulate thesis subjects in correspondence with these missions but also correlate to personal preferences. This resulted in six thesis topics which were presented to JPL after which the topic selection process was started. Together with the supervisors at the TU Delft and at JPL it was decided to work out one of these topics in particular and write it into a proposal. Because the expertise of the section is on orbits it was decided to focus on MSR, which also fits well with the current work of the Mars Program Formulation Office (MPFO) whom are designing the orbits for the Mars 2022 orbiter. The result is an initial thesis proposal that will be described in the next section.

### 2.2. INITIAL PROPOSAL

In this section the initial (starting) proposal is discussed based on the different aspects of a proposal as taught by the course Research Methodologies at the TU Delft. The initial working title is "**Mars Sample Return precise point rendezvous in Mars orbit**". Please note that this is not the final proposal and will change due to the knowledge gained and provided in this literature study.

#### 2.2.1. RESEARCH OBJECTIVE

The objective of this research is to find the optimum combination of the high-thrust MAV launch trajectory and the orbital changes required for the low-thrust orbiter in order to rendezvous at a certain point above Mars, depending on the desired design choices, and returning the orbiter to a save orbit by using TSI to propagate the trajectories, Q-law to determine the low-thrust orbiter thrust curve and using DE combined with and compared to MBH to optimise for mass, Time of Flight (ToF),  $\Delta V$ , Isp and/or  $\theta$ .

<sup>1</sup> All JPL missions: <http://www.jpl.nasa.gov/missions/>

### 2.2.2. RESEARCH PERSPECTIVE

It will be both Theory-testing research (**TSI**, **DE** and **MBH**) and Problem-analysis research (optimum problem). The problem will be solved through the writing and validation of an optimisation program based on orbital mechanics and from a(n) (initial) mission design standpoint. It is therefore an engineering problem, and is a result of preliminary research and discussions between researchers, supervisors and stakeholders.

### 2.2.3. RESEARCH FRAMEWORK

The framework has been set-up based on the guidelines provided in Research Methodologies and the corresponding literature [16] and is visualized in Figure 11.1.

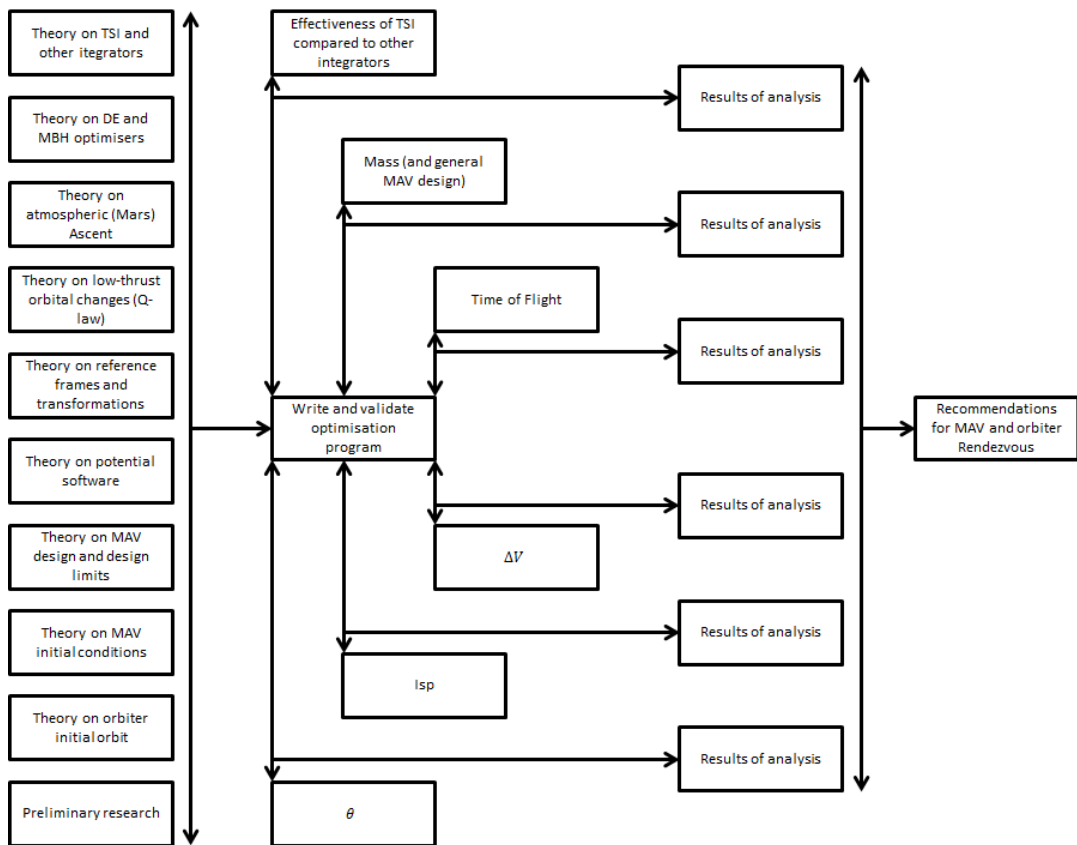


Figure 2.1: Research framework for the literature study (a) and the thesis work (b, c & d)

*Formulation:* (a) the study of the different theories and the preliminary research will result in a model (b) that can be used to write and validate an optimisation program to optimise for the different parameters and also determine the usefulness of **TSI**. (c) A comparison of the different optimisation results will help (d) establish the recommendations for the optimum **MAV** and orbiter rendezvous above Mars.

### 2.2.4. RESEARCH QUESTIONS

The corresponding research questions are listed:

- What are the current integration and optimisation methods used to perform ascent and transfer trajectory optimisation, how are the proposed methods different, and what are the expected results?
  - What is the difference between **TSI** and other frequently used integration methods in ascent and transfer trajectory calculations/optimisation and how do they work?
  - Which different optimisation methods are used in ascent and transfer trajectory optimisation and why have **DE** and **MBH** been chosen?

- What is the difference between **DE** and **MBH**, how do they work and what are the expected results?
- Which integration method(s) will **TSI** be compared to, why these particular integration methods and what are the expected improvements of **TSI** with respect to the other methods?
- Which aspects, parameters and equations are involved when designing ascent and transfer trajectories, what is the underlying theory and how can it be applied here?
  - What are the different aspects, parameters and equations when simulating an atmospheric ascent and how does that translate to Mars?
  - How can a low-thrust orbit transfer be performed and optimised for a rendezvous in Mars orbit?
  - Which perturbing bodies have to be accounted for in the Mars system in order to provide an accurate representation and which other perturbing sources have to be taken into account?
  - Which frame(s) of reference will need to be used, and if more than one frame is required, how do they relate to each other?
  - What will be the starting conditions of the **MAV** and the orbiter?
  - How do the different parameters affect the design of the **MAV**, how much can it be changed and what are the design limits, and thus also parameter limits, for the **MAV**?
  - When aiming for an orbit using Q-law, how can a precise orbit position be incorporated?
- What are the different optimal rendezvous situations given different design choices?
  - How does the orbit of the orbiter have to change in order to reach the desired rendezvous point based on the design choices?
  - What is the best **MAV** configuration and combination of launch parameters in order to reach the desired rendezvous point based on the design choices?
  - Which design is optimal for which design choice(s)?
- Would **TSI** be a good alternative for use in future optimisation programs?
  - How much more (or less) accurate is **TSI** compared to the other chosen integration methods?
  - How much faster (or slower) is **TSI** compared to the other chosen integration methods?
  - What are the advantages and disadvantages (besides the first two sub-questions) when using **TSI** in this kind of trajectory optimisation problem?
- Which of the two (or what kind of combination of the two) optimisation methods worked best in this kind of trajectory optimisation problem, what are the advantages and disadvantages of the different methods?

### 2.2.5. RESEARCH STRATEGY

The first step will be to perform a literature study on the subject and gather all the theory and become acquainted with this theory. The **TSI** should be explained in detail as well as the chosen reference integration method. The same will have to be done for **DE** and **MBH** as well as the Q-law method. After completion of the literature study, the optimisation program will have to be written, using the Taylor Series integration, to optimise (utilizing both **DE** and **MBH**) Martian ascent to a certain parking/rendezvous orbit starting at different elevations, azimuth and launch angle with respect to the horizon. This would also be used to compare the Taylor Series integration with one (or a number of) other integration method(s), for a small number of orbits, to identify the most suitable integrator for this problem. Once this is completed, the program should be updated such that this ascent optimisation will be able to not just optimise to a certain parking/rendezvous orbit but to also get to a specific point in that orbit (include time and  $\theta$ ) in order to perform a rendezvous manoeuvre with the orbiter. For the **MAV** this means that it could either directly go to the rendezvous point or first into a parking orbit (starting on the Martian surface) and then to the rendezvous orbit and point. It is assumed that during the entire ascent and manoeuvring phase the **MAV** uses a high-thrust propulsion system. As soon as this part of the program is validated, the orbiter can be added as well including Q-law. Provided that the orbiter, which uses a low-thrust propulsion system, starts from a scientific orbit, optimise the rendezvous orbit and point such that both **MAV** and orbiter will be at that point at the same time. After

which the orbiter will have to go back to a higher orbit in order to avoid getting caught in the gravity well of Mars. During each stage of the program writing it will have to be verified and validated. The validation will be performed based on the results from current [JPL](#) software used to perform orbit trajectory analyses and reference data from flown missions. Once the program validation has been completed, the actual optimisation process can commence and the optimisation will be performed for a number of different design choices while keeping within the limits of the [MAV](#) design and the orbiter design. Finally, recommendations will be provided based on the different optimised results and design choices.

#### **2.2.6. RESEARCH METHOD**

The research will be performed using a self-written software program and validated with programs used by [JPL](#) and flight data.

# 3

## MISSION HERITAGE

In early 2012 a group of scientists and engineers was set-up to devise an approach for the continuing exploration of Mars [17]. They had to combine all the requirements set by President Obama (to have humans in Mars orbit in the 2030s) and the 2011 NRC Decadal Survey for Planetary Science (science goals) while still keeping to the new proposed budget of the FY2013 U.S. Budget Submittal. Their conclusion was that a sample return mission would be the next logical step, because they deemed it to be the best combination between Human Exploration, Science and Technology. They also suggested different mission architectures to perform a [MSR](#) mission; using three, two or one launch(es). The first concept would first launch a rover to collect samples, then a [MAV](#) and a so-called *Fetch* rover to collect the sample case from the first rover and launch them into orbit, and the final launch would then send a sample return orbiter to collect the [MAV](#)/sample case and safely return it to Earth. The second concept would combine the last two launches into one using a smaller return orbiter propelled by a solar electric propulsion system. Finally, the third concept was to put all of these aspects into one launch, resulting in a sample collection rover with an on board [MAV](#) system and again a small return orbiter [17]. Currently NASA has decided to use a separate collector, orbiter and [MAV](#) system, which is what the research topic is based on. With the topic defined as in Chapter 2, it is required to determine what has already been done and what is currently being researched. This is called researching the missions heritage and is performed for every of the three phases involved: Mars atmospheric ascent (Section 3.1), low-thrust orbital transfers (Section 3.2) and rendezvous between an ascent vehicle and an orbiting vehicle above a planet (Section 3.3). Finally, the [MAV](#) heritage is examined in Section 3.4. To keep an overview, the reference missions and research will be discussed per phase and in the same order as mentioned.

### 3.1. MARS ATMOSPHERIC ASCENT REFERENCE MISSIONS

To date there have not been any launches from the Martian surface back into space. This does not mean that there exist no reference missions or any reference research. In principle every Earth launch can be compared to a launch from the Martian surface; there is a noticeable gravitational acceleration, rotational speed and atmosphere. However, the atmospheres are very different. In that sense, the moon might be a better reference body. In this section research on Mars ascent will be discussed first followed by actual flown Lunar sample return missions. Also, some Lunar ascent/sample return research will be discussed similar to the Mars research.

#### 3.1.1. MARTIAN ASCENT REFERENCE RESEARCH

Research has been performed on Martian ascent trajectories and is still being carried out for instance by the German Aerospace Center (Deutsches Zentrum für Luft- und Raumfahrt) ([DLR](#)). A list of reference research is shown in Table 3.1 followed by a short summary of each of the researched cases.

**Fanning and Pierson** In this study two different programs (gravity turn models and pitch-rate models) were used to observe the differences between them in the case of an optimisation for largest [MAV](#) payload mass using a two-stage vehicle and thus minimising the propellant mass required. During the optimisation different ascent profiles were tested in order to find the optimal ascent trajectory from the Martian surface to a circular orbit around Mars. For the first stage a liquid XLR-132 engine and for the

Table 3.1: Previous and current Mars ascent trajectory research

Person	Organization	Country	Year	Simulator
Fanning and Pierson [8]	Iowa State University	United States	1996	Unknown
Desai et al. [18]	NASA Langley and JPL	United States	1998	POST & OTIS
Whitehead [9, 19]	Lawrence Livermore National Laboratory	United States	2004	Unknown
Di Sotto et al. [20]	DEIMOS Engenharia and ESA	Portugal and The Netherlands	2007	Unknown
Trinidad et al. [3]	Northrop Grumman and JPL	United States	2012	MCAT
Dumont [21]	DLR	Germany	2015 (Ongoing)	TOSCA

second stage a liquid R-40B engine were assumed. The target parking orbit had a radius of 3862.92 km (where they assumed a Mars radius of 3389.92 km resulting in a 473 km altitude). Using a constant Gross Lift-Off Mass (**GLOM**) of 1400 kg, the gravity turn model resulted in a maximum payload mass of 367.8 kg whereas the pitch-rate model resulted in 366.4/366.8 kg. It was mentioned that the pitch-rate model might yield a better result overall if the aerodynamic effects are also taken into account but in the end it was concluded that the gravity turn model is a good choice in order to get a preliminary design for the **MAV**.

**Desai et al.** In this study a **MAV** ascent to a 300 km altitude circular orbit was simulated. The aerodynamic effects were simulated in a program called APAS, the aero-thermodynamic properties were simulated in LAURA and two different trajectory optimisation programs were used called POST and OTIS. For more information on these programs please see the reference [18]. Mars-Global Reference Atmospheric Model (**GRAM**) is used for the atmospheric model and the simulations also included mass, gravitational and propulsion models. Furthermore, a two-stage liquid propulsion system was assumed which had to deliver a payload mass of 30 kg into space. It was concluded that aero-thermodynamic effects are minimal. Also, the final nominal **MAV** lift-off mass was found to be 426 kg.

**Whitehead** In both papers the target orbit is taken at an altitude of 500 km and is circular. Also it is assumed to have a 100 kg **MAV** launch mass. Different trade-off's between staging, thrust, shape, and either liquid or solid propulsion are performed. In this case liquid propulsion shows a better performance with respect to the solid propulsion option. The problem was simulated as a simplified 2-D problem and coded into Fortran. It is also mentioned that miniaturisation of both liquid and solid propulsion systems would be required (down to a complete 10 kg system). A liquid single-stage to orbit is provided as a viable alternative.

**Di Sotto et al.** In this study the possible advantages of ascending to a 300 by 2000 km altitude parking orbit are discussed with respect to an ordinary 500 km altitude circular parking orbit. The optimisation of the trajectory has been split into an atmospheric part and a so-called exo-atmospheric part. The first part was then again split into a vertical rise phase, constant pitch rate phase, constant pitch phase and gravity turn phase respectively following **MAV** launch. The second part was also split into several phases: first an active propulsion phase then a coast phase followed by another active propulsion phase where the steering results from using an optimum guidance law derived from the "Primer vector". In this case it is assumed that both the first (four engines) and second stage (one engine) use liquid Rocketdyne RS-2101c engines. The used program optimises over 14 different optimisation variables and a number of constraints. It was concluded that a 300 by 2000 km altitude orbit could be achieved using the same architecture as for the 500 km altitude circular orbit. This would then also save 1000 kg in orbiter mass because of the higher altitude rendezvous. Unfortunately, nothing is known about the used optimisation program.

**Trinidad et al.** In this study the baseline design for the **MAV** is discussed. Several trade-off's are made concerning the kind of propulsion system and propellants. Also, five different launch angles are simulated

and compared. This trajectory analysis was performed using a three degrees of freedom tool developed by Northrop Grumman called Mission Capabilities Analysis Tool (MCAT). It used the Mars Geodetics and the 2010 atmosphere version of Mars-GRAM. The program was used to optimise (through the change of steepness and relative sizes of each stage) for a minimum MAV GLOM. The trajectory analysis was performed at an orbit of 466 km above the Martian surface. The resulting lowest GLOM was achieved using two liquid stages resulting in a MAV mass of 227 kg (283 to 391 kg including contingencies).

**Dumont**<sup>1</sup> Trajectory Optimisation and Simulation of Conventional and Advanced space transportation system (TOSCA) is a program that has been under development by DLR. It was initially created as an Earth launcher ascent simulator for early launcher design. Recently Dumont has started updating the program for both Lunar and Martian ascent, unfortunately nothing has been published yet on Martian ascent simulations. It incorporates both aerodynamic changes and propellant changes into the trajectory simulation and can also be used to optimise the trajectory based on several different optimisation parameters.

### 3.1.2. REFERENCE FLOWN LUNAR SAMPLE RETURN MISSIONS

As mentioned before, Lunar sample return missions can be considered similar to Mars sample return missions, the only difference being the atmosphere. This means that if the Martian atmosphere is neglected, Lunar flight data can be used to validate the ascent program (and then adding the atmosphere in a later phase). A comprehensive overview of all the sample return missions is presented in Table 3.2 for both manned and unmanned missions<sup>2</sup>. All successful soil and rock sample return missions were performed by the Soviet Union (robotic) and the United States (manned).

Table 3.2: Previous Lunar Sample Return Missions

Launch date	Country	Mission	Returned mass [kg]
16 July 1969	United States	Apollo 11	22
14 November 1969	United States	Apollo 12	34
12 September 1970	Soviet Union	Luna 16	0.101
31 January 1971	United States	Apollo 14	43
26 July 1971	United States	Apollo 15	77
14 February 1972	Soviet Union	Luna 20	0.055
16 April 1972	United States	Apollo 16	95
7 December 1972	United States	Apollo 17	111
9 August 1976	Soviet Union	Luna 24	0.17

Both Luna and Apollo missions first landed a craft on the Moon, then collected samples and returned these samples using a Lunar ascent vehicle. Unfortunately, the Luna missions cannot be used for validation since not enough data on the Lunar ascent phase is available. The Apollo missions however documented in detail and does include ascent flight data [22].

The Apollo programme was the first and only manned Lunar programme. It started in 1961 and lasted till 1972 [23]. The first missions were designed as tests and demonstrators for the actual Lunar landings. The first manned Lunar landing was performed by the Apollo 11 crew on the 20<sup>th</sup> of July 1969 [22]. Another five successful manned Lunar missions followed: Apollo 12, 14, 15, 16 and 17. All Apollo missions were able to bring back tens of kilograms of soil and rock samples. Both the astronauts and the samples ascended from the Lunar surface using the Lunar Ascent Module (LAM). Once back in Lunar orbit, the LAM would rendezvous with the Command and Service Module (CSM) at which time the astronauts and all the samples were transferred to the CSM. The LAM was discarded and the CSM was used to return to Earth. Both LAM and CSM are depicted in Figure 3.1<sup>3</sup>.

<sup>1</sup>Information based on personal communications with author as well

<sup>2</sup>Overview: [https://en.wikipedia.org/wiki/Sample\\_return\\_mission](https://en.wikipedia.org/wiki/Sample_return_mission)

<sup>3</sup>Source: NASA

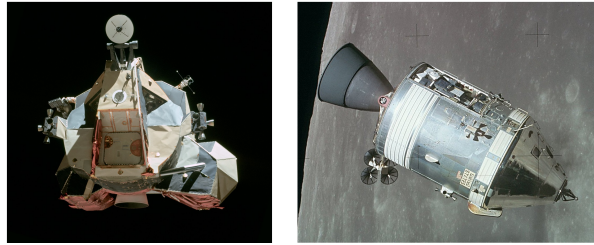


Figure 3.1: Left: Lunar Ascent Module, Right: Apollo Command and Service Module

### 3.1.3. LUNAR ASCENT REFERENCE RESEARCH

Research on Lunar sample return can also be used as reference data. Therefore a similar table to Table 3.1 can be set-up for Lunar research. An overview of different Lunar ascent/sample return research is provided in Table 3.3.

Table 3.3: Previous and current Lunar ascent trajectory research

Person	Organization	Country	Year	Program name
Sostaric and Merriam [24]	NASA Johnson Space Center	United States	2008 (Ongoing)	SORT
Dietrich et al. [25]	University of Colorado	United States	2015	Copernicus
Dumont [21]	DLR	Germany	2015 (Ongoing)	TOSCA

**Sostaric and Merriam** In this study a manned Lunar ascent and rendezvous trajectories were simulated and optimised. This was accomplished by dividing the ascent up into three different parts. A 100 m vertical rise, followed by a single axis rotation manoeuvre and ending in a powered explicit guidance phase to reach the target orbit. The problem was simulated in a 3 degrees of freedom simulation program called SORT. The single axis rotation algorithm calculates a time optimal single-axis rotation given the initial attitude and the final attitude. For the final phase of the ascent an optimiser called NPSOL was used, which is a non-linear programming solver. The initial target orbit was 15.24 by 75 km above the Lunar surface. The possibilities for emergency ascent were investigated together with a comparison between yaw steering and on-orbit plane changes. It was concluded that for large plane changes it is best to perform the plane changes on-orbit in order to reduce the required  $\Delta V$ .

**Dietrich et al.** In 2013 a new study was performed called Orion/MoonRise where the MoonRise mission would be combined with a manned mission to a halo orbit around the Earth-Moon L2 point [26]. In that case the MoonRise probe would be modified slightly and would have to ascent from the surface of the Moon to the Orion Spacecraft (s/c) in its halo orbit. The simulations performed showed a maximum theoretical sample return mass of 38 kg. The ascent vehicle would use a single solid STAR 48AX motor, based on the STAR 48A and 48B motor, and would have to be specially designed by Orbital ATK. In this follow up study two possible landing/ascent points on the moon were investigated: Schrödinger Crater and Tsiolkovsky Crater [25]. The simulator was developed in a tool called Copernicus combined with a MATLAB interface. The trajectories were simulated to ascent from the Lunar surface to a halo orbit around L2 and were split into four parts: ascent, trajectory correction manoeuvre, halo orbit insertion and halo orbit propagation.

**Dumont** Lunar ascent simulations were performed using TOSCA in light of the ROBEX project. In this paper, a re-usable concept Lunar ascent vehicle is described using a liquid oxygen/liquid hydrogen propulsion system with a specific impulse ( $I_{sp}$ ) of 440 s. The target orbit was 15 by 100 km after which the orbit would be circularised to 100 km. Ascent altitude-time profiles are provided for two different constant thrust settings: 25.9 kN and 34.5 kN.

## 3.2. LOW-THRUST ORBITAL TRANSFER REFERENCE MISSIONS

Because the planned Mars 2022 orbiter, which will likely collect the Martian sample from the MAV and return back to Earth, will have a low-thrust propulsion system it is important to identify previous missions and research. In the past few years, low-thrust propulsion systems have become increasingly popular in long duration missions because of the high  $I_{sp}$  and the low total system mass. Since the current defined topic will focus on a low-thrust problem in the Martian system, it is important to analyse previous low-thrust missions that have flown in planetary systems (see Section 3.2.1). As to date, no low-thrust missions have flown in the Martian system. However, research has been performed on low-thrust mission in both the Earth and Martian system as described in Section 3.2.2.

### 3.2.1. EARTH SYSTEM LOW-THRUST APPLICATIONS

Low-thrust applications in the Earth system were first implemented back in the 60s with the first non-experimental flight, using Electric propulsion (EP) for attitude control, performed by the Zond-2 [27]. The three main applications for EP in satellites have historically been in attitude control, (geosynchronous) station keeping and other general orbit adjustments. For the thesis problem it is interesting to investigate missions that used EP for orbit transfers and orbital phase changes. Table 3.4 provides an overview of different missions that used EP as a means to perform either orbital phase adjustments or orbit transfers (based on [27]). In the past few years EP has become increasingly popular for use as s/c main propulsion systems and now companies, such as Boeing and their 702SP series of communication satellites<sup>4</sup>, are even introducing fully electric s/c [28]. These new satellites are also included in Table 3.4 as well as a number of missions which had to use their EP systems for orbital transfer manoeuvres even though the electric thrusters were not intended for it<sup>56</sup>.

Table 3.4: Previous Low-thrust Earth Missions

Launch year	Country	Mission	EP use
1965	United States	Vela	Phase adjustment
1967	United States	Advanced Vela	Phase adjustment
1988	United States	Gstar-3	Orbit Transfer
2000	United States	MightySat II.1	Orbit Transfer
2001	Europe	Artemis	Orbit Transfer
2010	United States	AEHF(-1)	Orbit Transfer
2015	United States	ABS-3A	Orbit Transfer
2015	United States/France	Eutelsat 115 West B	Orbit Transfer

Compared to the intended use of the low-thrust EP on the Mars 2022 orbiter, where the propulsion system shall be used to perform several orbital transfer manoeuvres including orbit raising, orbit lowering and most likely inclination changes, the orbit transfer applications for the satellites shown in Table 3.4 are simply transferring the s/c from a Low Earth Orbit (LEO) or Geostationary Transfer Orbit (GTO) to Geostationary Earth Orbit (GEO). However, advanced low-thrust manoeuvring have been performed by interplanetary missions.

### 3.2.2. LOW-THRUST (MARTIAN) PLANETARY SYSTEM RESEARCH

Because low-thrust as a main propulsion system has become increasingly important, many studies are currently being conducted in the area of low-thrust trajectory optimisation for the Earth system, Mars system and mainly interplanetary transfers. However, since this problem deals with the orbit transfers in a planetary system the reference research will be selected based on Earth and Martian system applications. The reference research is presented in Table 3.5 again followed by a short description.

**Geffroy and Epenoy** In this study the possibility of using a generalised averaging method (bang-bang) is investigated. Two problems are considered: Minimum-time and fuel-saving both combined with several constraints. It is mentioned that rendezvous problems (similar to the problem described in this thesis

<sup>4</sup>Boeing company: <http://www.boeing.com/space/boeing-satellite-family/index.page>

<sup>5</sup>Artemis mission update: [http://www.esa.int/Our\\_Activities/Telecommunications\\_Integrated\\_Applications/Artemis\\_finally\\_reaches\\_operational\\_orbit](http://www.esa.int/Our_Activities/Telecommunications_Integrated_Applications/Artemis_finally_reaches_operational_orbit)

<sup>6</sup>AEHF-1 mission update: <http://spaceflightnow.com/atlas/av019/111009.html>

Table 3.5: Previous and current Mars low-thrust trajectory research

Person	Organization	Country	Year	Program name
Geffroy and Epenoy [29]	CNES	France	1997	Unknown
Kluever and Oleson [30]	University of Missouri-Columbia and NYMA, Inc.	United States	1998	Unknown
Bertrand et al. [31]	CNRS & CNES	France	2001	Unknown
Whiffen [32]	NASA JPL	United States	2006	Mystic
Sims et al. [33]	NASA JPL	United States	2006	MALTO
Kos et al. [34]	NASA JPL	United States	2006	MALTO, Mystic, Copernicus, OTIS, SNAP, CHEBYTOP, VARITOP, SEPTOP, NEWSEP and Sail
Derz and Seboldt [35]	DLR	Germany	2012	InTrance

topic) can be treated as well, but was not done this in this study. It is concluded that the method works well but needs to be combined with other methods in order to properly solve the numerical problem.

**Kluever and Oleson** In this study the low-thrust trajectories from LEO to GEO and GTO to GEO is optimised using a direct method (incorporating averaging techniques) and it is compared to the widely used SEPSPOT (which uses a shooting method to solve the two-point boundary value problem and is based on calculus of variation). The direct method used a sequential quadratic programming optimiser to optimise the problem. It is concluded that the developed direct method is a robust method that can be useful in preliminary design.

**Bertrand et al.** Here, low-thrust propulsion is used for the heliocentric stages and the Mars insertion and escape. Chemical propulsion is however still used for the final Mars rendezvous. In this case again a low-thrust planetocentric optimisation tool is used that is based on averaging techniques in optimal control. The used tool was developed by Centre National d'Études Spatiales (CNES) and is again solving the two point boundary value problem. In conclusion it is mentioned that improvements can be made to this tool: including variable power, mixed minimum-time/fuel-saving criterion, atmospheric drag and Van Allen degradation (in case of LEO insertion and better transition between planetocentric and heliocentric mission phases. It was also concluded that a fully electric vehicle would be a better choice (thus getting rid of the chemical propulsion for rendezvous) and will then be used for rendezvous as well, but this requires more research.

**Whiffen** This paper describes the Mystic program used for low-thrust trajectory calculations. The optimisation algorithm used is called Static/Dynamic Optimal Control and is a non-linear optimal control method that can optimise static and dynamic variables at the same time (it is based on Bellman's principle). It is used in the Dawn mission. The software can be used for planetocentric low thrust optimisation.

**Sims et al.** This paper describes the MALTO program used for low-thrust (and can also be used for high-thrust) trajectory optimisation. The trajectory problem is a non-linear optimisation problem which is then solved in MALTO using the non-linear programming software called SNOPT. In this paper the direct MALTO program is compared to the indirect SEPTOP program used previously for many mission design cases. MALTO showed similar final mass estimations but has much less convergence sensitivity and can incorporate many more intermediate flybys (up to 12 were tested).

**Kos et al.** This paper shows an overview of the different low-thrust trajectory analysis tools developed by NASA. A comparison is made between the different programs and it is specified that the users will have to decide for themselves which program fits best with their problem. SNAP is the primary tool to be

used for planetocentric optimisation of low-thrust trajectories. All the programs are coded in Fortran. The paper also provides information on how to obtain the programs (also through a website, which is not online anymore).

**Derz and Seboldt** In this paper a European [MSR](#) mission is envisioned through two different architectures (either two separate launches or one combined launch). In this study the orbiter utilises a low-thrust propulsion system as its main propulsion system. The orbiter would go into 1000 km parking orbit around Mars waiting for the sample to be brought into orbit by the [MAV](#). The low-thrust trajectories are optimised for minimal flight time using the InTrance program. This program optimises through the use of artificial neural networks and evolutionary algorithms. For the integration, Runge-Kutta-Fehlberg ([RKF45](#)) is used and JPLs DE405 ephemerides for Earth and Mars are incorporated as well. It was concluded that a low-thrust option for [MSR](#) is a good alternative to the European Space Agency ([ESA](#)) proposed high-thrust option. But, because of the power requirements, the [s/c](#) configuration should be investigated more.

This is a selection of research and programs that have been used in the last few years. Much more research has been performed concerning the Earth raising orbits.

### 3.3. ASCENT VEHICLE AND ORBITER DIRECT RENDEZVOUS REFERENCES

In this case, the definition of direct rendezvous is to get to the same point (or at least control box) in orbit at the same time as the orbiting [s/c](#) within one revolution. Often a certain rendezvous orbit is chosen and once in this orbit, the [s/c](#) performs a so-called phasing manoeuvre in order to get closer to the orbiting [s/c](#). Once inside the control box, the close rendezvous begins, which is not part of this study. In this section reference missions will be provided which have performed or which came close to single-revolution rendezvous. Also, the reference research performed in this particular field will be described.

#### 3.3.1. FLOWN MISSIONS

There have been many rendezvous missions, some of which specific to a celestial body launch and rendezvous with an orbiting vehicle. For example, all the Apollo missions were able to rendezvous with an orbiting [s/c](#) after ascending from the moon. And in more recent years there have been many rendezvous with the International Space Station ([ISS](#)). In Table 3.6 the missions with a low number of revolutions before rendezvous after launch are shown. It also shows an estimate of the amount of revolutions it took in order to successfully rendezvous with the orbiting [s/c](#).

Table 3.6: Previous (nearly) direct rendezvous Missions

Year	Country	Mission	Orbiting body	Revolutions
1965	United States	Gemini 6A and 7 [36]	Earth	4
1966	United States	Gemini 8 [37]	Earth	4
1967	Soviet Union	Kosmos-186 and 188 [38]	Earth	1
1969	United States	Apollo 11 [22]	Moon	2
2012	Russia	Progress-M-15M [39]	Earth	4

It is interesting to observe that so-far only the Russians have performed a single-revolution rendezvous<sup>7</sup>. However, it should be noted that this was achieved with two unmanned [s/c](#). Also, for the Gemini missions, single-revolution rendezvous (called first apogee plan) was one of the three rendezvous plans considered [37]. Though in the end it was decided that due to both extra stress on the astronauts, because all the same procedures would have to take place in a shorter time, and due to the inaccuracy of the orbit insertions at the time a first apogee rendezvous would be too risky and would need a back-up plan to deal with uncertainties. Instead it was decided to use the coelliptical plan.

A more recent application is the Russian rendezvous with the [ISS](#). As mentioned in the table, the Progress-M-15M was the first to demonstrate a shorter rendezvous strategy. Before this strategy was employed, the travel from Earth to the [ISS](#) took at least two days, however due to advancements in, among others, GPS technology, the transfer could now be achieved in a much shorter time [39]. This strategy is currently also applied to the

<sup>7</sup>Personal account: <http://www.svengrahn.pp.se/trackind/K186188/K186188.html>

manned Soyus missions to the ISS. Even shorter transfers are being considered. In the paper it is mentioned that a 3 revolution period is possible but it could even go down to 1 revolution.

### 3.3.2. DIRECT RENDEZVOUS REFERENCE RESEARCH

As mentioned in Section 3.3.1, research has already been performed in the past on the Gemini missions and is currently being done for mission to the ISS. However, more research has been conducted focused on single-revolution rendezvous or at least close to one revolution. An overview of this research can be found in Table 3.7 followed by a short description.

Table 3.7: Direct rendezvous reference research

Person	Organization	Country	Year	Application
de Almeida Prado [40]	Instituto Nacional de Pesquisas Espaciais	Brazil	1996	Rendezvous between two orbits
Woolley et al. [41]	NASA JPL	United States	2011	MSR

**de Almeida Prado** In this study, two orbits are taken and specifically two points in those orbits. Then the optimum rendezvous is computed starting in the first point in the initial (lower) orbit and arriving in the second point in the final (higher) orbit. This is achieved using less than one, one, or more revolutions. The Lambert problem is used and solved to find the required parameters for a given number of revolutions.

**Woolley et al.** In this study different strategies for Martian ascent and rendezvous are presented. Provided a set of requirements, the proper launch and rendezvous trajectories were found. In this case, the MAV is positioned in an orbit in front (could be slightly below) of the orbiter, because of the Line of Sight requirement in this case. It was concluded that optical detection and orbit determination for this particular MSR architecture would be a viable option.

As presented in Table 3.7 not much research has been conducted concerning the special case of direct launch single-revolution rendezvous. Also, considering that single-revolution rendezvous has been performed in the past and that for manned missions to the ISS it is still considered, it will be interesting to compare the results of the thesis work to other rendezvous options.

## 3.4. MAV DESIGN

Martian sample return has never been attempted, as a matter of fact a sample return from any celestial body with an atmosphere has never been done before. When designing a Martian sample return missions, a vital part is transporting the samples off of the planet, using a MAV. This vehicle can then either be sent directly to Earth or rendezvous with a s/c (either orbiting the planet or not). This section will focus on the different possible MAV designs that have been considered and/or proposed (Section 3.4.1). Most of these studies were based on a set baseline design that has changed over time due to a continuing changes in mission design and proposed date. Therefore Section 3.4.2 will outline the current MAV baseline design. There is however still some flexibility in the baseline design. This design space can be used during the optimisation to change the design slightly if required. The exact design space will be described in Section 3.4.3.

### 3.4.1. PREVIOUS INVESTIGATIONS

Many MAV design studies have been performed. A number of these studies are shown in Table 3.8. For each study, the main launch concept is provided and the kind of propellant(s) as well. The studies are presented in order of publication year.

From the table it is clear that all studies envision a rocket to bring the samples either into Martian orbit or directly back to Earth. Also, four clear propellant types have been investigated: the traditional solid and liquid propellant engines, the hybrid engine (which is a combination of a solid fuel and a liquid oxidizer) and the gel engine.

Table 3.8: Previous MAV studies

Person	Year	Launch method	Propellant(s)
Whitehead [42]	1997	two stage rockets (comparison study)	solid and liquid (and gel recommended as well)
Guernsey [43]	1998	two stage rocket	2x liquid
Desai et al. [18]	1998	two stage rocket	2x liquid
Stone [44]	1999	two stage rocket	hybrid
Stephenson [1]	2002	two stage rocket (three different designs)	2x Solid (Best), Solid and liquid or hybrid and 2x gel (Best)
Whitehead [19]	2005	one, two and three stage rockets (variational study)	solid and liquid
Stephenson and Willenberg [45]	2006	two stage rocket	2x solid
Sengupta et al. [46]	2012	two stage rocket	2x liquid
Trinidad et al. [3]	2012	two stage rocket	2x liquid
Mungas et al. [2]	2012	single stage rocket	liquid mono-propellant
Mars Program Planning Group [17]	2012	undefined rocket	solid and liquid

In [3] it is shown that the GLOM would be lowest when using a two stage liquid rocket. Nevertheless, a two stage gel rocket would be a reasonable alternative. However, a low GLOM is not the only requirement. A visual representation of some of the described designs is presented in Figure 3.2.



Figure 3.2: A number of rocket concepts visualized. a) Two stage solid rocket by Lockheed Martin [1], b) Single stage mono-liquid rocket by Firestar Technologies [2], c) Two stage gel rocket by TRW [1] and d) Two stage bi-liquid rocket by Boeing and Northrop Grumman [3]

### 3.4.2. CURRENT MAV BASELINE DESIGN

The latest baseline design for the MAV originates from a (number of) studie(s) conducted in 2012 (also see Table 3.8). The main properties of the current baseline is presented best by [3]. In this paper, the rocket depicted in d) of Figure 3.2 was analysed and put forward as the baseline design with the orbital sample container located in (and acting as) the nose of the rocket. A more detailed view of the baseline MAV is shown in Figure 3.3. Here, the samples are contained in the Orbiting Sample (OS), the thrust vector is controlled by the Thrust Vector Control (TVC) engines (or Reaction control system (RCS)) and the final attitude adjustments are made by the Attitude Control System (ACS) thrusters.

The design resulted from the requirements for a MAV put forward back in 2010. The main characteristics of the baseline MAV are summarised in Table 3.9.

It should be noted that since the current baseline design is a pressure regulated system, the thrust is

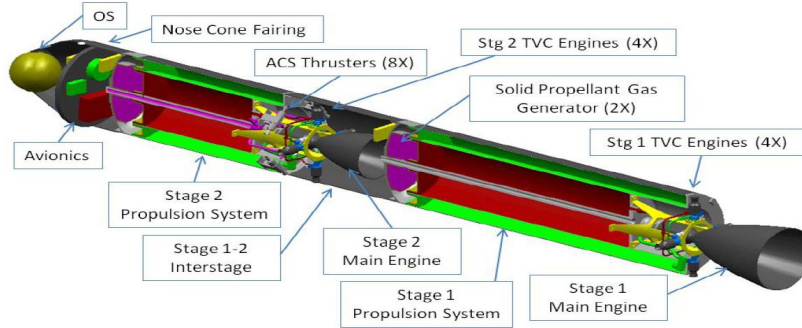


Figure 3.3: Two stage bi-liquid baseline MAV with descriptions of different components [3]

Table 3.9: MAV baseline design characteristics

Characteristic	Value or property
Martian Sample Payload	5 kg
Stage 1 main engine thrust	5.3 kN (restartable)
Stage 2 main engine thrust	2.7 kN (restartable)
Stage 1 RCS engines (4x)	445 N (4x)
Stage 2 RCS engines (4x)	445 N (4x)
Stage 2 ACS engines (8x)	4.4 N (8x)
Main engines propellants	MON-25 (Oxidizer), MMH (Fuel)
RCS propellant (hot-gas)	Segmented solid propellant gas generators (Also, liquid tank pressurant)
Total MAV mass	227 kg (283 kg with contingencies and 391 kg with extreme contingencies)
<i>Isp</i>	330.5 s Vacuum, 328.6 s in Martian atmosphere
Diameter	340 mm
Total length	approx. $\leq$ 3666 mm
Max. launch angle	$\pm 35^\circ$ off vertical axis
Target orbit	460 by 580 km

constant throughout the flight [47].

### 3.4.3. CURRENT DESIGN RESTRICTIONS

The baseline design described in Section 3.4.2 was based on early design restrictions set by the MAV Study Guidelines 2010 [3]. The design restrictions mentioned in [3] form the design space available for optimisation. The restrictions mentioned include those specified in [48].

- The total system, which is the MAV and the erector support system (tower) to launch it, have to have a total mass of less than 360 kg [3]
- Deliver a 5 kg Martian sample payload to orbit [3]
- The final orbit is 460 by 580 km [3]
- Initial MAV Study Guidelines volume requirement: 2850 mm long and a diameter of 700 mm [3]
- Updated volume requirement: ranging from 3666 mm long with a diameter of 350 mm to 3150 mm long with a diameter of 700 mm [3]
- $45^\circ \pm 0.2^\circ$  target orbit inclination [48]
- Ability to launch from  $\pm 30^\circ$  latitudes [48]
- Sample sphere diameter: 16 cm (5 kg) [48]

# 4

## OPTIMISATION

In this chapter, different mission design optimisation techniques will be discussed. There are two different kinds of optimisations: local optimisation, where a minimum (or maximum) is found which is the minimum for a small area in the function space and does not have to be the absolute minimum of the function, and global optimisation, where the found minimum (or maximum) is the minimum value of the entire function space [49]. Such a function space can contain multiple local minima but only one global minimum; one of the local minima is also the global minimum. A general description of the local and global optimisation techniques is provided in Sections 4.1 and 4.2 respectively. The different optimisation techniques are compared in Section 4.3 and the reason for choosing Differential Evolution and Monotonic Basin Hopping is provided in Section 4.4. Finally, DE and MBH will be described in more detail towards implementation in Sections 4.5 and 4.6 respectively. An optimisation problem can either be solved analytically, resulting in a direct solution, or numerically, approaching the exact solution [50]. When comparing different optimisation techniques usually cpu time is traded against accuracy of the result. Often a more accurate result requires more time and thus increases the cpu time required. From now on only minima are discussed, but every method can also be used to find the maximum.

### 4.1. DIFFERENT LOCAL OPTIMISATION METHODS

Local optimisation determines the local minimum of a function. The methods used are called Nelder-Mead, Newton-Raphson (1D), steepest descent (either along the axes or in an arbitrary direction), Sequential Quadratic Programming and Monotonic Basin Hopping [50, 51]. Some methods might get stuck at the local minimum, but sometimes can find several local minima and thus also find the global minimum. Local optimisation methods are usually fast and accurate, producing good results in a short time. But they only focus on a small area of the function space [52]. Therefore it is important to define a proper initial value for the local methods (for instance by first using a global optimiser).

### 4.2. DIFFERENT GLOBAL OPTIMISATION METHODS

In [50], two main numerical global optimisation categories are mentioned: sampling methods and meta-heuristics. In global optimisation the minimum value of the complete function is obtained, or at least an approximation of this value.

#### 4.2.1. SAMPLING METHODS

The sampling methods are based on selecting a value for the variable(s) in the function and then evaluating the function. This is done for many different values until a minimum is found and can be accomplished randomly (Monte Carlo) or using a certain pattern (grid search and Latin hypercube sampling<sup>1</sup>). These variable values can also be generated quasi-random, which often involves generating all the different values at the beginning of the optimisation and then evaluating the function for every of these values. An example of such a method is Sobol sequencing [53]. Sampling methods can be used to initially reduce the search space for a local optimiser since the resolution of sampling methods can be limited. However, should a sampling

<sup>1</sup>Online blog: <https://mathieu.fenniak.net/latin-hypercube-sampling/>

method be applied to a small function space, accurate results can still be obtained, which is why it can also be used for local optimisation.

#### 4.2.2. METAHEURISTICS

Metaheuristics are numerical optimisation techniques that directly propagate towards the solution. Unfortunately, convergence cannot always be detected, and usually a local optimisation gradient method is required to refine the final solution. The different methods are: Genetic Algorithm, Differential Evolution, Particle Swarm optimisation, (Adaptive) Simulated Annealing, Ant Colony optimisation, Dynamic Programming and Interval Analysis<sup>2</sup> [50, 51]. Often these methods require many iterations to reach a proper solution, however, they are very robust and to not require an accurate initial value.

### 4.3. TECHNIQUE COMPARISON

To gain a better understanding of the different methods mentioned in Sections 4.1 and 4.2, a comparison is made between all them. Table 4.1 shows the advantages and disadvantages of each method using a similar representation as provided in [50]. For metaheuristics the general advantages are: robust, do not depend on derivatives, do not require a good initial value and propagate directly towards a solution. The general disadvantages are: robust, does not depend on derivatives, does not require a good initial value and propagates directly towards a solution. Also, often metaheuristics require a local optimisation method to reach the precise final optimum. In the table the advantages and disadvantages that separate the different metaheuristic methods are mentioned.

Table 4.1: optimisation method comparison

Method	Type	Advantage	Disadvantage
Nelder-Mead	Local	simple	converges to local minimum
Newton-Raphson	Local	simple	convergence is slow near a flat optimum and converges to local minimum
Steepest descent	Local	simple, always finds a minimum and only requires previous gradient information (arbitrary direction results in better conversion)	can oscillate around minimum, has a slow convergence and converges to a local minimum (needs second derivatives/Hessian matrix for arbitrary directions)
Sequential Quadratic Programming	Local	works well on non-linearly constrained problems and neither initial point or iterate points have to be feasible [54]	converges to local minimum
Monotonic Basin Hopping	Local/ Global	can locate several local minima that are close together [51]	no guarantee that best found local minimum is also global minimum and normal Basin Hopping is preferred when searching one local minimum [55]
Monte Carlo	Global/ sampling	simple to implement and does not depend on derivatives	only simple problems (otherwise very slow), it is based on luck and can have bad resolution (approximation of value)
Grid search	Global/ sampling	simple to implement and does not depend on derivatives	slow and can have bad resolution (approximation of value)
Latin hypercube sampling	Global/ sampling	simple to implement, does not depend on derivatives and it provides more regular sampling	only simple problems (otherwise very slow), it is based on luck and can have bad resolution (approximation of value)
Sobol sequencing	Global/ sampling	good uniform distribution (regular sampling), faster convergence and does not depend on derivatives	all sampling values are generated at once [53]
Genetic Algorithm	Global	simple, easy to understand	uses binary numbers to encode variables

<sup>2</sup>Usually using a branch and bound method: <http://www.cs.sandia.gov/opt/survey/interval.html>

Differential Evolution	Global	simple, uses actual variable values	does not perform well for multi-objective problems and was not intended for binary code use [56]
Particle Swarm Optimisation [57]	Global	does not use mutations, very fast, simple, based on intelligence	does not perform well for a scattering problem, does not have a systematic calculation method
Simulated Annealing <sup>3</sup>	Global	easy to program, can be applied to many different problems, can deal with many constraints	the fine-tuning of the constraints and variables can be delicate, often Genetic Algorithms perform equally well or better
Ant Colony Optimisation [57]	Global	always solved using parallel computations, can handle dynamic problems	not well suited for theoretical problems
Dynamic Programming [58]	Global	solving sub-problems to find problem solution and stores solutions to sub-problems as to only evaluate every sub-problem once	can require much storage space with increase of different sub-problems
Interval Analysis [59]	Global	includes different error estimations, can be used for infinite data sets	can be complex

## 4.4. CHOSEN METHODS

As mentioned at the beginning of this chapter DE and MBH were chosen as the methods to be used in this particular thesis problem. In this section it is explained how this decision was reached. In order to choose the methods it was useful to understand which methods had been used before in the TU Delft Space department. Basing the decision on what knowledge already exists in the department would allow for use of resources that are already available and would make it easier to learn from experienced people. However, other used methods for similar subject problems could not be ignored, since one method might be better suited for the problem than the other. Therefore, Section 4.4.1 first describes a collection of methods that are frequently used for similar problems (this is a selection of the methods mentioned in Table 4.1) and then Section 4.4.2 will discuss the methods used in the Space department. Ultimately the TU Delft supervisors were also involved in deciding upon the final methods. The final decision of why DE and MBH were chosen is described in Section 4.4.3.

### 4.4.1. FREQUENTLY USED METHODS

The required method depends on the problem that needs to be solved. To help determine which methods to use for the thesis problem, reference optimisation research was consulted. An overview is presented in Table 4.2.

Most of the problems mentioned in Table 4.2 require metaheuristic methods. Addis et al. [69] mentions that Differential Evolution is very popular because of its robustness resulting in good results, but that Monotonic Basin Hopping might be a better alternative because it can produce even better results.

### 4.4.2. TU DELFT OPTIMISATION HERITAGE

At the Space department of the TU Delft, a toolbox was developed called Tudat. This toolbox can be used to solve and create programs for all kinds of astrodynamics problems. Since the introduction of this toolbox, students have been working on optimisation programs within this toolbox mainly based on Differential Evolution [70]. Such a program was developed by Musegaas [51]. These developed programs were also adjusted to incorporate specific problem needs such as was done by Miranda [71] where the original program used Differential Evolution and Particle Swarm optimisation was added to produce a better solution. It is however unlikely that Tudat programs itself will be used during this thesis, nonetheless the experience is there and can still be used.

### 4.4.3. CHOSEN CANDIDATE METHODS

The decision of which methods to use was based on the heritage, reference research, preference of the supervisors and personal preference. Currently, the method that is used most (and the method that most existing programs in the Tudat toolbox are programmed for) is DE. Therefore it was logical to use the DE optimisation

<sup>3</sup>Simulated Annealing overview, online document: <http://www.aiinfinance.com/saweb.pdf>

Table 4.2: Previous methods used for trajectory and orbit transfer optimisation problems

Person	Year	Subject	Method
Gage et al. [60]	1995	Interplanetary Trajectory (Mars missions)	Genetic Algorithm
Rauwolf and Coverstone-Carroll [61]	1996	Low-thrust orbit transfers (to Mars and Mercury)	Genetic Algorithm
Kim and Spencer [62]	2002	Spacecraft Rendezvous	Genetic Algorithms
Myatt et al. [63]	2004	Mission Analysis and Design (transfer orbits)	Differential Evolution (most robust)
Lee et al. [64]	2005	Low-thrust orbit transfers	Q-law with Genetic Algorithm and Q-law with Simulated Annealing
Abdelkhalik and Mortari [65]	2007	Transfer orbits	Genetic Algorithms
Vasile et al. [66]	2008	Space trajectories	Monotonic Basin Hopping
Garcia et al. [67]	2010	Optimisation of Mars entry vehicle for a mass of 40 tons	(Multi Objective) Genetic Algorithm
Li and Peng [68]	2011	Mars entry and descent	Sequential Quadratic Programming and Monte Carlo
Addis et al. [69]	2011	Space trajectories	Monotonic Basin Hopping

method for the current subjects problems. However, as [71] also showed, depending on the problem, it might be better to incorporate other methods as well. Based on the reference research it is clear that even though **DE** is very popular even outside of the TU Delft, **MBH** could be an attractive alternative. This is why it was decided to investigate both **DE** and **MBH**, compare the two methods and maybe even combine them to explore the results and possibilities for application in the current topic. This is also interesting from an academic point of view. The next two sections will discuss each of the chosen method in more detail and explain how they can be implemented.

## 4.5. IMPLEMENTATION OF DIFFERENTIAL EVOLUTION

Differential Evolution is a direct global method based on Genetic algorithms and was first introduced by Storn and Price back in 1995 [72]. The method became increasingly popular after performing well in two world wide optimisation competitions [73] and finally caught the interest of the scientific and engineering community in 1997 when two more papers were published of which the final paper ([4]) provided a clear and easy to understand description of the method. This description will also be used in Section 4.5.1 to explain the basics of **DE**. In Section 4.5.2 variations on the original **DE** method are explained as well.

### 4.5.1. THE WORKINGS OF DE

When using **DE** for a minimisation problem the objective is to find the minimum global function evaluation. For instance, if the aim is to find the minimum fuel mass in order to reach a certain point in a certain orbit then the function will be written to compute the required fuel mass given a combination of different variables (such as launch azimuth and lift-off mass). These variables are chosen randomly by the **DE** algorithm and their combination is optimised to reach a minimum fuel mass solution. In such a case, the minimum fuel mass function is called the cost function. Because **DE** is based on Genetic algorithms it works with "individuals", "population size", and "generations". An individual is a vector, with all the different variables in it, of size  $D$  (the number of variables). The values of these variables are initially randomly chosen for each individual before the **DE** optimisation, within the different variable constraints (parameter space). The population size ( $NP$ ) determines the number of individuals used during the optimisation. Before the start of the optimisation the first generation is generated randomly provided the mentioned constraints. Each time an optimisation run is performed, a new generation ( $G$ ) is created with new (improved) individuals, or including the best individuals of the previous generation depending on how well they performed. This means that the optimisation will run until a specific number of generations is achieved, which means that the number of generations is a set value by the user. The individual vectors per generation can be written as shown in Equation (4.1) [4].

$$x_{i,G} \quad \text{with } i = 1, 2, \dots, NP \quad (4.1)$$

In order to generate new individual vectors during the optimisation (new generation), DE adds the weighted difference between two individual vectors to a third vector, a process called mutation, and then mixes this new mutation vector  $v_{i,G+1}$  with the original, target, individual vector  $x_{i,G}$  resulting in a trial vector  $u_{i,G+1}$ , a process called crossover. Here the three individual vectors used to compile the mutation vector are all distinctly different from the original individual vector. This then calls for the requirement that NP is at least equal to 4. In equation form this means that first the mutant vector is created through the use of Equation (4.2) (visualized for a two-dimensional cost function in Figure 4.1).

$$v_{i,G+1} = x_{r_1,G} + F \cdot (x_{r_2,G} - x_{r_3,G}) \quad (4.2)$$

Where in Equation (4.2)  $r_1, r_2, r_3 \in \{1, 2, \dots, NP\}$  are all different and different from  $i$ . Also  $F \in [0, 2]$ , where  $F$  is called the amplification factor (or weight) which determines the impact of the difference vector to the first chosen  $x_{r_1,G}$  vector and is selected by the user. It should be noted that in case of a strictly constraint problem, such as the thesis topic problem (launching through the planet is impossible), each of the new variables created through mutation should be checked for plausibility. This means that the value for the different variables should always be within the respective parameter space.

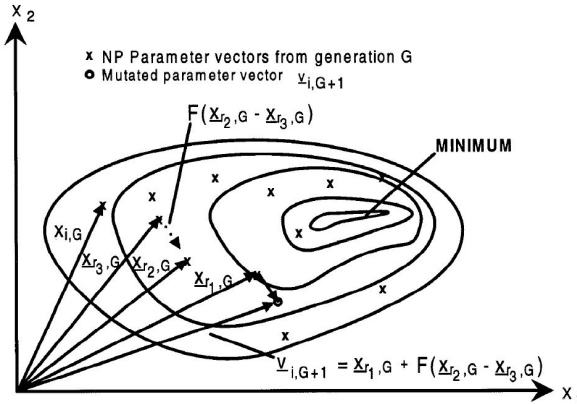


Figure 4.1: Construction of the mutation vector in a two-dimensional case [4]

The crossover/trial vector is composed of the variables from both  $x_{i,G}$  and  $v_{i,G+1}$ . Each different variable is denoted by its separate position number  $j$  (thus  $j = 1, 2, \dots, D$ ). Using this notation the trial vector can be described as  $u_{i,G+1} = (u_{1i,G+1}, u_{2i,G+1}, \dots, u_{Di,G+1})$  where the determination of which variable value originates from which vector ( $x_{i,G}$  or  $v_{i,G+1}$ ) is determined by Equation (4.3) and visualized by Figure 4.2 for a 7-dimensional case.

$$u_{ji,G+1} = \begin{cases} v_{ji,G+1}, & \text{if } (\text{randb}(j) \leq CR) \text{ or } j = rnbr(i) \\ x_{ji,G}, & \text{if } (\text{randb}(j) > CR) \text{ and } j \neq rnbr(i) \end{cases} \quad (4.3)$$

Where in Equation (4.3)  $\text{randb}(j) \in [0, 1]$  and is the  $j$ th evaluation obtained from a uniform random generator [4]. Also, CR is called the crossover constant which is chosen by the user  $\in [0, 1]$  and  $rnbr(i)$  is again a random chosen number. This ensures that at least one variable from the mutation vector will become part of the trial vector.

The last step is to determine whether the trial vector  $u_{i,G+1}$  generates a better value, or lower fuel mass in case of the example provided in the beginning of this example, than the original, target, individual vector  $x_{i,G}$ . If the trial vector performs better, then the  $i$ th individual vector in the next generation  $x_{i,G+1}$  becomes  $u_{i,G+1}$ . However if it performs worse than  $x_{i,G}$ , then  $x_{i,G+1}$  becomes  $x_{i,G}$ . This is done for every individual vector in the population. And once the entire population in a generation has been examined, and has either been replaced by a better combination or not, the next generation is examined until the final generation is reached.

A pseudo-code for this process written in C is provided in the paper of Storn and Price [4]. A specific example of this DE application is presented in [74] for both C and Matlab.

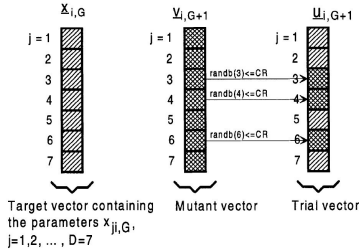


Figure 4.2: Construction of the trial vector in a 7-dimensional case [4]

#### 4.5.2. VARIATIONS OF DE METHOD

In their 1997 publication, Storn and Price also mention that the DE method described in Section 4.5.1 is not the only method to implement DE. In fact they make a selection of three distinct changes that can be made to vary the method. The first change would be to, instead of taking a random individual vector  $x_{r1,G}$  as the vector that will be mutated shown in Equation (4.2), one could also mutate the best individual vector (so the individual vector with the lowest value for the cost function that is not equal to the current ( $i$ ) vector being examined). In that case Equation (4.2) would change to Equation (4.4).

$$v_{i,G+1} = x_{best,G} + F \cdot (x_{r1,G} - x_{r2,G}) \quad (4.4)$$

The second change would be to use more difference vectors. In the case of Equations (4.2) and (4.4) only one difference vector is used. Should, for instance, two difference vectors be used then Equation (4.4) would change into Equation (4.5) [4]. This would however also affect the constraint for NP, which would in this case increase to a minimum of 6 (every added difference vector raises the minimum NP by 2).

$$v_{i,G+1} = x_{best,G} + F \cdot (x_{r1,G} + x_{r2,G} - x_{r3,G} - x_{r4,G}) \quad (4.5)$$

The final change would be in how the crossover is determined. Currently this is done using an independent binary (bin) experiment. The notation used to differentiate between the different options would be DE/rand/1/bin for the method described in Section 4.5.1, DE/best/1/bin if Equation (4.4) were to be used and if Equation (4.5) would be used, the notation would change to DE/best/2/bin, just to give a few examples.

Concerning the different control variables (NP, F and CR), a different optimiser could also be incorporated in order to optimise these parameters each time in order to gain the fastest result depending on the kind of problem. Storn and Price [4] do however provide a fair range and approximation of values for the control variables. As by Storn and Price: "F = 0.5 is usually a good initial choice. If the population converges prematurely, then F and/or NP should be increased. Values of F smaller than 0.4, like those greater than 1, are only occasionally effective. A good first choice for CR is 0.1, but since a large CR often speeds convergence, to first try CR = 0.9 or CR = 1.0 is appropriate in order to see if a quick solution is possible. For fastest convergence, it is best to pick the initial parameter range such that it covers the region of the suspected global optimum, although this choice doesn't seem to be mandatory." They also mention that a reasonable choice for NP is between 5 times D and 10 times D, however NP should always suffice to the minimum requirement as per number of difference vectors.

A more recent publication by A. Qing in 2009 [75] shows a decent overview of the different advances in the field of DE since 1997. In this book four different DE categories are described: classic, dynamic, modified and hybrid. Classic is the classic method described in Section 4.5.1 and slight modifications to it. As already mentioned it is important to deal with the fact that variables might need to stay within a certain parameter space. Qing describes two methods to deal with mutants that are not feasible: random reinitialization (where a new random variable is generated if the current variable is invalid) and bounce-back (where the value of the variable is brought back into the parameter space on either the lower bound or the upper bound depending on where it left the parameter space). It is also mentioned that should the optimum be known, the program can be terminated whenever the solution is found within a certain accuracy. The program could also be terminated if the population diversity is very small (smaller than a set limit). This means that almost all the individuals are the same and a solution might not be found. In [75] it is mentioned that Storn and Price recommend that NP = 10 times D, F = 0.8 and CR = 0.9. However, F = 0.5 and CR = 0.1 are also claimed to be a

good first choice, which is similar to the recommendations found in [4]. The book also states that it is claimed that convergence is more likely to occur but generally takes longer with larger populations and weaker mutation (smaller F). CR = 1 results in faster convergence if convergence occurs but CR = 0 is required to make DE robust enough for particular problems. Dynamic DE is similar to classic but is not based on generations. Dynamic DE has one population where the better children continuously replace the parents until a certain number of function evaluations has been reached. Also, the best individual is immediately updated every iteration round. Because it is all part of the new iteration, computations cannot be done in parallel any more. In modified DE one or several of the following core aspects of classic DE is modified: population initialization, differential mutation, crossover, objective and constraint function evaluation, and selection. An example of modified DE is provided in [74]. And finally hybrid DE involves combining DE with a deterministic and/or a stochastic optimiser [75]. Qing also shows different ways to determine the control parameters NP, F and CR. And different ways to perform a multi-objective DE, where one would like to optimise for different parameters at the same time.

It is clear that DE is flexible and can be adjusted to different kinds of problems, and what specifically to change depends on the user and the problem itself. It is the choice of the user to specify in what kind of configuration DE is to be used.

## 4.6. IMPLEMENTATION OF MONOTONIC BASIN HOPPING

Monotonic Basin Hopping is an optimisation method by Leary in 2000 [76] based on Basin Hopping first introduced by Wales and Doye in 1997 [77]. It depends on many local optimisations to eventually find a global optimum [51, 66, 78], which is why it can also be classified as a global optimiser (depending on the chosen definition). In 2008 Addis et al. [79] mentioned that MBH outperforms DE for given optimisation problems, which makes comparing these two methods for this particular thesis topic very interesting. In Section 4.6.1 the workings of MBH will be explained and any available variations on this method will be discussed in Section 4.6.2.

### 4.6.1. THE WORKINGS OF MBH

The basic form of MBH is probably best explained through the description provided in [78]. The method begins by setting a so called improvement counter to zero:  $N_{n,i} = 0$ . This counter is used to determine how many times a local optimisation does not result in a better solution than the existing best minimum. Then a set of randomly chosen variable values, from within the function space, is generated to use as an initial point/guess. This initial guess vector is called  $x$  and is used as the first input for a (by the user) chosen local optimiser. This local optimiser then tries to determine the local minimum point  $x^*$  (also called a "basin"), and if it finds a feasible solution, this local minimum is set as the current point and called  $x_{current}$ . If the local optimiser does not find a feasible solution, the program starts over again and chooses a new random point to serve as a new initial guess. This first step is visualized in Figure 4.3 for a one-dimensional case.

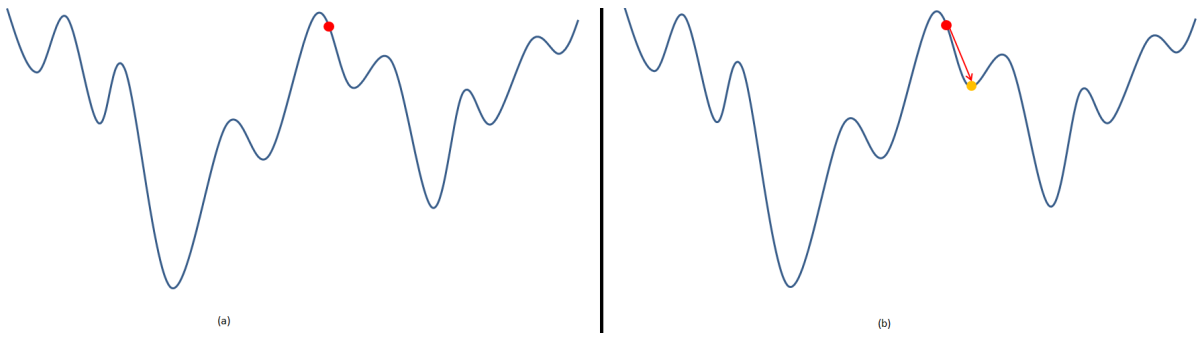


Figure 4.3: The first step of MBH where (a) first a random initial point  $x$  (red dot) is generated after which (b) the local minimum  $x^*$  (dark yellow point) is found through the use of a local optimiser. The local optimisation is visualized by a solid arrow.  $x^*$  becomes  $x_{current}$  if the local optimum is feasible.

The second step is to perturb (or mutate as it is called in genetic algorithms)  $x_{current}$  such that a new vector with variable values, called  $x'$ , is created. This perturbation is achieved by randomly choosing a deviation of the variable value through the use of a uniform probability distribution in  $[-\sigma, \sigma]$ , where  $\sigma$  is the standard

deviation. This process is visualized in Figure 4.4.

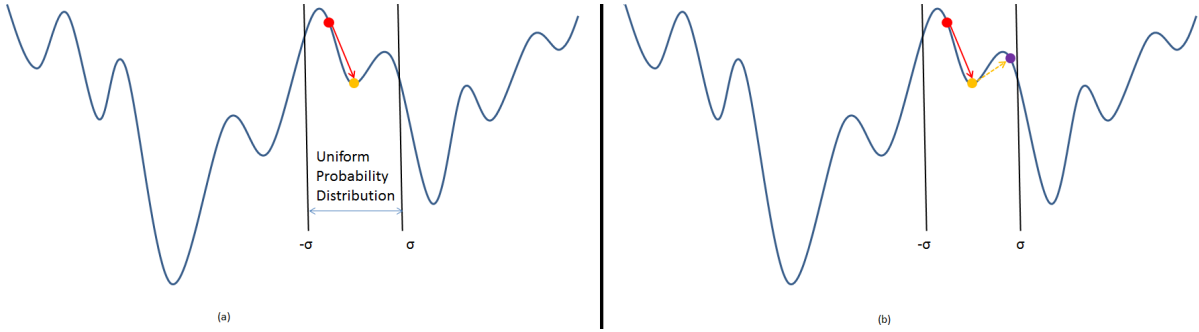


Figure 4.4: The second step of MBH where (a)  $x_{current}$  is perturbed within a uniform probability distribution creating (b) a new initial point  $x'$  (purple dot). The perturbation is visualized by a dashed arrow.

Using this new initial point, the local optimiser is run again. If this new  $x^*$  is feasible *and* better than the current minimum  $x_{current}$ , then  $x_{current}$  becomes  $x^*$  and the second and third steps are repeated. This can be seen in Figure 4.5. Also, at this point the  $N_{n,i}$  is set to zero again, because the minimum was improved.

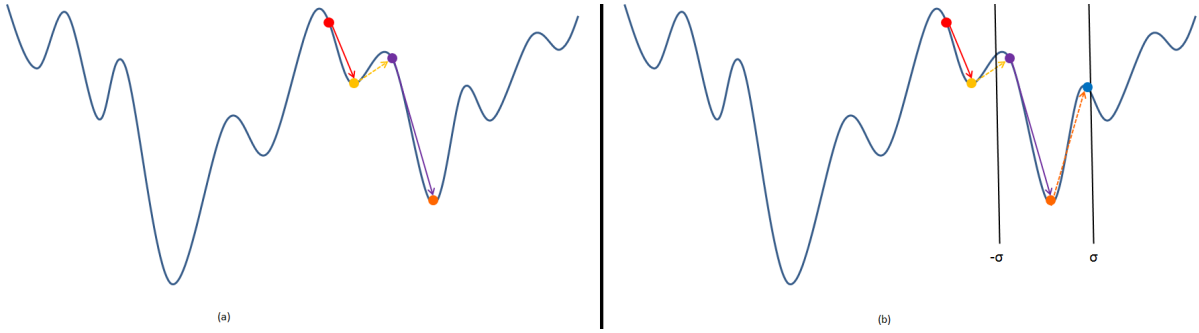


Figure 4.5: The third step of MBH where (a) the new local minimum  $x^*$  (orange dot) is compared to the current local minimum  $x_{current}$  and is set as  $x_{current}$  if it is better. Then (b) the second step repeats from the new  $x_{current}$  creating a new perturbed point  $x'$  (dark blue dot).

However, it could be possible that at a certain point the minimum does not improve, such as shown in Figure 4.6. In this case  $x_{current}$  is not updated and remains the same, and the loop starts again with the second step, thus perturbing the same minimum point as before. Also, for each consecutive moment that this occurs, a counter is put on  $N_{n,i}$ . It could be that the minimum value does not improve for a large number of iterations, which means that it is stuck at the best local minimum for that region. MBH works with the assumption that basins tend to be close together and thus finds a certain minimum within that set of basins (called a "funnel", which could be the right part of the function curve illustrated in Figure 4.6).

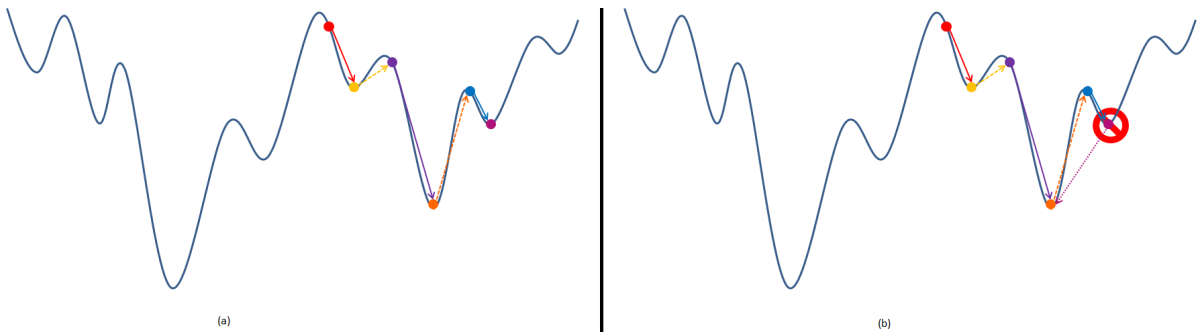


Figure 4.6: (a) A new local optimum is found (magenta dot), but (b) it is not better than the current optimum (orange dot), which is why it is disregarded visualized by the dotted arrow.

However, if the minimum point does not improve, it means that it is stuck in such a funnel. The search

space however likely contains a number of these funnels which all have their own best minimum and one of these funnels thus contains the global minimum, which is the minimum that the algorithm attempts to find. So in order to escape a certain funnel and try to find the next one a maximum on the number of not improved iterations is set called  $Max_{n,i}$ . Once this maximum is reached, **MBH** is set to start at the first step again while saving the best found local minimum for that particular funnel.

This process is repeated (see Figure 4.7, until either the maximum number of total iterations (step 1 to 3), or a maximum CPU time is reached. These two criteria are called the cut-off criteria.

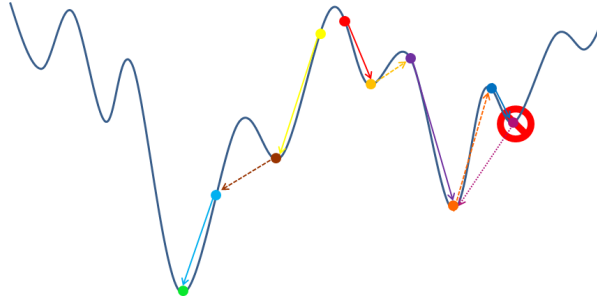


Figure 4.7: The process is repeated for another initial guess (yellow dot). In this case, the current funnel contains the global minimum, however the process is still repeated until one of the cut-off criteria has been met.

At the end of the **MBH** run, the best found local minimum is presented and should be the global minimum (unless the global minimum could not be reached before one of the cut-off criteria was met). One of the advantages of this method is, because **MBH** uses a local optimiser to determine the final values of the variables, the obtained global minimum will be very accurate and convergence to a minimum is guaranteed (whether it is the global minimum or not). An example pseudo-code for the described process is provided in [78]. It is thus important to choose a proper local optimiser for **MBH**. The choice of the local optimiser is further discussed in the next section, together with different methods to create variations on the **MBH** method.

#### 4.6.2. VARIATIONS OF THE MBH METHOD

There are several ways in which the **MBH** method can be changed. First the manner in which the values for point  $x$  are created can be bound to a certain parameter space for each of the variables. This could result in more feasible points and thus less iterations. Secondly the local optimiser can be chosen by the user themselves depending on the problem that needs to be solved, so different **MBH** methods with different local optimisers can exist. Many reference research that has been focussed on space trajectory problems use the Sparse Nonlinear Optimizer (**SNOPT**), such as [80–83]<sup>4</sup>. **SNOPT** was introduced in 2002 by Gill et al. [84] as a Sequential Quadratic Programming (see Sections 4.1 and 4.3) method. **SNOPT** requires the first function derivatives and is very effective with highly constrained problems such as trajectory optimisation. More information on the detailed workings of **SNOPT** can be found in [84, 85]. Musegaas [51] also mentioned that **SNOPT** should be very useful in future research given the fact that it is a powerful local optimiser. Based on all the reference research and provided that similar problems to the thesis topic have all used or recommended **SNOPT**, this local optimisation tool is chosen to be used in the **MBH** method. Finally, a different distribution from the original uniform probability distribution [83], used to perturb  $x_{current}$ , can be used to improve the efficiency and robustness of **MBH**. In [78] two different distributions called Cauchy<sup>5</sup> and bi-polar Pareto<sup>5</sup> were used in order to find a better performance of the **MBH** optimiser. In conclusion the paper recommends a bi-polar Pareto distribution, because it improved the performance most compared to the original distribution.

<sup>4</sup>The last reference is not a space problem application

<sup>5</sup>Also used in [81]

# 5

## INTEGRATORS

Integration can be used to model/predict the manner in which a function will progress (in time) usually given an initial condition. In orbital computations, integration is often used to model the stability of an orbit or predict where an object or spacecraft will be after a certain time or provided a certain disturbance. Because orbits and launch trajectories are multi-dimensional problems, the functions cannot be integrated analytically and therefore have to be approximated using numerical integration methods [86]. A short summary of available integration methods will be provided in Section 5.1. Determining a suitable integration method requires a trade-off between accuracy of the results and cpu time [6]. In Section 5.2 a comparison will be made between the different integration methods, which will provide an indication of the accuracy and time efficiency. In Chapter 2 it was already mentioned that Taylor Series integration (TSI) was chosen as the main integrator for the thesis problem. However, it should be compared to more commonly used integrators for space applications. Therefore, in Section 5.3 a selection is made of the most appropriate integrators based on the TU Delft heritage and external experience with problems similar to the subject provided in Chapter 2. This section shall also explain why TSI was initially chosen. Unfortunately, because the methods are numerical, and thus never result in an absolute accurate answer, there is always a sudden inaccuracy. This inaccuracy is represented by the truncation error. These truncation errors are usually the largest errors, however there can also be an additional error caused by the fact that computers round-off values up to a certain amount of decimal figures. The more computations are performed in sequence, the bigger this round-off error will become. There are also specific errors that are associated with the integration of a space related problem as described in [87]. If the simulated system is chaotic or if the step-size is too large, instability errors can occur. There can also be errors in the physical model used to simulate the system caused by mistakes in the assumptions made to create the physical model such as forces and disturbances that are not (properly) taken into account. Many methods exist to handle, or at least give an approximation of, these errors. These methods are then sometimes combined with existing integration methods to create new integration methods. This chapter will thus focus on the different integration methods and not the different methods of determining the different errors.

### 5.1. DIFFERENT INTEGRATORS

There are many different integration methods available. In this section the methods have been split into single-step (Section 5.1.1) and multi-step methods (Section 5.1.2) based on [6]. The methods can further be categorised by either using a fixed or a variable step-size and by being explicit or implicit. An explicit method only uses the information of the current  $\mathbf{x}_i$  (and sometimes past) point(s) to determine the next point value  $\mathbf{x}_{i+1}$ . An implicit method also uses the next point value to determine this same next point value, which requires iteration. Numerical integration to the next point can be defined by the current point plus the step-size  $h$  times the increment function  $\Phi$  as shown by Equation (5.1). The increment function changes depending on the used method. Here,  $\eta$  represents the numerical approximation.

$$\mathbf{x}(t_0 + h) \approx \mathbf{x}_0 + h\Phi = \eta(t_0 + h) \quad (5.1)$$

### 5.1.1. SINGLE-STEP

In single-step methods, only the information at the current (starting) point is taken into account and the information of previous points is neglected and not saved [6]. Some simple explicit, fixed step-size, single-step methods are Euler, Mid-point and **RK4** [86]. Euler uses the properties of the initial point to directly calculate the value at the next point. Mid-point already takes an extra point at half a step-size into account, and **RK4** takes the weighted average of four points (the starting point, two mid-points and a final point) into account. Many derivative methods exists based on these functions. A method based on the Mid-point method for instance is the high-order extrapolation (a.k.a. DIFEX2) (explicit) [88]. And some examples based on the original **RK4** integrator are Runge-Kutta-Nyström (a.k.a. DOPRIN) (implicit) [89], High-order Runge-Kutta-Nyström (**RKN12**) (implicit) [89] and **RKF45** [90, 91]. This last integrator is slightly different since it is still explicit, but uses a variable step-size.

### 5.1.2. MULTI-STEP

A multi-step method uses the information from the current point and the information of previous points, usually reaching as far back as the previous three points such as the Adams-Bashforth 4 (**AB4**) method [6]. This explicit method is similar to **RK4** where it uses a weighted average of four points, but in this case uses three previous points as well. A derivative of this method is the Adams-Bashforth 6 (**AB6**) (explicit) method. Another example of an implicit multi-step method is the Taylor Series integration (**TSI**) method, which uses a variable step-size and is based on Taylor Series expansion in order to compute the next set of variables [92]. An implicit, fixed step-size, multi-step method is the Adams-Moulton method which uses a polynomial to interpolate the function values [6]. Combining both these explicit and implicit methods creates what is called a Predictor-Corrector where the initial guess for the next point value follows from the explicit function and the implicit function is then used to correct or improve the estimate. Such methods are Low-order Predictor-Corrector (**ABM4**) and High-order Predictor-Corrector (**ABM12**) [6, 89]. These all use a fixed step-size, however there are also variable step-size methods based on these methods such as Shampine-Gordon (**SG**) (sometimes referred to as DE, not to be confused with Differential Evolution), which is an explicit method [93, 94] and Störmer-Cowell (**SC14**), which is again both implicit and explicit (based on Predictor-Corrector) [89, 93].

## 5.2. TECHNIQUE COMPARISON

A representation (based on [6]) of the mentioned methods is provided in Table 5.1 and can be used to compare the different methods. The sources for these advantages and disadvantages are the same as mentioned in Sections 5.1.1 and 5.1.2, and should an extra source be used, it will be mentioned separately. Also, please note that the comparison is sometimes based on astrodynamical problems specifically and are not necessarily true for other physical problems.

Table 5.1: Integration method comparison

Method	Type	Advantage	Disadvantage
Euler	Single-step, fixed step-size, explicit	simple, easy to implement	poor accuracy, better solution requires very small step-sizes, so an increase in cpu time
Mid-point	Single-step, fixed step-size, explicit	simple, easy to implement	not very accurate
<b>RK4</b>	Single-step, fixed step-size, explicit	simple, stable, and has small round-off error accumulation	step-size has to be determined through trial and error which requires more cpu time
DIFEX2	Single-step, fixed step-size, explicit	useful for numerically stable second order differential equations	not very accurate and not very fast
DOPRIN	Single-step, fixed step-size, implicit	includes local truncation error estimate [95], can be used for a wide range of accuracies [5]	not very accurate and not very fast
<b>RKN12</b>	Single-step, fixed step-size, implicit	high accuracy, efficient (fast)	high order (can be complex) and not the best method if the system is velocity dependent [5]

RKF45	Single-step, variable step-size, explicit	includes local truncation error estimate	poor accuracy and slow
AB4	Multi-step, fixed step-size, explicit	simple, stable, efficient if previous results are stored, faster than RK4 for identical step-size and has small round-off error accumulation	step-size has to be determined through trial and error which required more cpu time, and needs a different technique to determine the previous point values at the beginning
AB6	Multi-step, fixed step-size, explicit	very fast	very poor accuracy and instability at large step-sizes [5]
TSI	Multi-step, variable step-size, explicit	very fast and very accurate [92]	can be complex
Adams-Moulton	Multi-step, fixed step-size, implicit	accurate, stable, and has small round-off error accumulation	step-size has to be determined through trial and error which required more cpu time, and needs a different technique to determine the previous point values at the beginning
ABM4	Multi-step, fixed step-size, both implicit and explicit	very fast and includes local truncation error estimate	poor accuracy and not efficient if high accuracies are required
ABM12	Multi-step, fixed step-size, both implicit and explicit	fast, high accuracy and includes local error estimate	not efficient if low accuracies are required
SG	Multi-step, variable step-size, explicit	very accurate, high efficiency, includes local truncation error estimate and stable [5]	not very fast
SC14	Multi-step, variable step-size, both implicit and explicit	very accurate, fast and very stable [5]	can be complex

A graphic performance comparison, performed by [5], was made between (several of) these methods for single-step and multi-step (Figure 5.1). It should be mentioned though that the graphs show more methods than mentioned in this and the previous section, because more variations exist but it was chosen to discuss a selection of different methods only.

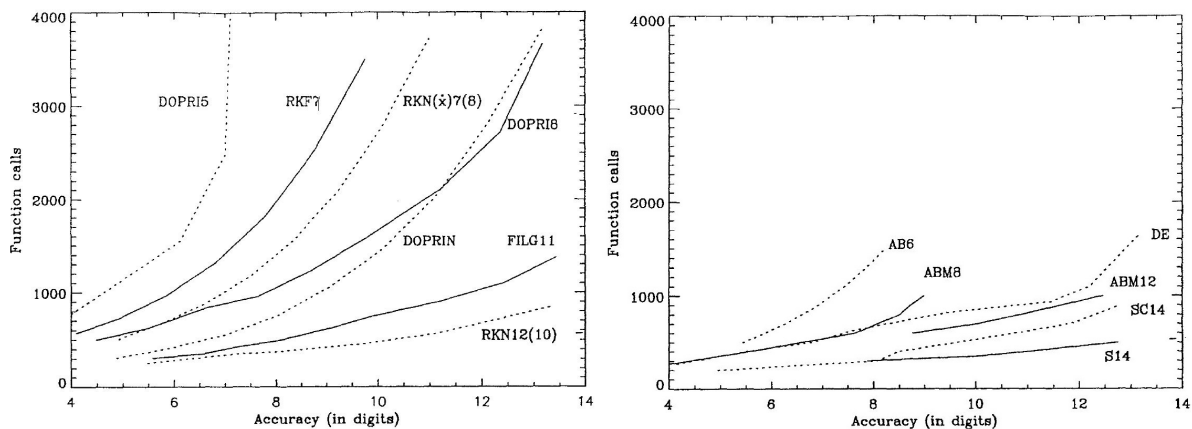


Figure 5.1: Comparison of single-step (left) and multi-step (right) methods for an eccentricity of 0.1 [5]

### 5.3. CHOSEN METHODS

For the integration method selection, it is beneficial to know which methods are used in industry and which methods have already been implemented within the space department at the TU Delft. Some of the references used in Sections 5.1 and 5.2 were already focussed on space missions but discussed a number of different methods. Section 5.3.1 elaborates on the implemented methods for space problems. The past TU Delft experience is discussed in Section 5.3.2 and finally the methods are chosen in Section 5.3.3.

#### 5.3.1. FREQUENTLY USED METHODS IN RELATED SPACE PROBLEMS

Table 5.2 provides an overview of reference research and the used integrators. Should a reference discuss different methods, then the method that the author deems most suited for a space related mission will be cited. However, in some cases several methods are mentioned, since the detailed scope of the subjects was not set yet. In those cases, the proper application of the methods will be provided as well.

Table 5.2: Previous integration methods used for trajectory and orbit (transfer) problems

Person	Year	Subject	Method
Quinn et al. [96]	1991	Orbit propagation	Störmer (so without Cowell implicit correction)
Montenbruck [5]	1992	Orbital motion (very low and very high elliptic orbits)	High-order Runge-Kutta-Nyström (if $EoM \neq f(V)$ ) else Shampine-Gordon
Van der Houwen et al. [97]	1998	High-precision orbit computations	Störmer-Cowell
González et al. [98]	2000	long-term satellite orbit prediction	high order RKN
Berry [93]	2004	Space surveillance	Störmer-Cowell
Scott and Martini [92]	2008	Orbital motion, planetocentric and heliocentric trajectories	Runge-Kutta-Fehlberg and Taylor Series integration

A completely different category of integrators is the symplectic integration methods. These are used in orbit mechanics when dealing with a pure Hamiltonian system [86] and in the case of very long term orbit integrations. However, since they deal with such a specific problem they are not considered useful for this thesis problem.

#### 5.3.2. TU DELFT INTEGRATION HERITAGE

Within the space department, integration work has been performed by Van Kints in 2005 [6] (with SC14 performing best with Cartesian coordinates), Gondelach in 2012 [99] (using RK4) and Hofsteenge in 2013 [86] (recommends DOPRI8, which is similar to DOPRIN). Although most methods used here are quite different, it is still important to understand which knowledge exists in the department. Research has also been performed on the TSI by Römgens et al. in 2011 [100].

#### 5.3.3. CHOSEN METHODS

As mentioned in Chapter 2 TSI was already considered for the main integration method. This was done on the advice of the TU Delft supervisors mainly because not much research has been done in the field of launch and space trajectories using this method. It is therefore very interesting to use this method in such an application and compare it to other methods. However, at this point the focus will be on the optimisation and therefore the use of TSI has become a secondary objective. This means that initially a simpler integration method will be used to model the trajectories and should time permit TSI will be implemented. In [92] TSI was compared to RKF45 because the used program (SNAP) had this last integration method already incorporated. For a s/c spiralling out of the Earth's gravity field, the cpu time required to integrate the problem with TSI was found to be at least 19 times less than the time required to perform the same integration using RKF45, which means that eventually it will be useful to try and use TSI for the thesis problem as well. However, by recommendation of the TU Delft supervisors, a simple initial integration method will suffice and can then later be compared to TSI should time allow. Therefore, it will be best to start with the simplest integration method, the work-horse of the integration methods: RK4. This is why this method will be discussed in more detail in Section 5.5.

## 5.4. IMPLEMENTATION OF TAYLOR SERIES INTEGRATION

Taylor Series integration has been used to solve ordinary differential equations since the early 1960s [92]. However, the first modern implementation of TSI in a space trajectory problem was provided by Montenbruck in 1992 [101, 102]. In 2008 Scott and Martini were able to implement this TSI method into the SNAP trajectory propagator [92] which is the implementation that will be used during this explanation. The method used is described in Section 5.4.1 and possible improvements on the method are mentioned in Section 5.4.2.

### 5.4.1. THE WORKINGS OF TSI

In [92] an example situation is used to describe the TSI method: the thrust-less motion around a central body. For consistency the same example and formulation will be used. The state vector is represented by  $\bar{X}$  with the corresponding vector for the initial conditions  $\bar{X}_0$ . Each of the variables can at any point be represented by  $x_n(t)$  and thus the Taylor series expansion for an order  $K \in \mathbb{R}$  (chosen by the user) can be written as shown by Equation (5.2) with  $n = 1, \dots, 7$  in this case (7 variables; three position, three velocity and one mass) and  $T_{n,K}$  is the truncation error for the  $n^{th}$  variable using  $K$  terms.

$$x_n(t) = \sum_{k=0}^K \frac{x_n^{(k)}(t_0)}{k!} (t - t_0)^k + T_{n,K} \quad (5.2)$$

This particular TSI method uses recurrence relations in order to determine the  $k^{th}$  order derivatives and only requires the first derivatives shown in Equation (5.3) for the 7 variables and two newly introduced variables to ease the use of recurrence relations. Here  $GM$  represents the standard gravitational parameter (also known as  $\mu$ ).

$$\begin{aligned} x'_1 &= x_4 \\ x'_2 &= x_5 \\ x'_3 &= x_6 \\ x'_4 &= -GM \frac{x_1}{(x_1^2 + x_2^2 + x_3^2)^{3/2}} = -GM \frac{x_1}{x_9} \quad \text{with } x_9 = x_8^{3/2} \quad \text{and } x_8 = x_1^2 + x_2^2 + x_3^2 \\ x'_5 &= -GM \frac{x_2}{(x_1^2 + x_2^2 + x_3^2)^{3/2}} = -GM \frac{x_2}{x_9} \quad \text{with } x_9 = x_8^{3/2} \quad \text{and } x_8 = x_1^2 + x_2^2 + x_3^2 \\ x'_6 &= -GM \frac{x_3}{(x_1^2 + x_2^2 + x_3^2)^{3/2}} = -GM \frac{x_3}{x_9} \quad \text{with } x_9 = x_8^{3/2} \quad \text{and } x_8 = x_1^2 + x_2^2 + x_3^2 \\ x'_7 &= 0 \\ x'_8 &= 2x_1x_4 + 2x_2x_5 + 2x_3x_6 \\ x'_9 &= \frac{3}{2} \frac{x_9x'_8}{x_8} \end{aligned} \quad (5.3)$$

The general recurrence relations for products ( $w(t) = f(t)g(t)$ ) and quotients ( $w(t) = \frac{f(t)}{g(t)}$ ) that are required are provided in Equation (5.4) respectively.

$$\begin{aligned} \text{For products } W(k) &= \sum_{j=0}^k F(j) G(k-j) \\ \text{For quotients } W(k) &= \frac{1}{g(t_0)} \left[ F(k) - \sum_{j=1}^k G(j) W(k-j) \right] \\ \text{Both with } W(k) &= \frac{w^{(k)}(t_0)}{k!}, \quad F(j) = \frac{f^{(j)}(t_0)}{j!} \quad \text{and} \quad G(k-j) = \frac{g^{(k-j)}(t_0)}{(k-j)!} \end{aligned} \quad (5.4)$$

Now let  $u_n^{(k-1)} = x_n^k$  for  $k = 1, \dots, K$ , then  $\frac{u_n^{(k-1)}}{(k-1)!} = \frac{x_n^k}{(k-1)!}$ , and also  $\frac{x_n^k}{k!} = X_n(k)$ . Combining this results in Equation (5.5).

$$U_n(k-1) = kX_n(k) \Rightarrow X_n(k) = \frac{U_n(k-1)}{k} \quad (5.5)$$

Then also introducing  $w_4 = \frac{x_1}{x_9}$ ,  $w_5 = \frac{x_2}{x_9}$ ,  $w_6 = \frac{x_3}{x_9}$ ,  $w_{8,1} = x_1x_4$ ,  $w_{8,2} = x_2x_5$ ,  $w_{8,3} = x_3x_6$  and  $w_9 = \frac{x_9u_8}{x_8}$ , the equations presented in Equation (5.3) can be rewritten to arrive at the recurrence relations using the given definitions. These relations are provided in Equation (5.6).

$$\begin{aligned} U_1(k) &= X_4(k) = \frac{U_4(k-1)}{k} & U_4(k) &= -GMW_4(k) & U_7(k) &= 0 \\ U_2(k) &= X_5(k) = \frac{U_5(k-1)}{k} & U_5(k) &= -GMW_5(k) & U_8(k) &= 2W_{8,1}(k) + 2W_{8,2}(k) + 2W_{8,3}(k) \\ U_3(k) &= X_6(k) = \frac{U_6(k-1)}{k} & U_6(k) &= -GMW_6(k) & U_9(k) &= \frac{3}{2}W_9(k) \end{aligned} \quad (5.6)$$

Where the expressions for  $W_4(k)$ ,  $W_5(k)$ ,  $W_6(k)$ ,  $W_{8,1}(k)$ ,  $W_{8,2}(k)$ ,  $W_{8,3}(k)$  and  $W_9(k)$  are shown in Equation (5.7).

$$\begin{aligned} W_4(k) &= \frac{1}{x_9} \left[ X_1(k) - \sum_{j=1}^k X_9(j) W_4(k-j) \right] = \frac{1}{x_9} \left[ \frac{U_1(k-1)}{k} - \sum_{j=1}^k \frac{U_9(j-1)}{k} W_4(k-j) \right] \\ W_5(k) &= \frac{1}{x_9} \left[ X_2(k) - \sum_{j=1}^k X_9(j) W_5(k-j) \right] = \frac{1}{x_9} \left[ \frac{U_2(k-1)}{k} - \sum_{j=1}^k \frac{U_9(j-1)}{k} W_5(k-j) \right] \\ W_6(k) &= \frac{1}{x_9} \left[ X_3(k) - \sum_{j=1}^k X_9(j) W_6(k-j) \right] = \frac{1}{x_9} \left[ \frac{U_3(k-1)}{k} - \sum_{j=1}^k \frac{U_9(j-1)}{k} W_6(k-j) \right] \\ W_{8,1}(k) &= \sum_{j=0}^k X_1(j) X_4(k-j) = x_1 \frac{U_4(k-1)}{k} + x_4 \frac{U_1(k-1)}{k} + \sum_{j=1}^{k-1} \frac{U_1(j-1)}{j} \frac{U_4(k-j-1)}{k-j} \\ W_{8,2}(k) &= \sum_{j=0}^k X_2(j) X_5(k-j) = x_2 \frac{U_5(k-1)}{k} + x_5 \frac{U_2(k-1)}{k} + \sum_{j=1}^{k-1} \frac{U_2(j-1)}{j} \frac{U_5(k-j-1)}{k-j} \\ W_{8,3}(k) &= \sum_{j=0}^k X_3(j) X_6(k-j) = x_3 \frac{U_6(k-1)}{k} + x_6 \frac{U_3(k-1)}{k} + \sum_{j=1}^{k-1} \frac{U_3(j-1)}{j} \frac{U_6(k-j-1)}{k-j} \\ W_9(k) &= \frac{1}{x_8} \left[ \sum_{j=0}^k X_9(j) U_8(k-j) - \sum_{j=1}^k X_8(j) W_9(k-j) \right] \\ &= \frac{1}{x_8} \left[ \sum_{j=0}^k \frac{U_9(j-1)}{j} U_8(k-j) - \sum_{j=1}^k \frac{U_8(j-1)}{j} W_9(k-j) \right] \end{aligned} \quad (5.7)$$

With the Taylor series coefficients now defined as provided in Equation (5.5), Equation (5.2) can be used to determine the parameter values at time  $t$  (or  $t_1$ ) for the known previous parameter values at time  $t_0$ . The same can then be done to determine the values at  $t_2$  using the parameter values at  $t_1$ , etc. In its simplest form, a constant step-size  $h$  ( $t - t_0$ ) is taken which determines the next  $t$ .

#### 5.4.2. VARIATIONS OF TSI METHOD

Many of the different aspects of TSI can be varied upon: The manner in which the truncation error is estimated, using a variational step-size and method of determining the next step size, and the order until which the series is evaluated  $K$ .

As mentioned before  $K$  can be chosen by the user, however in [92] it is mentioned that the maximum number of series terms cannot exceed 30 using this particular method.

When considering the variable step-size, [92] uses two different methods to determine the next step size. The first method is using Equation (5.8), where  $\eta$  is the chosen step multiplication factor and has to be smaller than 1,  $h$  is the current step-size,  $\tau$  is the chosen local error tolerance (or preferred accuracy),  $e_{max}$  is the

estimate of maximum truncation error and  $M$  is the order of the maximum truncation error estimate which follows from the maximum number of series terms.

$$h_{next} = \eta h \left( \frac{\tau}{e_{max}} \right)^{\frac{1}{M}} \quad (5.8)$$

In this case  $e_{max}$  is determined through Equation (5.9). Where the maximum estimated truncation error over all variables  $n$  is chosen.

$$e_{max} = \text{Max}_n [ |X_n(K-1)| h^{K-1} + |X_n(K)| h^K ] \quad (5.9)$$

Another method mentioned in the same paper is to directly use the local error tolerance  $\tau$  to determine the next step size. This method assures that the step-size is small enough that all variables satisfy the error condition directly. The step-size is determined using a so-called fixed-point iteration performed using Equation (5.10). The initial step-size  $h_1$  can be chosen to be the current step-size  $h$  as an easy estimate. Then the iteration is performed over  $l$  until a certain required convergence is reached.

$$h_{l+1} = \exp \left( \frac{1}{K-1} \ln \frac{\tau}{|X_n(K-1)| + h_l |X_n(K)|} \right) \quad (5.10)$$

Again this is done for all variables and the smallest required step-size is chosen. This is then used to determine the next step-size through  $h_{next} = \eta h_{chosen}$ . Scott and Martini preferred this second method over the first mentioned method of determining the next step-size because the first method requires previous step information ( $e_{max}$ ), nonetheless the performance of both methods was very similar [92].

Finally, there are several techniques to estimate the (local) truncation error that results from every series evaluation. Simply put  $e_{max}$  is the estimation of the maximum value that  $T_{n,K}$  can take. One example of how to determine this estimate was already shown by Equation (5.9). Another approach would be to calculate the estimate from the  $K+1$  term in the series, however, this is discouraged in [92] because it would require an extra computation and is not a reliable error estimate.

## 5.5. IMPLEMENTATION OF RK4

As mentioned, RK4 is known as the work-horse of engineering problems when it comes to the integration of functions. It is a slightly more complicated form of the Euler and Mid-point methods. In this case four points/state vectors are used to determine the next parameter value(s). The exact workings of RK4 will be explained in Section 5.5.1 and other variations are discussed in Section 5.5.2.

### 5.5.1. THE WORKINGS OF RK4

Runge-Kutta 4 (RK4) is based on the formulation provided by Equation (5.1) where in this case the increment function for RK4 is presented in Equation (5.11). The principle behind RK4 is well described by [6]. This method is a single-step, fixed step-size, explicit method and thus does not use any previous step information to determine the next step. Only the current parameter values are used to predict the next step as is visualised in Figure 5.2. In this figure it can also be seen that this method uses four derivative evaluations of the function to determine the next point indicated as  $x(t_0 + h)$ .

$$\Phi_{RK4} = \frac{1}{6} (k_1 + 2k_2 + 2k_3 + k_4) \quad (5.11)$$

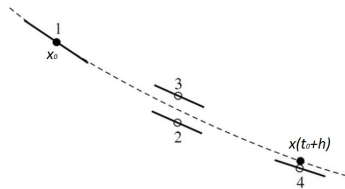


Figure 5.2: Principle of RK4 for a single parameter [6]

First the time-derivative of the current point/state vector is taken and called  $k_1$  as shown by Equation (5.12) (including the whole sequence). This is used to evaluate the local state vector halfway through the interval at

$h/2$  from the current time and for a parameter value of  $x_0 + h \frac{k_1}{2}$  and is called  $k_2$ . This  $k_2$  is then used instead of  $k_1$  to perform the same evaluation as before, resulting in  $k_3$ . Finally,  $k_3$  is used to evaluate the local state vector at the end of the interval resulting in  $k_4$ . These four derivative values are then added in a weighted fashion to produce the increment function as shown by Equation (5.11), which is in turn used to determine the next point/state vector (see Equation (5.1)).

$$\begin{aligned} k_1 &= f'(t_0, x_0) \\ k_2 &= f'(t_0 + h/2, x_0 + hk_1/2) \\ k_3 &= f'(t_0 + h/2, x_0 + hk_2/2) \\ k_4 &= f'(t_0 + h, x_0 + hk_3) \end{aligned} \quad (5.12)$$

In Equation (5.12)  $f'$  depicts the evaluation of the derivative. It is also mentioned in [6] that performing this integration will result in a local truncation error that is  $\leq O(h^5)$ . Therefore, Equation (5.1) can be adapted to include the truncation error as depicted by Equation (5.13).

$$\mathbf{x}(t_0 + h) = \mathbf{x}_0 + h\Phi + \mathbf{T} \quad (5.13)$$

### 5.5.2. METHODS BASED ON RK4

The **RK4** method is often seen as the classic method and has thus been expanded and varied upon substantially (also see Section 5.1.1). There are three direct means in which to modify the method: the order (so number of intermediate points used to evaluate the final point), including the next estimation in order to improve the next parameter values (making it implicit) and the manner in which the step-size is chosen, which can even be done such that the method changes to a variable step-size method. Examples of implicit methods based on **RK4** are **DOPRIN** and **RKN12**, and an example of a method which is based on **RK4** but uses a variable step-size is **RKF45**. The **RKF45** uses an estimate of the truncation error to determine the next step-size [90], similar to a variation of **TSI**. This is accomplished by computing a fourth and fifth order Runge-Kutta and then using the difference between those two as an estimate for the truncation error.

# 6

## ATMOSPHERIC (MARTIAN) LAUNCH

As mentioned in Section 3.1 no Marian launches have occurred to date, however there have been numerous Earth launches. Also, similar research has already been performed using different simulation programs as was discussed in Section 3.1. Section 6.1 will elaborate on this research. For the launch in the Martian atmosphere, a similar model to the one used for Earth launches can be implemented provided it is adapted for the Martian atmosphere. The model and the assumptions including the resulting EoM are provided in Section 6.2. The launch trajectory itself can consist of different phases with their own characteristics. The preferred launch trajectory for the desired final conditions is described in Section 6.3 and finally Section 6.4 discusses the initial conditions of the launch site on the Martian surface based on the landing sites currently under consideration for the Mars 2020 rover.

### 6.1. PREVIOUS RESEARCH

In Section 3.1 the different successful Lunar sample return missions were provided. The flight data of these missions (readily available for all Apollo missions in the Apollo mission reports) can be used for initial validation of the dynamic model and the EoM. The reference Lunar research can also be used for initial validation. Other validation will have to be performed using the reference Mars ascent research mentioned in Section 3.1.1. The most important characteristics that could be used for the validation are mentioned in Table 6.1 for each of the different papers. Unfortunately, Dumont [21] has not yet performed any Marian ascent simulations which is why it cannot be used for validation at this time. Should information not be available at the moment, the cell will read Not Available (N/A). For Fanning and Pierson the thrust values originate from a second source<sup>1 2</sup>.

Table 6.1: Reference characteristics from Mars Ascent research

Characteristic	Fanning and Pierson [8]	Desai et al. [18]	Whitehead [9, 19]	Di Sotto et al. [20]	Trinidad et al. [3]
GLOM [kg]	1400	426	100	919.2	227
Payload mass [kg]	367.8	30	Max. 20	4	5
Target orbit [km]	473 (circular)	300 (circular)	500 (circular)	300 by 2000	460 by 580
Propulsion type	Liquids	Liquids	Liquid(s)	Liquids	Liquids
No. of stages	2	2	1 or 2	2	2
Thrust per engine [N] first/second stage	16700 <sup>1</sup> / 4000 <sup>2</sup>	3559 (Max. vacuum)(2x)/222 (Max. vacuum)(4x)	1000	1503 (vacuum)(4x)/1687 (vacuum)	5300 (plus 4x 445 TVC)/2700 (plus 4x 445 TVC plus 8x 4.4 ACS)

<sup>1</sup> First stage engine thrust: <http://www.astronautix.com/engines/xlr132.htm>

<sup>2</sup> Second stage engine thrust: <http://www.astronautix.com/engines/r40b.htm>

$I_{sp}$ per engine [s]	338/309	323 (vacuum)/308 (vacuum)	310	306/306	328.6 (330.5 vacuum)/328.6 (330.5 vacuum)
Point-mass?	Yes	No	No	N/A assumed yes	N/A assumed no
Initial vertical rise? (Time [s])	Yes (3±2)	N/A	Yes (N/A)	Yes (2.3)	Yes (in 90° case 2.15 incl. 1.5 coast)
Launch latitude [ $^{\circ}$ ]	0	between 30 N and 15 S	N/A assumed 0	N/A	N/A assumed 0
Launch azimuth [ $^{\circ}$ ]	90	N/A	N/A assumed 90	N/A	90 (?)
Target inclination [ $^{\circ}$ ]	N/A assumed 0	30	N/A assumed 0	45	N/A assumed 0
Drag coefficient	0.88	0.7 (at Mach 0.8), 1.38 (> Mach 3.0)	0.2 (Max. 0.6 and 0.3 > Mach 4)	N/A	N/A

## 6.2. DYNAMIC MODEL AND EQUATIONS OF MOTION

There are many different approaches to the ascent problem of the MAV. Therefore it is important to choose the proper dynamic model to simulate the ascent and formulate the corresponding EoM. The model and initial assumptions are discussed in Section 6.2.1, and the EoM are described in Section 6.2.2.

### 6.2.1. DYNAMIC MODEL AND INITIAL ASSUMPTIONS

When performing trajectory calculations it is important to understand in which RF the parameters are defined and computed and which set of state variables (or coordinate system) is used. The different reference frames and coordinate systems will be discussed in more detail in Chapter 8. During the ascent phase of a rocket there are two coordinate systems that can be used, either the Cartesian coordinate system [103] (Earth) or the spherical coordinate system [8, 104, 105] (Mars and Earth). An advantage of the Cartesian system is that there are no singularities when using the position:  $x, y, z$  and velocity:  $V_x (\dot{x}), V_y (\dot{y}), V_z (\dot{z})$  which makes it easier to use during the integration and optimisation. A disadvantage is that Cartesian coordinates do not provide a proper insight into the behaviour of the MAV during ascent. If spherical coordinates are used however, the trajectory of the ascent is better visualized and it is easier to identify any changes that have to be made to the trajectory. The spherical coordinate system is presented in Figure 6.1. Here the position is represented by the distance  $r$ , the longitude  $\tau$  and the latitude  $\delta$ . The velocity is defined by the ground speed  $V$ , the flight-path angle  $\gamma$  and the heading angle  $\chi$ . The problem with using spherical coordinates however, is that singularities occur whenever  $\gamma$  and/or  $\delta = \pm 90^{\circ}$  and/or  $V=0$  m/s. This means that during the optimisation not every scenario can accounted for which limits the simulation.

Even though there are several solutions to handle the singularities, none of them provide absolute optimisation freedom. This is why it was decided to use the Cartesian coordinate system for the EoM.

The results of each iteration (the position and velocity) can easily be transformed to spherical coordinates (see Chapter 8) to gain insight into the trajectory. When formulating the EoM the definition of the different forces acting on the MAV are required (the EoM will then be formulated using the Cartesian coordinates). A two-dimensional representation of the forces acting on the MAV is provided in Figure 6.1. In this case it will be assumed that there is no wind acting on the MAV. This can be done because the atmosphere is very thin and because a simplified model will make it easier for the optimiser to converge, since convergence will be less and less likely if there are increasingly more optimisation parameters.

In the model presented in Figure 6.1  $\epsilon$  (from now on  $\epsilon_T$ ) is the thrust elevation gimbal angle and the lift  $L$ , drag  $D$  and thrust  $T$  are defined by Equation (6.1) [106].

To simulate out of plane motion and thus making it a three-dimensional model, a second thrust gimbal angle is introduced. This angle is defined in the x-y plane of the body frame, or B-frame, where it should be noted that the positive x-axis is defined through the vehicle centreline in the direction of flight, the z-axis is

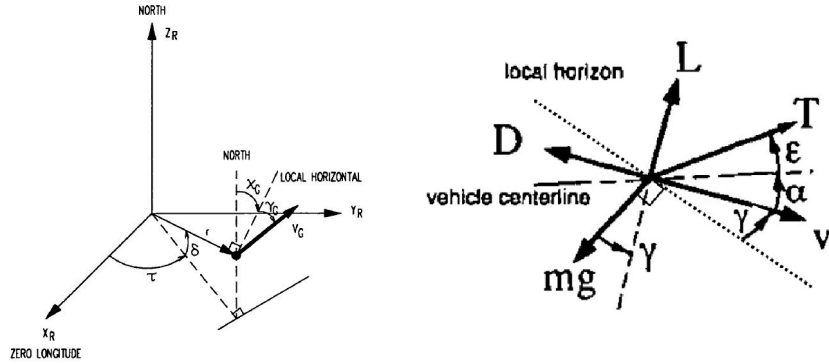


Figure 6.1: (Left) Graphical definition of the spherical coordinate system. The angles are all defined positive in the direction of the arrow [7] (Right) Graphical definition of the force model [8]

defined pointing down in Figure 6.1 perpendicular to the vehicle centreline and the y-axis is then pointing out of the x-z plane by the convention of the Right-hand-rule (R.H.R.). This second gimbal angle is called the thrust azimuth gimbal angle  $\psi_T$  as by [7].

In the equations for  $L$ ,  $D$  and  $T$ ,  $\rho$  is the air density,  $S$  is the reference surface area,  $C_L$  the lift coefficient,  $C_D$  the drag coefficient,  $\dot{m}$  the mass flow rate ( $= \frac{dm}{dt}$ ),  $g_0$  the gravitational acceleration at Earth sea-level (not Mars),  $c_{eff}$  the effective expulsion velocity,  $c$  the expulsion velocity,  $A_e$  the exit surface area of the nozzle,  $p_e$  the exit pressure and  $p_0$  the pressure of the surrounding air.

$$\begin{aligned} L &= \frac{1}{2} \rho V^2 S C_L \\ D &= \frac{1}{2} \rho V^2 S C_D \\ T &= \dot{m} g_0 Isp = \dot{m} c_{eff} = \dot{m} c + A_e (p_e - p_0) \end{aligned} \quad (6.1)$$

All the provided equations depend on the altitude  $h$ :  $\rho = f(h)$  and  $p_0 = f(h)$ . Also, both coefficients are a function of the Mach number  $\mathcal{M}$  and the angle of attack  $\alpha$ . In this thesis problem, it is assumed that the angle of attack is constant (also see Section 6.2.2). This means that the drag coefficient is only a function of the Mach number. If a simple "pencil" shape is assumed, which is a reasonable assumption when looking at the baseline model in Figure 3.3, then [9] provides an estimation of the drag coefficient for different Mach numbers as can be seen in Figure 6.2.

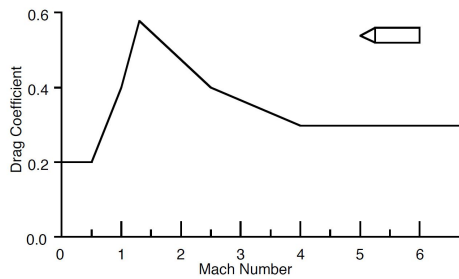


Figure 6.2: Drag coefficient as a function of Mach number [9]

This drag coefficient plot can be used to determine the drag at different velocities (since  $\mathcal{M} = f(V, \mathcal{A})$  where  $\mathcal{A}$  is the speed of sound in the Martian atmosphere at that particular point which can be obtained through the atmospheric model that will be chosen). Thus given a certain atmospheric model, the air density and pressure at different altitudes, and the Mach number can be computed. The atmospheric model will be selected and discussed in Chapter 9.

The gravity force  $mg$  depends on the local gravitational acceleration  $g$ . This  $g$  can be determined assuming a homogeneous gravity field and a spherical Mars using Equation (6.2) where  $g_{M0}$  is the standard

gravitational acceleration on the surface of Mars ( $3.71 \text{ m/s}^2$ ) [107],  $R_M$  is the (local) radius of Mars,  $G$  the gravitational constant,  $M_M$  the mass of Mars,  $\mu_M$  the standard gravitational parameter of Mars and  $r$  the position radius of the vehicle.

$$g = g_{M0} \left( \frac{R_M}{r} \right) = \frac{GM_M}{r^2} \frac{\mu_M}{r^2} \quad (6.2)$$

This equation can then be used to determine the gravitational acceleration at any distance from Mars. It is assumed that the mass of the MAV, the orbiter(s) and the two Martian moons can be neglected with respect to the mass of Mars (the mass of Phobos is an order of 7 smaller than the mass of Mars) [107]. Also, during the ascent the gravitational perturbations  $J$  can be neglected because the time spent in ascent is relatively short.

### 6.2.2. CORRESPONDING EoM AND INITIAL ASSUMPTIONS

The general equations of motion can be derived using the described model, and are based on [7]. Because the motion of the Mars 2022 orbiter will be described in an Inertial Mars frame it was decided to write the EoM for the MAV ascent in the same frame. The current conditions can be described as shown by Equation (6.3), where  $m_{MAV}$  is the mass of the MAV and the subscript  $I$  refers to the inertial frame.

$$\mathbf{r} = \begin{pmatrix} x_I \\ y_I \\ z_I \end{pmatrix} \quad \mathbf{V} = \begin{pmatrix} V_{x_I} \\ V_{y_I} \\ V_{z_I} \end{pmatrix} \quad m_{MAV} \quad (6.3)$$

The EoM can now be described by Equation (6.4). Here,  $a$  represents the acceleration.

$$\begin{aligned} \dot{x}_I &= V_{x_I} & \ddot{x}_I &= \dot{V}_{x_I} = a_{x_I} \\ \dot{y}_I &= V_{y_I} & \ddot{y}_I &= \dot{V}_{y_I} = a_{y_I} \\ \dot{z}_I &= V_{z_I} & \ddot{z}_I &= \dot{V}_{z_I} = a_{z_I} \end{aligned} \quad \dot{m}_{MAV} = -\frac{T}{g_0 Isp} \quad (6.4)$$

The accelerations follow from Newton's  $F = m \cdot a$  and can thus be described as a function of the mass and the different forces and accelerations acting on the MAV. These are all described in different reference frames unfortunately, which means that the forces acting on the MAV will have to be translated into the Inertial Mars frame. This is done through reference frame transformations (which will be discussed in detail in Chapter 8). A transformation is always performed by rotating around the different axes in a particular order which requires the different rotational angles. Each rotation around a certain axis has a corresponding transformation matrix, for instance  $T_x(\phi)$  where  $T$  is the symbol for a transformation matrix, the subscript  $x$  shows that it is a rotation around the x-axis and the  $\phi$  is in this case the angle of rotation. This particular rotation is a positive rotation around the x-axis (following the R.H.R. and the angle is positive). Should the rotation be negative then the transformation matrix would have been presented as  $T_x(-\phi)$ . First it is important to define the reference frames in which the different forces are acting. In this case the thrust is acting in a propulsion frame or P-frame (with the corresponding gimbal angles as rotation angles), the drag is acting in the aerodynamic frame or A-frame and the gravity is acting in the Mars rotational frame or R-frame. Before describing the relation between the different frames, a number of assumptions are made.

- No wind; It is assumed that there is no wind and thus no corresponding effects or changes in the MAV attitude to simplify the simulation [7].
- No side-slip; Because there is no wind, there will be no side-slip [7].
- No lift; It can be assumed that there is no lift, based on the thin atmosphere [8]
- No angle of attack; Because there is no lift, the angle of attack can be assumed to be zero [7].
- No bank angle; Because the system is a point mass system and there is no lift and no wind, the assumption of an absence of a bank angle is valid [105]

From these assumptions it is clear that the A-frame is in this case identical to the body frame or B-frame. Therefore the body is always pointing into the same direction as the velocity vector. This provides another set of angles to transform to the inertial frame as can be seen in Figure 6.1. These angles are the flight-path angle

$\gamma$  and the azimuth (or heading angle)  $\chi$ . The subscript  $G$  shows that this frame is set-up for the flight-path angle, azimuth and velocity based on the ground-speed as suppose to airspeed, but since there is no wind this is irrelevant in this case. Rotating over these angles would result in transforming to the vertical frame or V-frame. In the vertical frame the x-axis points towards the northern hemisphere, the z-axis points towards the centre of mass of the orbiting body and the y-axis points towards the east [7]. Figure 6.1 then also shows the rotation angles required to transform from the V-frame to the R-frame. These angles are the latitude  $\delta$  and the longitude  $\tau$  in a rotating frame. The final transformation involves the rotation from the R-frame to the I-frame. This rotation depends on the location of the prime meridian (the meridian of zero longitude) at the time that the inertial reference frame was set  $\Omega_P$ , the rotational velocity of Mars  $\dot{\Omega}_M$  and the time between when the inertial frame was set and the current time  $t_O$ . The rotational angle between the R-frame and the I-frame can then be defined to be  $\dot{\Omega}_M t_O - \Omega_P$  (where the motion and angles are defined towards the east).

Now including all the forces, accelerations and rotations and using the notation for transformation matrices as defined earlier, the expressions for the accelerations in the I-frame can be described by Equation (6.5). In this notation, each vertical line depicts the point a new reference frame is reached and the letter shows which one. Also, because the transformations require matrix multiplications, the transformation should be read from right to left.

$$\begin{pmatrix} a_{x_I} \\ a_{y_I} \\ a_{z_I} \end{pmatrix} = \left|_{\mathbf{I}} \mathbb{T}_{\mathbf{z}}(-\dot{\Omega}_M t_O + \Omega_P) \right|_{\mathbf{R}} \begin{pmatrix} -\mu_M \frac{x_R}{r^3} \\ -\mu_M \frac{y_R}{r^3} \\ -\mu_M \frac{z_R}{r^3} \end{pmatrix} + \left|_{\mathbf{R}} \mathbb{T}_{\mathbf{z}}(-\tau) \mathbb{T}_{\mathbf{y}}\left(\frac{\pi}{2} + \delta\right) \right|_{\mathbf{V}} \mathbb{T}_{\mathbf{z}}(-\chi) \mathbb{T}_{\mathbf{y}}(-\gamma) \left|_{\mathbf{B}} \right\{ \begin{pmatrix} -\frac{D}{m_{MAV}} \\ 0 \\ 0 \end{pmatrix} + \dots \right. \\ \left. \dots + \left|_{\mathbf{B}} \mathbb{T}_{\mathbf{z}}(-\psi_T) \mathbb{T}_{\mathbf{y}}(-\epsilon_T) \right|_{\mathbf{P}} \begin{pmatrix} \frac{T}{m_{MAV}} \\ 0 \\ 0 \end{pmatrix} \right\} \quad (6.5)$$

The corresponding transformation matrices will be written out in Chapter 8. Also, the position and velocity will change each time step, which means that the angles  $\tau$ ,  $\delta$ ,  $\chi$  and  $\gamma$  will also change. These angles can all be described in the R-frame. Thus in order to determine the updated values, the position and velocity will have to be transformed from the I-frame to the R-frame. Then using the transformation between Cartesian and spherical coordinates, the angles can be obtained. This transformation is also described in Chapter 8. Following from the haversine formula based on great circles, the change in the ground distance travelled  $S_G$  (in the R-frame) can be computed as a function of the longitude and latitude as shown by Equation (6.6).

$$S_G = 2R_M \arcsin \left( \sqrt{\sin^2\left(\frac{\dot{\delta}}{2}\right) + \frac{1}{2} (\cos(\dot{\delta}) + \cos(2\delta + \dot{\delta})) \sin^2\left(\frac{\dot{\tau}}{2}\right)} \right) \quad (6.6)$$

### 6.3. REQUIRED LAUNCH TRAJECTORY

When examining the different possible launch trajectories, one mainly looks at different ways to control the ascent vehicle in such a manner that reduces losses. Four different possible launch trajectories (usually followed by each other) are a vertical rise phase, a constant pitch-rate phase, a constant pitch phase and a gravity turn phase. Also, sometimes a control program for the pitch/pitch-rate is followed instead of a constant pitch/pitch-rate. The pitch angle is defined as  $\alpha + \gamma$ , however since there is no angle of attack in this case, the pitch angle is equal to the flight-path angle  $\gamma$  (in the R-frame and V-frame). The ascent is then followed by a coasting phase and a final burn phase to place the s/c into a desired orbit [8, 20, 103, 106]. In this case however, since it is assumed that the engines can be gimballed ( $\psi_T$  and  $\epsilon_T$ ) the phase between the vertical rise and the gravity turn can be optimised and thus not need a constant pitch-rate and constant pitch phase. This transition phase shall be known as the first thruster control phase. During the gravity turn, the stage-separation will take place. Then the second stage ignites and will continue the gravity turn. At some point in the second stage burn, it could be more beneficial to change the flight program to a second thruster control phase. This is to avoid an early zero flight-path angle and to position the MAV such that a certain apocentre can be reached. After the second stage is burned-out, the coasting phase will start. At the end of this coasting

phase (at apocentre of the ascent) a final burn is provided to propel the MAV into the desired final orbit. It should however be noted that a vertical rise might not be optimal, which is why the set of equations mentioned in Equation (6.5) allow for an initial heading ( $\chi$ ) and launch angle ( $\gamma$ ) to be defined at the beginning of the simulation. The different ascent phases will be discussed in this section.

### 6.3.1. VERTICAL RISE

The vertical rise phase can be used to penetrate the thickest layers of the atmosphere before performing the gravity turn [8, 106]. This will reduce the effect of drag significantly but will increase the gravity losses. During the vertical ascent the flight-path angle is equal to  $90^\circ$  (or  $\frac{\pi}{2}$ ). The heading angle during this phase is undefined, which means that the orientation of the MAV is not defined at this stage. Also, during the vertical ascent both gimbal angles are set equal to zero. Therefore the flight-path angle and heading angle do not change during the vertical ascent and since the value of the heading angle is not important, it can be set equal to zero. As soon as the first thruster control phase starts, the heading angle will be defined automatically as a result of the gimbal angles, and the flight-path angle will change as well. With these trajectory characteristics the expressions in Equation (6.5) can be rewritten for the vertical phase (see Equation (6.7)). It is worth mentioning that the first two rotations are now both around the y-axis, which means that they can be performed at once (resulting in a positive rotation  $\delta$ ) however, for clarity it is written such that the V-frame is included.

$$\begin{pmatrix} a_{x_I} \\ a_{y_I} \\ a_{z_I} \end{pmatrix} = \left| \mathbb{T}_z(-\dot{\Omega}_M t_O + \Omega_P) \right|_{\mathbf{R}} \begin{pmatrix} -\mu_M \frac{x_R}{r^3} \\ -\mu_M \frac{y_R}{r^3} \\ -\mu_M \frac{z_R}{r^3} \end{pmatrix} + \left| \mathbb{T}_z(-\tau) \mathbb{T}_y\left(\frac{\pi}{2} + \delta\right) \right|_{\mathbb{V}} \mathbb{T}_y\left(-\frac{\pi}{2}\right) \left| \begin{pmatrix} T - D \\ m_{MAV} \\ 0 \\ 0 \end{pmatrix} \right|_{\mathbf{B}}$$
(6.7)

For the optimisation of this phase the only control variable can be the vertical ascent time  $t_v$  (if not pre-set).

### 6.3.2. FIRST THRUSTER CONTROL PHASE

To transition from the vertical phase to the gravity turn, a change in the heading and flight-path angle is required. These changes can be set in motion by gimbaling the thruster, or in other words by providing a thrust elevation ( $e_{T1}$ , where the subscript 1 refers to the first thruster control phase) and/or thrust azimuth angle ( $\psi_{T1}$ ). These two angles are both optimisation parameters. In this case, it is necessary to use the complete set of equations for the accelerations (see Equation (6.5)). A third optimisation parameter for the first thruster control phase is the time spend in this phase  $t_{T1}$ . During this phase a reduced thrust could be required. This would then introduce another optimisation parameter: the thrust level during the first thruster control phase  $T_{T1}$ . At the end of this phase, the thrust level is again set to full thrust (if it was changed) and both  $e_{T1}$  and  $\psi_{T1}$  are again set to zero which will be the start of the gravity turn phase.

The current baseline design does not assume an engine that can be gimballed (see Section 3.4) but uses control thrusters instead. However, for this thesis it can be assumed that in the future either gimballing will be introduced on the MAV or the trajectory adjustments will indeed have to be made by control thrusters instead.

### 6.3.3. GRAVITY TURN AND SECOND THRUSTER CONTROL PHASE

After the vertical rise and the first thruster control phase, a so-called gravity turn is initiated. The gravity turn results in a rotation of the MAV into a (near) horizontal flight orientation which reduces the gravity losses and is usually initiated after passing through the thickest layers of the atmosphere in order to reduce drag. Because at the beginning of this phase the flight-path angle is  $0 < \gamma < \frac{\pi}{2}$  (in the R-frame), the gravity force will cause a change in this flight-path angle. This will cause the MAV to turn towards a lower flight-path angle automatically without the use of the gimbal feature. Therefore, during this manoeuvre, the gimbal angles are both zero, which means that the thrust is again acting directly in the B-frame simplifying the acceleration equation. However, in this case there is a flight-path angle and there is also a heading angle. The resulting acceleration equation can be represented by Equation (6.8).

$$\begin{pmatrix} a_{x_I} \\ a_{y_I} \\ a_{z_I} \end{pmatrix} = \left| \mathbf{I} \right| \mathbb{T}_z(-\dot{\Omega}_M t_O + \Omega_P) \left| \mathbf{R} \right| \begin{pmatrix} -\mu_M \frac{x_R}{r^3} \\ -\mu_M \frac{y_R}{r^3} \\ -\mu_M \frac{z_R}{r^3} \end{pmatrix} + \left| \mathbf{R} \right| \mathbb{T}_z(-\tau) \mathbb{T}_y\left(\frac{\pi}{2} + \delta\right) \left| \mathbf{V} \right| \mathbb{T}_z(-\chi) \mathbb{T}_y(-\gamma) \left| \mathbf{B} \right| \begin{pmatrix} \frac{T-D}{m_{MAV}} \\ 0 \\ 0 \end{pmatrix} \quad (6.8)$$

At the start of the gravity turn, there is also a certain heading angle. This heading angle (in the I-frame) will determine the final inclination of the orbit together with the MAV latitude at the start of the gravity turn. The relation for the inclination is shown by Equation (6.9). During the gravity turn (and the rest of the ascent phase) both the heading angle and latitude will change, however the eventual inclination which the MAV will reach will stay the same (assuming  $\psi_{T2} = 0$  during the second thruster control phase). If at the beginning of the gravity turn, the desired inclination has not been reached, it means that the first two phases were not ideal and will have to be changed. Also, in this case the inclination is an optimisation parameter since different orbital inclinations will have to be investigated combined with the Mars 2022 orbiter trajectory.

$$\chi_0 = \arcsin\left(\frac{\cos(i)}{\cos(\delta_0)}\right) \quad (6.9)$$

During the gravity turn phase, the first stage will burn out, be ejected (simulated by an instant reduction in mass; the empty mass of stage 1) and the second stage will be ignited and will burn until its burn-out. The first stage will completely follow the gravity turn, however as mentioned before, the second stage could be set to follow a second thruster control program. Because there is no need to change the inclination (which was already set by the first thruster control phase) this second thruster control phase will only use the elevation gimbal angle  $\epsilon_{T2}$  to change the MAV attitude, resulting in the acceleration equation given by Equation (6.10).

$$\begin{pmatrix} a_{x_I} \\ a_{y_I} \\ a_{z_I} \end{pmatrix} = \left| \mathbf{I} \right| \mathbb{T}_z(-\dot{\Omega}_M t_O + \Omega_P) \left| \mathbf{R} \right| \begin{pmatrix} -\mu_M \frac{x_R}{r^3} \\ -\mu_M \frac{y_R}{r^3} \\ -\mu_M \frac{z_R}{r^3} \end{pmatrix} + \left| \mathbf{R} \right| \mathbb{T}_z(-\tau) \mathbb{T}_y\left(\frac{\pi}{2} + \delta\right) \left| \mathbf{V} \right| \mathbb{T}_z(-\chi) \mathbb{T}_y(-\gamma) \left| \mathbf{B} \right| \left\{ \begin{pmatrix} -\frac{D}{m_{MAV}} \\ 0 \\ 0 \end{pmatrix} + \dots \right. \\ \left. \dots + \left| \mathbf{B} \right| \mathbb{T}_y(-\epsilon_T) \left| \mathbf{P} \right| \begin{pmatrix} \frac{T}{m_{MAV}} \\ 0 \\ 0 \end{pmatrix} \right\} \quad (6.10)$$

This manoeuvre could also be chosen to begin some time after the ignition of the second stage. Another aspect that could be used for the optimisation is the coasting time between the separation of the first stage and the second stage. All these different options result in a number of optimization parameters which can be chosen to be active or not (either optimised or set as a constant parameter). These parameters are: burn-time of the first stage  $t_1$ , the first coasting time between the first and second stage  $t_{c1}$ , the elevation gimbal angle  $\epsilon_{T2}$  (with possible thrust control  $T_{T2}$ ), the burn-time of the second stage  $t_2$  and (if chosen to delay the second thruster manoeuvre) the time at which the second thruster control step starts  $t_{T2}$ .

#### 6.3.4. COASTING AND ORBIT BURN

The final coasting phase starts at the second stage burn-out. There will still be some remaining propellant mass in the second stage at that point which will be used to perform the final orbit burn. The required propellant mass is a direct result of the necessary change in velocity required to propel the MAV into its final orbit from the current coasting trajectory. In order to compute this propellant mass, first the apocentre and pericentre of the current (elliptic) trajectory have to be determined [8] (see Equation (6.11)).

$$r_{ap} = \frac{-\mu_M r \pm \sqrt{(\mu_M r)^2 + r(rV^2 - 2\mu_M)(rV \cos(\gamma))^2}}{rV^2 - 2\mu_M} \quad (6.11)$$

Here  $r_{ap}$  represents the pericentre  $r_p$  for the negative and apocentre  $r_a$  for the positive sign. At this point, a check is performed to assure that the reached  $r_a$  is equal to the apocentre of the desired orbit (in case of a circular orbit) or equal to the pericentre of the desired orbit (in case of an elliptic orbit). The general equations that can be used for this check are provided in Equation (6.12) [108] where  $a$  and  $e$  are the semi-major

axis and eccentricity of the desired orbit respectively, which can be optimisation parameters as well, and the underscore  $c$  stands for check.

$$\begin{aligned} r_{a,c} &= a(1 - e) \\ r_{p,c} &= a(1 + e) \end{aligned} \quad (6.12)$$

The velocity at the apocentre can then be computed using Equation (6.13).

$$V_a = \sqrt{V^2 - 2\mu_M \left( \frac{1}{r} - \frac{1}{r_a} \right)} \quad (6.13)$$

The required  $\Delta V$  to reach the desired orbit is then given by Equation (6.14).

$$\Delta V = \sqrt{\mu_M \left( \frac{2}{r} - \frac{1}{a} \right)} \quad (6.14)$$

Now that the required velocity change is known, the corresponding required propellant mass  $\Delta m_b$  can be computed through the use of Tsiolkovsky's equation as the difference between the mass of the second stage at burn-out  $m_2$  and the final mass of the second stage  $m_{2,f}$  after the orbit burn. The expression for  $\Delta m_b$  is then provided by Equation (6.15).

$$\Delta m_b = m_2 \left( 1 - \exp \left( \frac{-\Delta V}{g_0 Isp} \right) \right) \quad (6.15)$$

During the coasting and the final burn, the only optimisation parameters are the eccentricity and the semi-major axis of the desired orbit. Thus the maximum number of optimisation parameters for the ascent phase is 14 and are:  $t_v$ ,  $t_{T1}$ ,  $T_{T1}$ ,  $\epsilon_{T1}$ ,  $\psi_{T1}$ ,  $t_1$ ,  $t_{c1}$ ,  $t_2$ ,  $t_{T2}$ ,  $\epsilon_{T2}$ ,  $T_{T2}$ ,  $a$ ,  $e$  and  $i$ .

## 6.4. MARS 2020 LANDING SITE CONDITIONS

In the beginning of August 2015 the second Workshop on the Mars 2020 Landing Site was held in Monrovia, California <sup>3</sup>. Directly following this workshop, a meeting was held in order to select eight potential landing sites for the Mars 2020 rover. These sites are (alphabetically) presented in Table 6.2 including the position data. Please note that the latitude and longitudes are within an accuracy of approximately 5 km.

Table 6.2: Current candidate landing sites (source:[JPL](#))

Landing site	Altitude w.r.t. MOLA geoid [km]	Latitude [°N]	Longitude [°E]
Columbia Hills/Gusev	-1.9	-14.4	175.6
Eberswalde	-1.4	-23.0	327.0
Holden	-2.1	-26.4	325.1
Jezero	-2.5	18.5	77.4
Mawrth	-2.3	24.0	341.1
NE Syrtis	-2.2	17.8	77.1
Nili Fossae	-0.6	21.0	74.5
SW Melas	-1.9	-12.2	290.0

There are also several landing site constraints that are important to the thesis problem:

- **Elevation** The elevation of the landing site must be below +0.5 km MOLA elevation. Which is with respect to the MOLA geoid (defined to be at a radius of 3396 km [109–111], not to be confused with the volumetric mean radius mentioned in [107])
- **Latitude** The landing site latitude has to be between  $\pm 30^\circ$  of the equator
- **Landing Ellipse** And the current best landing ellipse would be 18 km long and 14 km wide.

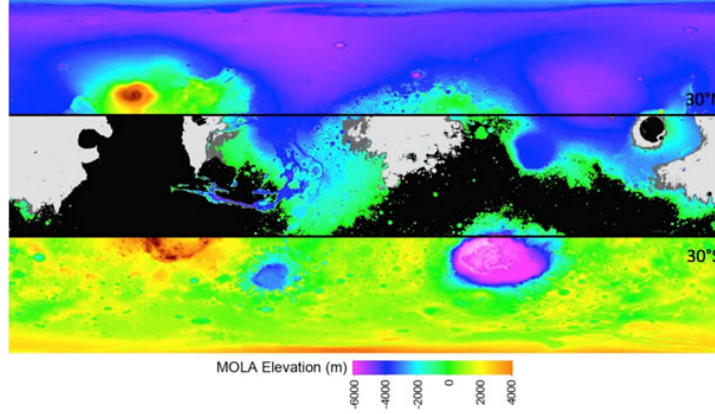


Figure 6.3: Constrained landing area on Mars between the  $30^{\circ}\text{N}$  and  $30^{\circ}\text{S}$  line. In that area, black land has an elevation above +0.5 km w.r.t. the MOLA geoid and the grey areas are lower thermal inertial constrained areas

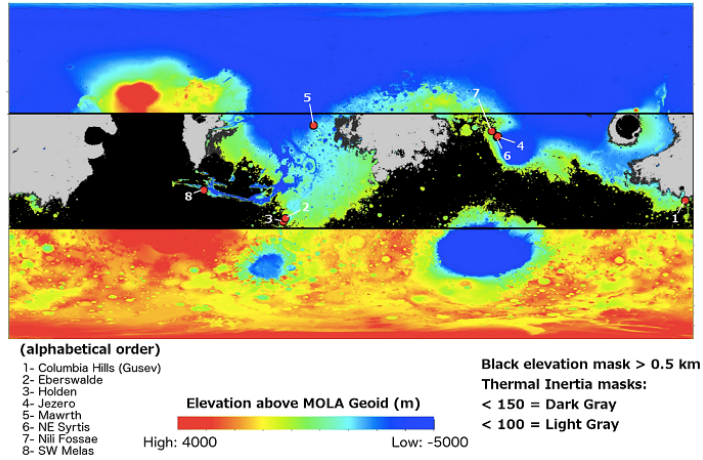


Figure 6.4: Locations of the eight potential landing sites within the constrained area

These constraints result in a band where the landing sites can be chosen, as visualised in Figure 6.3<sup>3</sup>. The location of the eight chosen potential landing sites are indeed located in this band as shown by Figure 6.4<sup>3</sup>.

The position data is all provided in the R-frame. With the different latitudes, the respective local rotational velocity  $V_{yR,0}$  (due East or in the y-direction in the R-frame), as viewed from the I-frame can be determined. These velocities provide the values for the initial velocity vector. The relation for  $V_{yR,0}$  is given in Equation (6.16) and the initial velocity vector is then provided through Equation (6.17). Here,  $\dot{\Omega}_M$  is the rotational velocity of Mars, the L-frame is attached to the landing site and  $R_M$  is the (local) radius of Mars.

$$V_{yR,0} = \dot{\Omega}_M R_M \cos(\delta_0) \quad (6.16)$$

$$\begin{pmatrix} V_{xI,0} \\ V_{yI,0} \\ V_{zI,0} \end{pmatrix} = \left| \begin{matrix} \mathbf{I} & \mathbb{T}_{\mathbf{z}}(-\dot{\Omega}_M t_O + \Omega_P) & \mathbb{T}_{\mathbf{z}}(-\tau_0) \\ & \mathbf{R} & \mathbf{L} \end{matrix} \right| \begin{pmatrix} 0 \\ V_{yR,0} \\ 0 \end{pmatrix} = \begin{pmatrix} -\sin(\tau_0 + \dot{\Omega}_M t_O - \Omega_P) V_{yR,0} \\ \cos(\tau_0 + \dot{\Omega}_M t_O - \Omega_P) V_{yR,0} \\ 0 \end{pmatrix} \quad (6.17)$$

<sup>3</sup> Landing site workshop: <http://marsnext.jpl.nasa.gov/>

# 7

## TRANSFER ORBITS

The second part of the thesis problem involves (transfer) orbits around Mars. After the ascent phase of the MAV, the vehicle will be inserted into an orbit around Mars. Since it will use its high-thrust second stage engine to perform the final burn to do this it is required to understand the different possible orbits that can be reached using high-thrust. Therefore Section 7.1 will discuss the different high-thrust orbits. At this time, the orbiter should already be in position to rendezvous with the MAV. The orbiter will therefore have to travel from its original (scientific) orbit to the rendezvous orbit around Mars after which it will have to return to a higher/safer orbit as to not be trapped in the gravitational well of Mars. However, compared to the MAV, the orbiter will be using a low-thrust propulsion system. These propulsion systems can be turned on for longer amounts of time to provide a continuous thrust. The low-thrust trajectories are discussed in Section 7.2. Because low-thrust transfers are relatively new, all available planetocentric reference missions have been flown in the Earth system (also see Section 3.2). The reference mission for low-thrust missions will be discussed and the most important information will be summarized in Section 7.2 as well. Section 7.3 describes the models and the general EoM required to represent the motion of the orbiter. The thrust history for the orbiter can be constructed using Q-law. This control law is described in Section 7.4. Finally, the Mars 2022 orbiter initial conditions and constraints will be provided in Section 7.5.

### 7.1. HIGH-THRUST

Two types of high-thrust transfer orbits are high energy transfer and minimum energy transfer orbits [112]. This last transfer method is referred to as a Hohmann transfer [10] and is the most common transfer orbit. It is a direct transfer method, which means that it will directly transfer a s/c from one orbit to the other by travelling less than  $360^\circ$  (within one rotation) around the main body. In case of a Hohmann transfer, the s/c travels  $180^\circ$  around Mars before arriving at the destination orbit. This transfer orbit, from one circular orbit to another circular orbit, is characterized by two propulsive shots, one at the departing orbit and one at the destination orbit as illustrated in Figure 7.1 for a heliocentric case<sup>1</sup>. The elliptic orbit touches both the departing and destination planet orbits.

A Hohmann transfer orbit, in itself, could also be a desired elliptical orbit, in which case only the first burn will have to take place. The process of reaching this desired orbit was described by the equations in Section 6.3.4. For a Hohmann transfer the planets have to be aligned such that the angle between the departing planet at the time of departure and the destination planet at the time of arrival is  $180^\circ$  which only happens every so often. In create more opportunities to reach a certain set point in an orbit, as well as faster, high energy transfer orbits can be applied. In Figure 7.2 the four different trajectory types for the ordinary two dimensional case are described for a transfer from Earth to a planet further from the Sun (as an example).

Figure a) displays the fastest trajectory which is called a type I trajectory. Figure b) represents a so called type II trajectory where the planet is intercepted at the second crossing of the orbit. Figures c) and d) are similar but for a different starting position of the Earth. Even though the type I trajectory requires more energy, it might be preferred if time is an important factor. A good example of the benefits is provided in [10], where it is said that a flight time reduction of 50% only requires an increase in  $\Delta V$  of 19% but reduces the transferable payload mass by 27%. This does not however include the plane change that might need to

<sup>1</sup>Source: <http://www.braeunig.us/space/interpl.htm>

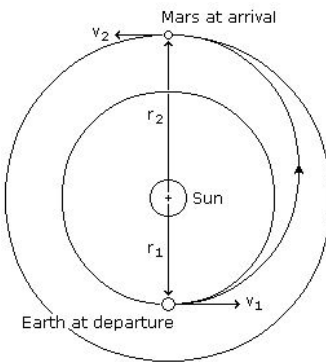


Figure 7.1: Graphical representation for Earth-Mars Hohmann transfer burns

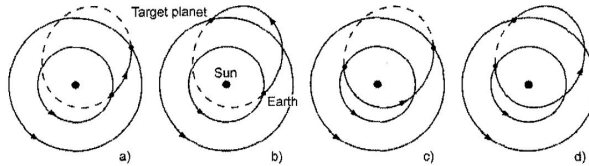


Figure 7.2: Graphical representation of the four different high energy transfer orbit possibilities based on an arbitrary ellipse crossing both orbits [10]

be performed. It should be mentioned that any required inclination changes between the MAV orbit and the orbit of the Mars 2022 orbiter should be performed by the orbiter because a low Mars orbit inclination change with a high-thrust propulsion system requires a lot more energy and thus propellant mass than an inclination change performed by the low-thrust propulsion system of the Mars 2022 orbiter at a much higher orbit [10].

Both Hohmann and high-energy transfer orbits could be used by the MAV should it be required to transfer from its original (parking) orbit to a different orbit. At this point it is assumed that rendezvous will take place in the injected original (parking) orbit of the MAV, but in future mission design these transfer orbits can be used to bring the MAV to the higher Mars 2022 orbiter orbit should that be required.

## 7.2. LOW-THRUST

The Mars 2022 orbiter will be using a low-thrust electric propulsion system and will be orbiting the planet to gather scientific data and perform observations. It will also be required to collect the Martian sample from the MAV and bring it back to Earth. On a Martian planetocentric level this means that the orbiter will have to travel from its scientific orbit to the lower MAV orbit and then back to a higher Martian orbit in order to escape Mars' gravity well and to reach a suitable Earth return orbit. The low-thrust transfer orbit is described in Section 7.2.1 and Section 7.2.2 describes the reference missions for the Mars 2022 orbiter transfer orbits.

### 7.2.1. LOW-THRUST ELECTRICAL PROPULSION TRANSFER

Low-thrust electric propulsion is characterised by a high specific impulse ( $I_{sp}$ ) but very low thrust levels. It is very useful for long duration missions and these engines can thrust continuously if necessary. This continuous thrusting would result in a spiralling orbit as depicted in Figure 7.3, however the thrust can also be applied in increments where there are thrusting periods and coasting periods in the transfer orbit. This was for instance done by the Dawn spacecraft in combination with gravity assists (see Figure 7.4).

### 7.2.2. REFERENCE MISSIONS

The Mars 2022 orbiter will be propelled by an EP system, thus a spiralling transfer motion can be expected. The reference missions and research mentioned in Section 3.2 also used EP. Deep Space 1 is considered to be the first modern s/c to use EP as its main propulsion system used to perform orbital transfer manoeuvres. The engine was a Xenon ion engine. Ever since this mission Xenon engines have become increasingly popular and almost all modern low-thrust missions now use Xenon engines [10]. These engines are either Hall thrusters or full ion engines. In Table 7.1 all flown reference missions that used either of these engines are mentioned

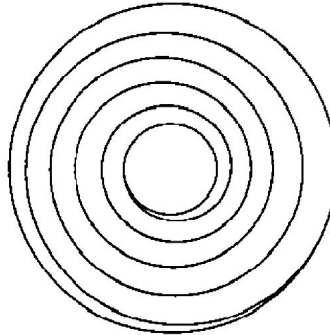


Figure 7.3: Example of continuous low-thrust trajectory[11]

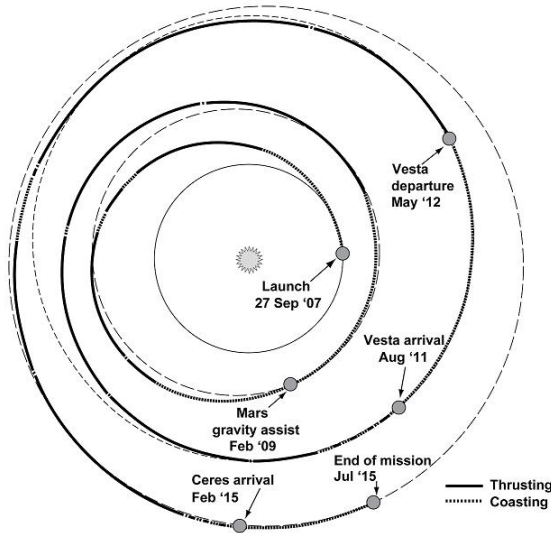


Figure 7.4: Example of a segmented low-thrust interplanetary trajectory: the Dawn spacecraft[10]

and their engine characteristics are specified. This table also includes interplanetary missions.

Table 7.1: Flown low-thrust missions using Xenon engines and their characteristics (provided per thruster)

Year	Mission/ <i>s/c</i>	Engine	Thrusters	Thrusters active at once	Engine power [kW]	Isp [s]	Thrust [mN]	Ref.
1998	Deep Space 1	Ion	1	1	2.5 (max)	3120	92.4	[10, 27, 113]
2001	Artemis	Ion	4	1	0.57	3370	$15 \pm 0.9\%$	[114] <sup>2</sup>
2003	Hayabusa	Ion	4	3	0.38	3160	8	[10]
2003	SMART-1	Hall	1	1	1.19	1631	68	[10]
2007	Dawn	Ion	3	1	2.6	3058	92	[10]
2010	AEHF(-1)	Hall	4	2	4.5	2020	267	Updates <sup>3 4</sup>
2015	Boeing 702SP	Ion	4	1 <sup>5</sup>	4.5	3500	165	[28, 115] <sup>6</sup>

There are already many different programs available that can simulate low-thrust trajectories. In three of

<sup>2</sup>Artemis mission update: [http://m.esa.int/Our\\_Activities/Telecommunications\\_Integrated\\_Applications/Artemis\\_finally\\_reaches\\_operational\\_orbit](http://m.esa.int/Our_Activities/Telecommunications_Integrated_Applications/Artemis_finally_reaches_operational_orbit)

<sup>3</sup>AEHF-1 mission update: <http://spaceflightnow.com/atlas/av019/111009.html>

<sup>4</sup>Online catalogue Aerojet Rocketdyne: <https://www.rocket.com/propulsion-systems/electric-propulsion>

<sup>5</sup>Assumed 1 provided that the maximum available power is 9 kW, or 2 if no other system is active, which is less likely

<sup>6</sup>Boeing company: <http://www.boeing.com/space/boeing-satellite-family/index.page>

the mentioned papers in Section 3.2.2 the different used methods, dynamic equations and EoM are described. [29] and [30] used the classical non-singular equinoctial orbital elements, instead of the Kepler elements, and their corresponding EoM to determine the orbit trajectories, whereas [32] describes a method of using Cartesian coordinates and the corresponding EoM. These reference methods can be used in the next section to set-up the dynamic model and corresponding EoM for the thesis problem.

## 7.3. DYNAMIC MODEL AND EQUATIONS OF MOTION

For the simulation of the orbiter it is important to have an accurate representation of reality. However, it should also still be possible to find a solution to the problem, which means that the model should also not be too complex. Most of the low-thrust model will be based on the work of Gebbett [116] and thus the same assumptions will be made and equations will be used. The dynamic model is described in Section 7.3.1 and the corresponding EoM are provided in Section 7.3.2.

### 7.3.1. DYNAMIC MODEL AND INITIAL ASSUMPTIONS

The motion of a s/c around a body can be described by the Kepler elements (Figure 8.10) where  $a$  is the semi-major axis,  $e$  is the eccentricity,  $i$  the orbit inclination,  $\omega$  the argument of periapsis,  $\Omega$  the right ascension of the ascending node and  $\theta$  the true anomaly. In a normal stable orbit all these elements except for  $\theta$  are constant. The elements are in this case described in an inertial planet-centred reference frame.

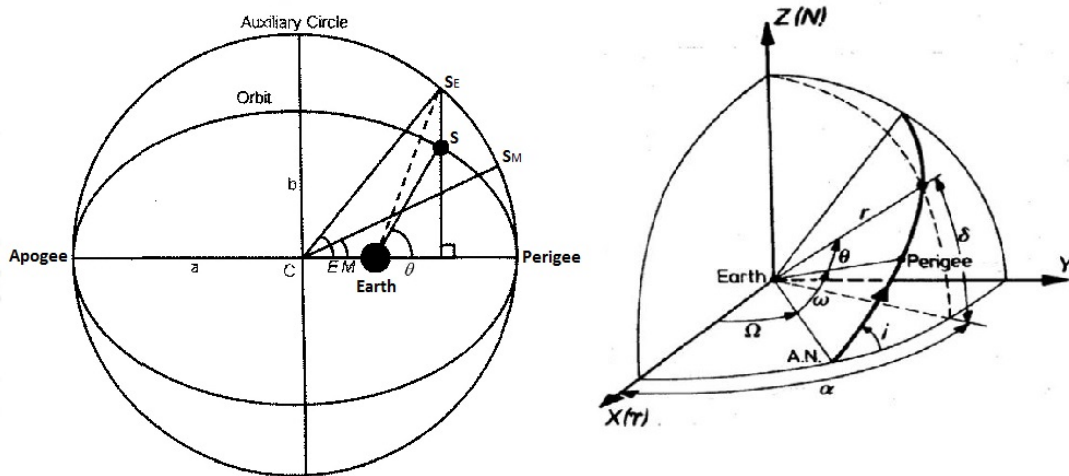


Figure 7.5: Definition of the Kepler elements in 2D (left) and 3D (right) [12, 13]

A stable orbit can however be disturbed which will cause the orbital elements to change and thus result in a different orbit. These disturbances are called orbital perturbations. During the orbital change of the Mars 2022 orbiter, the low-thrust propulsion system will cause a perturbation in order to change from one orbit to the other, however there are also other effects that can cause the orbit to change. The most important perturbations that were taken into account by [116] and that are meaningful to take into account in an orbit around Mars are the  $J_2$  gravitational (flattening) effect, and the third body perturbation caused by the Sun. Both effects will be discussed in the next section. Another element that is taken into account in the low-thrust orbital model is the shadowing effect of the planet. The orbiter will be using a propulsion technology called Solar Electric Propulsion (SEP) which requires such a great amount of power that it can only be used when the s/c is in direct sunlight. Therefore the propulsion system cannot be used during eclipse, which has to be taken into account when designing the propulsion scheme for the low-thrust orbit trajectory. More information on the application of the shadowing effect in the simulation tool can be found in [116].

### 7.3.2. CORRESPONDING EoM AND INITIAL ASSUMPTIONS

In order to model the changes in the orbital elements as a result of the thrust and the different perturbations Gauss' form of the Lagrange's planetary equations as shown by Equation (7.1) can be used [10, 116, 117]. Here  $f_S$ ,  $f_N$  and  $f_W$  are defined as in Figure 7.6 and  $p$  is the semi-latus rectum defined as  $a(1 - e^2)$ .

$$\begin{aligned}
 \frac{da}{dt} &= 2 \frac{a^2}{\sqrt{\mu_M p}} \left[ e \sin(\theta) f_S + \frac{p}{r} f_N \right] \\
 \frac{de}{dt} &= \frac{1}{\sqrt{\mu_M p}} \left[ p \sin(\theta) f_S + ((p+r) \cos(\theta) + r e) f_N \right] \\
 \frac{di}{dt} &= \frac{r}{\sqrt{\mu_M p}} \cos(\theta + \omega) f_W \\
 \frac{d\omega}{dt} &= \frac{1}{e \sqrt{\mu_M p}} \left[ -p \cos(\theta) f_S + (p+r) \sin(\theta) f_N \right] - \frac{r \sin(\theta + \omega) \cos(i)}{\sqrt{\mu_M p} \sin(i)} f_W \\
 \frac{d\Omega}{dt} &= \frac{r}{\sqrt{\mu_M p} \sin(i)} \sin(\theta + \omega) f_W \\
 \frac{d\theta}{dt} &= \frac{\sqrt{\mu_M p}}{r^s} + \frac{1}{e \sqrt{\mu_M p}} \left[ p \cos(\theta) f_S - (p+r) \sin(\theta) f_N \right]
 \end{aligned} \tag{7.1}$$

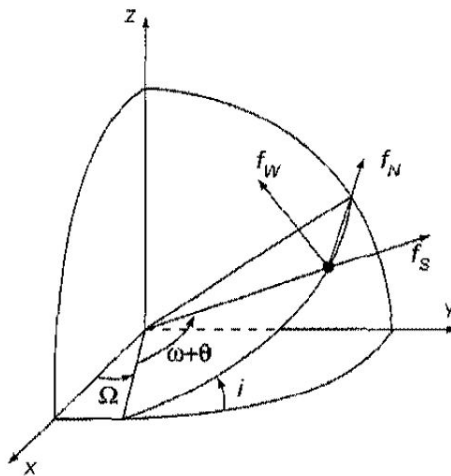


Figure 7.6: Definition of the perturbing accelerations [10]

However, it is clear that for  $e = 0$  and/or  $i = 0^\circ$  or  $180^\circ$  this set of equations results in singularities. Therefore a slightly modified set of elements is used to eliminate these singularities. In [116] the MEE were deemed most suited based on the survey performed in [118] because this set is non-singular. The definition of the six elements is provided in Equation (7.2), where the semi-latus rectum is still the same as was defined before but now directly used. More information on the MEE will be provided in Chapter 8.

$$\begin{aligned}
 p &= a(1-e^2) & h &= \tan^I \left( \frac{i}{2} \right) \cos(\Omega) \\
 f &= e \cos(\omega + I\Omega) & k &= \tan^I \left( \frac{i}{2} \right) \sin(\Omega) \\
 g &= e \sin(\omega + I\Omega) & L &= \omega + \theta + I\Omega
 \end{aligned} \tag{7.2}$$

In Equation (7.2)  $I$  is the retrograde factor and has a value of +1 for posigrade orbits and -1 for retrograde orbits. This is done to avoid singularities when  $i = 180^\circ$  and thus making the set non-singular.

The corresponding time differential equations are also provided in [118] and corrected by [116]. These corrected equations are shown in Equation (7.3) where  $s^2 = 1 + h^2 + k^2$  and  $w = p/r = 1 + f \cos(L) + g \sin(L)$ . These equations are used to propagate the orbit.

$$\begin{aligned}
\frac{dp}{dt} &= \frac{2p}{w} \sqrt{\frac{p}{\mu_M}} f_N \\
\frac{df}{dt} &= \sqrt{\frac{p}{\mu_M}} \left[ \sin(L) f_S + ((w+1) \cos(L) + f) \frac{f_N}{w} - (h \sin(L) - k \cos(L)) g \frac{f_W}{w} \right] \\
\frac{dg}{dt} &= \sqrt{\frac{p}{\mu_M}} \left[ -\cos(L) f_S + ((w+1) \cos(L) + g) \frac{f_N}{w} + (h \sin(L) - k \cos(L)) f \frac{f_W}{w} \right] \\
\frac{dh}{dt} &= \sqrt{\frac{p}{\mu_M}} \frac{s^2 f_W}{2w} \cos(L) \\
\frac{dk}{dt} &= \sqrt{\frac{p}{\mu_M}} \frac{s^2 f_W}{2w} \sin(L) \\
\frac{dL}{dt} &= \sqrt{\mu_M p} \left( \frac{w}{p} \right)^2 + \frac{1}{w} \sqrt{\frac{p}{\mu_M}} (h \sin(L) - k \cos(L)) f_W
\end{aligned} \tag{7.3}$$

When it comes to the other perturbations, these can simply be added as an extra effect in any of the three perturbation acceleration directions.  $J_2$  on Mars has a value of  $1960.45 \cdot 10^{-6}$  [107]. The general equations for gravitational perturbations in normal Kepler elements are discussed in [119], however in this case, the same equations are needed for the MEE. Fortunately, these are provided by [120] and are given in Equation (7.4). Here  $s$  is again defined as was for Equation (7.3).

$$\begin{aligned}
f_{S,J_2} &= -\frac{3\mu_M J_2 R_M^2}{2r^4} \left( 1 - 12 \frac{(h \sin(L) - k \cos(L))^2}{s^4} \right) \\
f_{N,J_2} &= -\frac{12\mu_M J_2 R_M^2}{r^4} \left( \frac{(h \sin(L) - k \cos(L))(h \cos(L) + k \sin(L))}{s^4} \right) \\
f_{W,J_2} &= -\frac{6\mu_M J_2 R_M^2}{r^4} \left( \frac{(h \sin(L) - k \cos(L))(1 - h^2 - k^2)}{s^4} \right)
\end{aligned} \tag{7.4}$$

The perturbing acceleration caused by a third body are important to take into account if the third body has a high mass compared to the primary (orbiting) body. Mars has two natural satellites: Phobos and Deimos. However, the mass of these two satellites are relatively small compared to Mars. Thus it is assumed that the Martian moons do not have to be taken into account in the third body perturbations, however should this decision change, they can always be added in the future. The Sun however is a body that will definitely have to be taken into account. In [116] a method by Battin ([121]) is used to determine the accelerations caused by the third body, which in this case is the Sun. Battin's function is described in Equation (7.5) where  $\mathbf{r}$  is the position vector of the orbiter with respect to Mars and  $\mathbf{r}_{MS}$  is the position vector of the Sun with respect to Mars.

$$f(q) = q \left[ \frac{3 + 3q + q^2}{1 + (1 + q)^{\frac{3}{2}}} \right] \quad \text{where} \quad q = \frac{\mathbf{r} \cdot (\mathbf{r} - 2\mathbf{r}_{MS})}{\mathbf{r}_{MS} \cdot \mathbf{r}_{MS}} \tag{7.5}$$

The third body acceleration can then be described by Equation (7.6). Please note that these accelerations are described in the inertial Mars-centred frame in Cartesian coordinates and will thus have to be transformed to the s/c centred frame in order to be added to the other accelerations that are acting on the orbiter. This transformation will be described in Chapter 8.

$$\mathbf{a}_S = -\frac{\mu_S}{(\mathbf{r} - \mathbf{r}_{MS})} (\mathbf{r} + f(q) \mathbf{r}_{MS}) \tag{7.6}$$

Here the standard gravitational parameter for the perturbing body, in this case the Sun, is used. For a given position of the celestial bodies and the orbiting s/c the most important perturbations can now be computed.

## 7.4. Q-LAW

During the transfer of the orbiter, the low-thrust engine will be used to perform the orbital changes. However, unlike high-thrust engines, low-thrust engines can be active for a long period of time. They can also be turned off and on again. Determining the time that the engines have to be active and in which direction the thrust has to be pointed can be very difficult and time consuming. This is why, at JPL back in 2003, Petropoulos developed a feedback control law called Q-law [122], which can very accurately provide a good representation of the thrusting behaviour required to get from a starting orbit to a target orbit. The specific point in that orbit  $\theta$  can not be pre-set. In the years following, Q-law was refined ([117, 123]) and the latest version of Q is presented in Equation (7.7).

$$Q = (1 + W_P P) \sum_{\alpha} W_{\alpha} S_{\alpha} \left[ \frac{d(\alpha, \alpha_T)}{\dot{\alpha}_{xx}} \right]^2, \quad \text{for } \alpha = a, e, i, \omega, \Omega \quad (7.7)$$

Here  $W_P$  and  $W_{\alpha}$  are weights which have a scalar value equal to or greater than 0.  $P$  is a penalty function depending on the problem, but in [117] it was used to define a minimum periapsis radius which the orbit had satisfy. This function is defined in Equation (7.8).  $S_{\alpha}$  is a scalar function as defined by Equation (7.9) and  $d(\alpha, \alpha_T)$  is a distance function (see Equation (7.10)) where the subscript  $T$  stands for target. Finally,  $\dot{\alpha}_{xx}$  represents the maximum rate of change of the orbital elements over the thrust direction and true anomaly as defined by Equation (7.11).

$$P = \exp \left[ k \left( 1 - \frac{r_p}{r_{p,min}} \right) \right] \quad (7.8)$$

Here  $k$  is a scalar that can be adjusted if required. For instance, if at the end of the propagation it turns out that during the propagation the orbit went 2 km below the allowed minimum perigee radius and it is preferred to only go 1 km below the allowed minimum perigee radius, then the value for  $k$  should be increased. Initial trial and error.

$$S_{\alpha} = \begin{cases} \left[ 1 + \left( \frac{a - a_T}{ma_T} \right)^n \right]^{\frac{1}{r}}, & \text{for } \alpha = a \\ 1, & \text{for } \alpha = e, i, \omega, \Omega \end{cases} \quad (7.9)$$

In Equation (7.9) the nominal values for  $m$ ,  $n$  and  $r$  are respectively 3, 4 and 2.

$$d(\alpha, \alpha_T) = \begin{cases} \alpha - \alpha_T, & \text{for } \alpha = a, e, i \\ \arccos[\cos(\alpha - \alpha_T)], & \text{for } \alpha = \omega, \Omega \quad \text{where } \cos(\alpha - \alpha_T) \in [0, \pi] \end{cases} \quad (7.10)$$

$$\dot{\alpha}_{xx} = \begin{cases} \dot{\alpha}_{xx} = \max_{\alpha, \beta, \theta}, & \text{for } \alpha = a, e, i, \Omega \\ (\dot{\omega}_{xxi} + b\omega_{xxo}) / (1 + b), & \text{for } \alpha = \Omega \end{cases} \quad (7.11)$$

Here  $\dot{\alpha}$  are provided by Equation (7.1),  $\alpha \in [-\pi, \pi]$  is the in-plane thrust angle and  $\beta \in [-\frac{\pi}{2}, \frac{\pi}{2}]$  is the out-of-plane thrust angle [116]. The subscript x means that it is a maximum. In this case two x's are used because first the maximum is taken using a combination of  $\alpha$  and  $\beta$  resulting in  $\dot{\alpha}_x$  and then the maximum is taken using  $\theta$  thus resulting in the notation  $\dot{\alpha}_{xx}$ . Also,  $b$  is a non-negative constant with a nominal value of 0.01 and both  $\dot{\omega}_{xxi}$  and  $\dot{\omega}_{xxo}$  are defined in Equation (7.12).

$$\begin{aligned} \dot{\omega}_{xxi} &= \max_{\alpha, \theta} (\dot{\alpha} |_{\beta=0}) \\ \dot{\omega}_{xxo} &= \max_{\theta} (\dot{\alpha} |_{\beta=\pi/2}) \end{aligned} \quad (7.12)$$

Now using Equation (7.13), the equations in Equation (7.1) can be written such that  $Q$  is not a function of  $\alpha$ ,  $\beta$  and  $\theta$  as described in [117].

$$\begin{aligned} f_S &= f_{Thrust} \cos(\beta) \sin(\alpha) \\ f_N &= f_{Thrust} \cos(\beta) \cos(\alpha) \\ f_W &= f_{Thrust} \sin(\beta) \end{aligned} \quad (7.13)$$

$Q$  is zero at the target orbit and positive elsewhere. The greater the value of  $Q$  the further away the **s/c** is from the target orbit. The idea is to reduce  $Q$  to zero as soon as possible. Therefore at every time step, the largest difference in  $Q$  is required. This can be computed through Equation (7.14). Here the subscript  $n$  denotes that it is a minimum.

$$\frac{dQ}{dt} = \dot{Q} = \sum_{\alpha} \frac{\delta Q}{\delta \alpha} \dot{\alpha}$$

$$\dot{Q}_n = \min_{\alpha, \beta} \dot{Q}$$
(7.14)

From this it can be determined in which direction the thrust has to be directed. The next step is to determine whether it is useful to provide this thrust at this instance or not. This is done through the so-called effectivity. The absolute and relative effectivity are defined as in Equation (7.15).

$$\eta_a = \frac{\dot{Q}_n}{\dot{Q}_{nn}}$$

$$\eta_r = \frac{\dot{Q}_n - \dot{Q}_{nx}}{\dot{Q}_{nn} - \dot{Q}_{nx}}$$

$$where \quad \dot{Q}_{nn} = \min_{\theta} \dot{Q}_n$$

$$where \quad \dot{Q}_{nx} = \max_{\theta} \dot{Q}_n$$
(7.15)

It is up to the user to determine which of the two effectivities to use, because it is problem dependent. But both values will have to be higher than a certain cut-off value  $\eta_{cut}$  for the control law to accept it as a point where thrust has to be applied. If the effectivity is lower than this  $\eta_{cut}$  it means that no thrust will be applied and the **s/c** is thus in a coasting phase. According to Petropoulos it is better to use the relative effectivity for near circular orbits.

The equation for the Q-law itself is used to determine the direction in which thrust has to be applied and the Q-law effectivity determines whether this thrust should be applied or not. This results in a thrust which is incorporated in the orbit propagation. However, in its current form, singularities can occur, which is why [116] wrote the Q-law in MEE using the Gauss' equations provided in Equation (7.3). This form will also be used in the thesis problem to avoid any singularities and to be able to optimise for every kind of orbit.

The simplified form of the Q-law using MEE is provided by Equation (7.16)[116]. This formulation is similar to the original Q-law formulation that was introduced in 2003 [122].

$$Q_{MEE} = \sum_{\xi} W_{\xi} \left[ \frac{\xi - \xi_t}{\dot{\xi}_x} \right]^2, \quad for \quad \xi = p, f, g, h, k$$
(7.16)

Again  $W_{\xi}$  are weights with a scalar value equal to or greater than 0 and  $\xi$  depicts the MEE. Also, since only one maximum is taken (only the maximum with respect to  $L$ ) the notation for  $\dot{\xi}_x$  has one  $x$  in the subscript. In this case Gebbett found that it is more computationally efficient to use the expressions for the accelerations in the different directions directly instead of using the two thrust angles. Therefore, the expressions for  $\dot{\xi}_x$  are found through the EoM given by Equation (7.3) and applying Equation (7.17).

$$\dot{\xi}_x = \max_L (\dot{\xi}) \quad for \quad \xi = p, f, g, h, k$$
(7.17)

For  $p_x$ ,  $h_x$  and  $k_x$  the analytical expressions for the critical points can be found for which  $L$  is maximum. The value for  $p_x$ ,  $h_x$  and  $k_x$  is then the maximum of both critical values resulting from the equations mentioned in Equation (7.18) [116].

$$\begin{aligned}
\dot{p}_x &= \max(\dot{p}_{cr}), & \dot{p}_{cr} &= \frac{2p}{1 \pm \frac{f}{\sqrt{\frac{g^2}{f^2} + 1}} \pm \frac{g}{f\sqrt{\frac{g^2}{f^2} + 1}}} \sqrt{\frac{p}{\mu_M} f_{Thrust}} \\
\dot{h}_x &= \max(\dot{h}_{cr}), & \dot{h}_{cr} &= \frac{\pm \sqrt{1-g^2}}{1 \pm f\sqrt{1-g^2-g^2}} \sqrt{\frac{p}{\mu_M} \frac{s^2}{2}} f_{Thrust} \\
\dot{k}_x &= \max(\dot{k}_{cr}), & \dot{k}_{cr} &= \frac{\pm \sqrt{1-f^2}}{1 \pm g\sqrt{1-f^2-f^2}} \sqrt{\frac{p}{\mu_M} \frac{s^2}{2}} f_{Thrust}
\end{aligned} \tag{7.18}$$

Because  $\dot{f}$  and  $\dot{g}$  are a function of all the three acceleration directions, a direct analytical solution was deemed impossible to find by [116]. Therefore the functions have to be evaluated numerically for  $L$  to determine the critical values for the three different accelerations. The equations for  $\dot{f}$  and  $\dot{g}$  (see Equation (7.3)) can be slightly rewritten to single out the different accelerations as shown in Equation (7.19). Here the  $H(L)$ ,  $J(L)$  and  $K(L)$  are simply the rewritten parts of the original expression and are shown in Equation (7.20) for both  $\dot{f}$  and  $\dot{g}$  respectively.

$$\begin{aligned}
\dot{f} &= H_f(L)f_S + J_f(L)f_N + K_f(L)f_W \\
\dot{g} &= H_g(L)f_S + J_g(L)f_N + K_g(L)f_W
\end{aligned} \tag{7.19}$$

$$\begin{aligned}
H_f &= \sqrt{\frac{p}{\mu_M}} \sin(L) & H_g &= -\sqrt{\frac{p}{\mu_M}} \cos(L) \\
J_f &= \sqrt{\frac{p}{\mu_M}} \frac{(w+1)\cos(L)+f}{w} & J_g &= \sqrt{\frac{p}{\mu_M}} \frac{(w+1)\cos(L)+g}{w} \\
K_f &= -\sqrt{\frac{p}{\mu_M}} \frac{h\sin(L)-k\cos(L)}{w}g & K_g &= \sqrt{\frac{p}{\mu_M}} \frac{h\sin(L)-k\cos(L)}{w}f
\end{aligned} \tag{7.20}$$

It is mentioned that this method is very slow, but it does result in a robust system that can handle both elliptic and circular orbits. In order to have a slightly faster evaluation [116] decided to evaluate  $\dot{f}_x$  and  $\dot{g}_x$  only once every revolution because the orbital elements do not show a significant difference in that one revolution. This is only an approximation but in Equation (7.16) the weights can be used to make the contribution of both  $\dot{f}_x$  and  $\dot{g}_x$  less important and have a lower influence on the solution.  $Q_{MEE}$  is again zero at the target orbit and positive elsewhere. In this case Equation (7.21) (based on Equation (7.15)) is used to determine the largest rate of change of  $Q_{MEE}$ . For further information see [116].

$$\begin{aligned}
\frac{dQ_{MEE}}{dt} &= \dot{Q}_{MEE} = \sum_{\xi} \frac{\delta Q_{MEE}}{\delta \xi} \dot{\xi} \\
\dot{Q}_{MEE,n} &= \min_{f_S, f_N, f_W} \dot{Q}_{MEE}
\end{aligned} \tag{7.21}$$

With the minimum value of  $\dot{Q}_{MEE}$  now known, the expressions for the absolute and relative effectiveness (see Equation (7.15) used for the normal Q-law) can be applied here again to determine whether the thrust has to be applied or not. However, as was mentioned in Section 7.3.1 the orbiter is unable to thrust when it is in the shadow of the planet. Therefore when using the minima and maxima (with respect to  $L$  in stead of  $\theta$ ) there is also a limit put on  $L$  to avoid positions in the orbit that would be in the shadow of Mars [116]. Another important consideration is the fact that the program might decide to show thrust-on-off behaviour called on-off-chatter, which is caused by a  $\eta$  close to the cut-off value [117]. A second type of chatter is the thrust direction chatter, where first the thrust is directed forward and then backward and then forward again (for instance) etcetera. Both types of chatter can be dealt with as described by Petropoulos [117] and Gebbett [116] but can never be completely eliminated.

The non-singular form of the Q-law  $Q_{MEE}$  does not include a penalty function as is the case with the normal Q-law. The described penalty function in Equation (7.8) provides a minimum condition for the pericenter radius. As will be discussed in the next section, the initial orbit of the Mars 2022 orbiter is at a relatively low altitude. This is why, in consultation with Petropoulos, it was decided that this penalty function might have to be added to  $Q_{MEE}$  depending on the behaviour during the simulation. This would change the partial derivatives for  $\frac{\delta Q_{MEE}}{\delta \xi}$  and therefore the program written by Gebbett [116] would have to be updated.

## 7.5. MARS 2022 ORBITER INITIAL CONDITIONS

According to JPL the Mars 2022 orbiter shall be used to bring a Martian sample back to Earth. In the current architecture the orbiter will be launched from Earth two years before the MAV will. This means that the orbiter will also perform several scientific missions in the Martian system. Therefore, at the start of the thesis simulations the orbiter will be in a scientific orbit. In this case that means that the orbiter will be in a sun-synchronous orbit at an altitude of 320 km. The precise orientation of the orbit with respect to an Inertial Mars reference frame ( $\omega$  &  $\Omega$ ) will depend on the simulated exact date at the beginning of the simulation. It is assumed that this initial orbit will be a circular orbit ( $e = 0$ ). The precise point in this orbit ( $\theta$ ) will have to be chosen before the start of the simulation. Given that the starting orbit is a sun-synchronous orbit at an altitude of 320 km, the orbit characteristics  $a$  and  $i$  can be computed. In [107] it is mentioned that the volumetric mean radius of Mars  $R_M$  is 3389.5 km thus resulting in a semi-major axis of 3709.5 km or 3,709,500 m. With this information, Equation (7.22) [119] can be solved for a pure  $J_2$  (for Mars  $1960.45 \cdot 10^{-6}$  [107]) sun-synchronous orbit around Mars with the orbital period of Mars around the Sun  $T_{MS} = 5.9355 \cdot 10^7$  s and  $\mu_M = 4.283 \cdot 10^{13} \text{ m}^3/\text{s}^2$ .

$$\cos(i) = -\frac{4\pi}{3T_{MS}J_2} \left( \frac{a(1-e^2)}{R_M} \right)^2 \sqrt{\frac{a^3}{\mu_M}} \quad (7.22)$$

From this it can be computed that the inclination will be  $92.6979^\circ$ . Thus the initial parameters will be  $a = 3,709,500$  m,  $e = 0$  and  $i = 92.6979^\circ$ , and  $\omega$ ,  $\Omega$  and  $\theta$  are not specifically defined yet.

Besides the characteristics of the initial orbit, the engine parameters and the total mass of the orbiter at the start of the simulation are required. Currently, two different Xenon engines are under consideration. Table 7.2 shows the different characteristics depending on the type of engine that will be chosen. The Max. engine power is the maximum power available for the worst case (which is at Mars Aphelion).

Table 7.2: The two different engines currently under consideration for use on the Mars 2022 orbiter

Engine	Start Mass [kg]	Max. engine power [kW]	Isp [s]	Thrust [mN]
Hall	2500	10.0877	2600	250
Ion	2000	7.2055	3300	170

The Ion engine is based on the same engine used by Boeing's 702SP satellite.

# 8

## REFERENCE SYSTEMS AND TRANSFORMATIONS

When considering the position, speed and acceleration of a space vehicle, different reference frames are usually used. Why there are different frames, which frames are required, what they are used for and how to transfer from one frame to the other will be discussed in Sections 8.1 and 8.2. In case of, for instance, a car travelling on the road, a certain coordinate system has to be used in order to measure the speed in a certain direction. For the car it can be said that a Cartesian system is used with  $x$  in the direction of motion,  $z$  pointing towards the ground and  $y$  then pointing to the right if looking in the direction of motion (using the so-called **R.H.R.** to complete the frame). The speed is then measured and expressed in the  $x$ -direction. This works well when a vehicle is travelling in a straight line or on a flat plane, but in orbital mechanics the motion usually has to be described just above or in an orbit around a (spherical) body. Therefore it is important to know which coordinate system is used and how to change between these coordinate systems should the other system become more convenient to use at a certain point. In Section 8.3 the difference between these coordinate systems and how to transfer from one to the other is explained.

### 8.1. REQUIRED REFERENCE SYSTEMS

In the example of the car, the frame of reference is fixed to the Earth. However, when considering two cars driving on the same road, one might like to investigate the difference in velocity between both vehicles. In that case a **RF** is chosen that is fixed to one of the two cars. This makes it easier to determine the relative speed of one car with respect to the other car. The same can be done for **s/c** (think of formation flying). There are therefore a number of different **RFs** that can be used. In this section the required **RFs** and their application will be presented.

#### 8.1.1. MARS-CENTRED INERTIAL (MCI) RF (I-FRAME)

The Mars-centred inertial reference frame is a **RF** that is, as the name implies, fixed to the centre of mass of Mars [14]. It is a frame in which Mars still rotates with respect to that frame, or in other words it is an inertial frame with respect to Mars. The  $x$ -axis is defined through a certain meridian which can be set by the user. This means that the user can determine his or her own inertial frame. A frame that is often used (and which is based on J2000<sup>1</sup>) is the MARSIAU frame [124, 125]. This is a Mars inertial frame that is translated from the Earth J2000 frame. For the translation a point through the mean equator of Mars is specified where the equator ascends through the mean equator of Earth. The  $x$ -axis is defined through this point. The  $z$ -axis is then defined through the rotational axis of Mars and the  $y$ -axis completes the frame through the **R.H.R.**. The translation is described in [124, 125] using the J2000 numbers from [126]. The generic inertial frame is shown in Figure 8.1. The centre of the frame is represented by the letter 'A'. The MARSIAU frame is required if certain data from outside sources will have to be incorporated into the simulation, however for the actual simulation and optimisation it will be easier and much more straightforward to define a custom Mars inertial reference frame for the thesis problem.

<sup>1</sup>J2000 is an Earth referenced inertial frame that was set through the rotational axis of Earth ( $z$ -axis) and through the vernal equinox of the year 2000 ( $x$ -axis). The reference was set on the Julian date of 2451545.0 or 01-01-2000 at 12:00 Greenwich Mean Time (**GMT**).

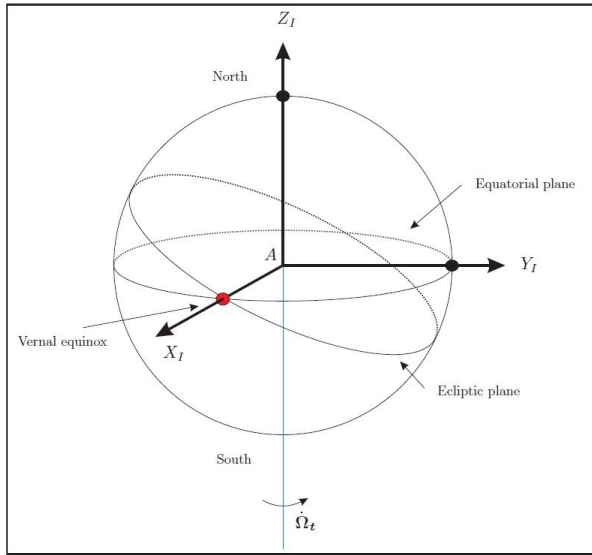


Figure 8.1: Graphical definition of the Mars-centred inertial reference frame [14]

This reference system is very useful if the motion of the **s/c** with respect to the **s/c** ground-track is not important.

### 8.1.2. MARS-CENTRED MARS-FIXED (MCMF) RF (R-FRAME)

The Mars-centred Mars-fixed frame is exactly the same as the **MCI** frame except for one distinct difference. The x-axis of the **MCMF** frame ( $x_R$ ) is defined through the 0.5 km wide Airy-0<sup>2</sup> crater which has a latitude of -5.07829° [127]. The associated meridian is called the Prime meridian. On the 1<sup>st</sup> of January 2000 at 12:00 the Prime meridian of Mars was 176.630° east of the x-axis in the **MARSIAU** frame (which is important when transforming from the **MARSIAU** frame to the current **MCMF** frame)[125, 126]. Because the Airy-0 crater is fixed to the surface of Mars and rotates around the Martian rotational axis (in both **MCI** and **MCMF** the z-axis), the **MCMF** is also a rotational frame. This frame rotates with Mars and can therefore be very useful for ground observation purposes. In the case of the **MAV** it is important to take the rotational velocity of Mars into account, since Mars will be rotating underneath the **MAV** causing rotational effects. A graphical representation of the **MCMF** frame is presented in Figure 8.2. An angle  $\Omega_P$  is defined as the relative angle between the prime meridian and the x-axis of the **MCI** frame at the time that the inertial frame was defined.

### 8.1.3. VERTICAL RF (V-FRAME)

This next **RF** can be used to describe the motion of a **s/c** in orbit around a planet. The centre of the vertical frame is defined in the centre of gravity of the **s/c** [14] but is not rotationally fixed to it. This means that the frame can rotate with respect to the **s/c** itself. This is because the x-axis is set to point to the north pole of Mars. The z-axis is perpendicular to Mars' surface (or points to the centre of Mars assuming Mars is a sphere) and the y-axis then points due east. The x-y plane is tangent to Mars' geoid. Figure 8.3 shows the vertical frame denoted by the letter 'V' at an arbitrary position around Mars compared to the **MCI** frame. The centre of the Vehicle-carried normal Mars (**VCNM**) frame is defined by the letter 'G'. The vertical frame relates to the Mars rotational frame through the latitude and longitude (also see Figure 6.1).

### 8.1.4. BODY-FIXED (BF) RF (B-FRAME)

The body-fixed frame is fixed to the **s/c** body and therefore rotates with the **s/c** as well. The origin of the **BF** **RF** is usually defined in the centre of mass (often equal to the centre of gravity) [14]. The axis orientation can be chosen to be in any direction. In this case the x-axis is defined through the vehicle-centre line and goes through the "nose" of the **s/c**, the z-axis is defined towards the orbiting body and the y-axis completes the frame through the **R.H.R.**. An example of a body frame used for the Apollo Command and Service module is provided in Figure 8.4<sup>3</sup>. In this case the z-axis was however defined by the main hatch of the vehicle.

<sup>2</sup>ESA website: [http://www.esa.int/Our\\_Activities/Space\\_Science/Mars\\_Express/Where\\_is\\_zero\\_degrees\\_longitude\\_on\\_Mars](http://www.esa.int/Our_Activities/Space_Science/Mars_Express/Where_is_zero_degrees_longitude_on_Mars)

<sup>3</sup>Source: NASA

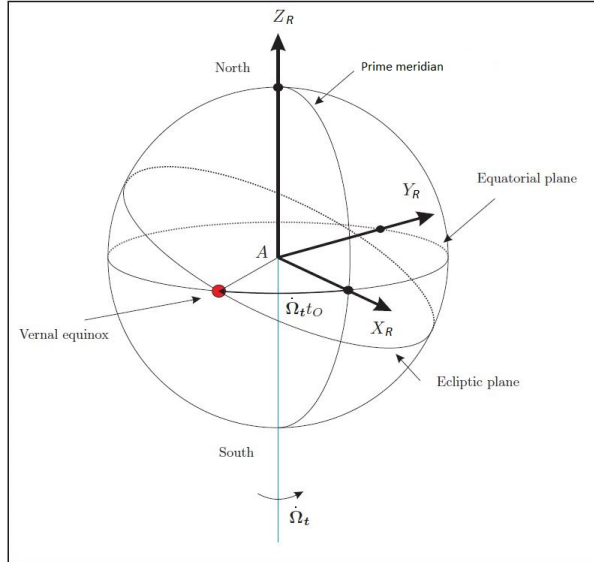


Figure 8.2: Graphical definition of the Mars-centred Mars-fixed reference frame [14]

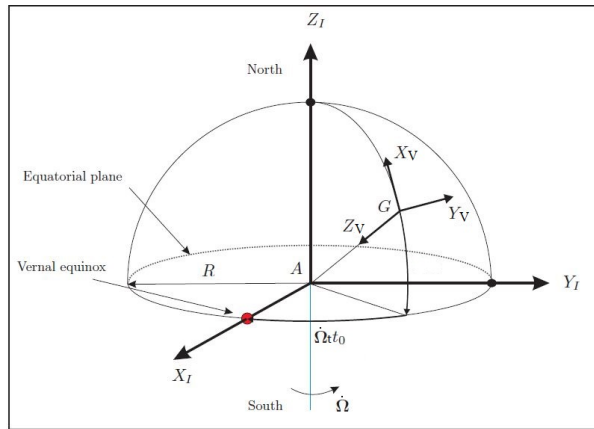


Figure 8.3: Graphical definition of the Vertical reference frame compared to the Mars-centred inertial frame [14]

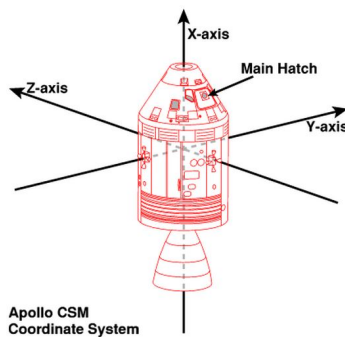


Figure 8.4: Graphical example of a Body-fixed reference frame used on the Apollo Command and Service module

The axes of the body frame are denoted by a 'B' in this report. In the thesis problem the body frame relates directly to the vertical frame through the flight-path angle  $\gamma$  and the heading (or azimuth) angle  $\chi$ , because the x-axis of the body frame coincides with the velocity vector of the s/c (also see Figure 6.1).

### 8.1.5. PROPULSION RF (P-FRAME)

The propulsion or thrust frame is a body frame where the x-axis is defined by the thrust vector. The y and z-axis are defined as depicted in Figure 8.5.

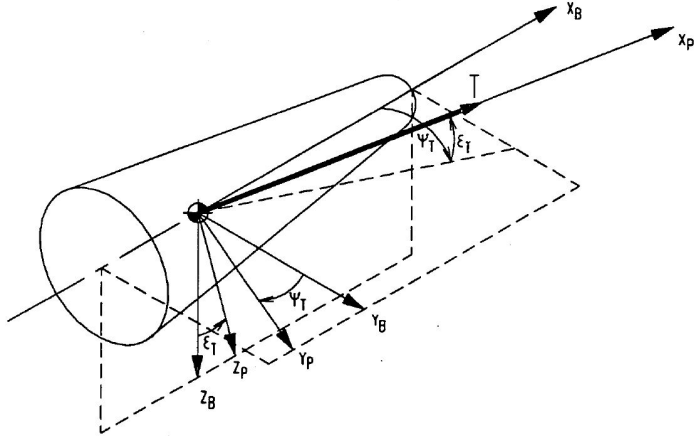


Figure 8.5: Propulsion frame relative to the body frame [7]

The B-frame and P-frame are related through the thrust elevation gimbal angle  $e_T$  and the thrust azimuth gimbal angle  $\psi_T$ .

## 8.2. TRANSFORMATION BETWEEN REFERENCE FRAMES

Because different problems and situations are easier to understand and to formulate in different RFs, it is important to understand how to transform from one RF to the other. In this case only transformations for a set point in time, called static transformations, are required for the described thesis problem. The required transformations from Chapter 6 are described in this section.

For transformation between two RFs, a correlation has to exist. This correlation (orientation) can be described using a set of angles, called the Euler angles, that can be described between the different RFs [15]. In a 3 dimensional space, there are three axes. So in order to get from one RF to the other, a maximum of 3 rotations (translations/transformations) have to take place; one over each axis. However, often fewer rotations are necessary because some of the axes are already properly aligned. Sometimes two reference frames are not directly related through known angles, which means that other (intermediate) RFs will have to be used. In this case more than 3 rotations are possible, but again a maximum of three rotations are needed to go from one RF to an intermediate RF given the known angles. Since a 3 dimensional space is described, three dimensional coordinates have to be translated to the next reference frame. For this, Cartesian coordinates are used. A rotation around the x-axis can be described by the change in the y and z coordinates due to an angle ( $\phi$ ) in the y-z plane as visualized in Figure 8.6. The rotation around the x-axis follows the R.H.R. of rotation, which states that if the thumb of your right hand is pointed in the axis direction, then the rest of your fingers show the direction of positive orientation. Therefore the described rotation is positive. Should the rotation have been to the other direction (clockwise around the x-axis as seen in Figure 8.6), the angle would have been negative. This is very important in transformations, and its usefulness becomes more obvious when more transformations are performed after each other. But first a system of equations is required to transform from the 'i' frame to the 'j' frame.

From Figure 8.6 a relation can be described between the coordinates in the 'i' frame and the 'j' frame in matrix form. This relation (convention as by [15]) is shown by Equation (8.1). Here  $\mathbf{r}$  is the state vector containing the coordinate values and  $T_x(\phi)$  represents the x-axis transformation matrix and is the standard matrix to be used if a transformation around an x-axis is performed. The only parameter that changes is the angle (and sometimes the sign of the angle as mentioned).

$$\begin{pmatrix} x \\ y \\ z \end{pmatrix}^j = \begin{bmatrix} 1 & 0 & 0 \\ 0 & \cos(\phi) & \sin(\phi) \\ 0 & -\sin(\phi) & \cos(\phi) \end{bmatrix} \begin{pmatrix} x \\ y \\ z \end{pmatrix}^i \Rightarrow \mathbf{r}^j = T_x(\phi) \mathbf{r}^i \quad (8.1)$$

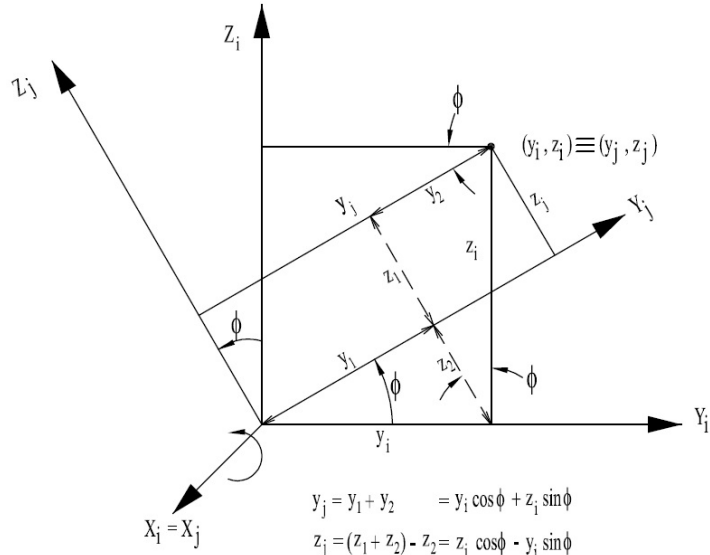


Figure 8.6: General rotation around the x-axis [15]

This rotation described by Figure 8.6 and Equation (8.1) can also be described for the y-axis and the z-axis. The complete set of axis transformation matrices is then presented in Equation (8.2).

$$\mathbb{T}_x(\phi) = \begin{bmatrix} 1 & 0 & 0 \\ 0 & \cos(\phi) & \sin(\phi) \\ 0 & -\sin(\phi) & \cos(\phi) \end{bmatrix}, \mathbb{T}_y(\phi) = \begin{bmatrix} \cos(\phi) & 0 & -\sin(\phi) \\ 0 & 1 & 0 \\ \sin(\phi) & 0 & \cos(\phi) \end{bmatrix}, \mathbb{T}_z(\phi) = \begin{bmatrix} \cos(\phi) & \sin(\phi) & 0 \\ -\sin(\phi) & \cos(\phi) & 0 \\ 0 & 0 & 1 \end{bmatrix} \quad (8.2)$$

From now on, the cosine notation will be shortened to 'c' and the sine notation will be shortened to 's' to make the transformation matrices more comprehensive. Also, because the matrices are orthogonal, the inverse of the matrix is simply the transpose of the matrix. And the inverse of a rotation matrix is the rotation in the other direction.

The order, or sequence, in which these transformations are performed is very important. This is because the sequence results in a matrix multiplication equation, and from linear algebra it is known that  $\mathbf{A} \cdot \mathbf{B} \neq \mathbf{B} \cdot \mathbf{A}$ . Therefore, if the sequence of transformations is not correct, the resulting RF will not be the desired RF. Also, as mentioned before, it is not always possible or easy to transform from one RF directly into the other. So usually one of the afore mentioned RF is used as an intermediate RF. It is therefore possible to transform from the P-frame all the way to the I-frame using all the other mentioned RFs with a maximum of three rotations between each frame. For convenience it has been chosen to adopt the convention mentioned in [14] and [15] to describe the transformations. Therefore the I-frame, R-frame, V-frame, B-frame and P-frame will be known as  $F_I$ ,  $F_R$ ,  $F_V$ ,  $F_B$  and  $F_P$  respectively when used to indicate the RFs in equations. And because these equations involve matrix multiplications, they have to be read from right to left. Therefore it can be said that the transformation matrix to go from  $F_B \rightarrow F_R$  is  $\mathbb{T}_{RB} = \mathbb{T}_{RV}\mathbb{T}_{VB}$ . This is one of the transformations required for the MAV trajectory. The other two transformations are more straight forward:  $F_P \rightarrow F_B$  is  $\mathbb{T}_{BP}$  and  $F_R \rightarrow F_I$  is  $\mathbb{T}_{IR}$ . For the  $\mathbb{T}_{IR}$  matrix, a transition is performed from  $F_R \rightarrow F_I$ . This is done over the angle  $\dot{\Omega}_t t_O$  as defined in Figure 8.2.  $\dot{\Omega}_t$  is the rotational velocity of Mars and  $t_O$  is the time from the set inertial frame. This is also where  $\Omega_{P0}$  is required (not depicted) since this angle describes the position of the prime meridian at the time that the inertial frame was set. Because the angle is defined east of the  $x_I$ -axis, it has to be subtracted from  $\dot{\Omega}_t t_O$  since  $\Omega_{P0}$  is defined positive in the same direction as  $\dot{\Omega}_t t_O$  which is defined to be positive going from  $x_I$  to  $x_R$ . The rotation around the z-axis is positive in the same direction according to the R.H.R. for rotation. In this case the rotation is performed in the negative direction around the z-axis with an angle  $-\dot{\Omega}_M t_O + \Omega_P$ . The complete RF transformation with the written out matrix for this rotation is given by Equation (8.3). Please note that the signs of the angles changed in the matrix due to the sine and cosine functions.

$$\mathbb{T}_{\text{IR}} = \left| \begin{array}{c} \mathbb{T}_{\text{z}}(-\dot{\Omega}_M t_O + \Omega_P) \\ \hline \text{I} \end{array} \right|_{\text{R}} = \begin{bmatrix} c(\dot{\Omega}_M t_O - \Omega_P) & -s(\dot{\Omega}_M t_O - \Omega_P) & 0 \\ s(\dot{\Omega}_M t_O - \Omega_P) & c(\dot{\Omega}_M t_O - \Omega_P) & 0 \\ 0 & 0 & 1 \end{bmatrix} \quad (8.3)$$

Here the vertical lines with the letter designations depict when a certain reference frame is reached. The same notation was already shown in Chapter 6. The transformations for  $\mathbb{T}_{\text{RB}}$  and  $\mathbb{T}_{\text{BP}}$  can now be written in a similar manner and are described in Equations (8.4) and (8.5) respectively.

$$\begin{aligned} \mathbb{T}_{\text{RB}} &= \left| \begin{array}{c} \mathbb{T}_{\text{z}}(-\tau) \mathbb{T}_{\text{y}}\left(\frac{\pi}{2} + \delta\right) \\ \hline \text{V} \end{array} \right|_{\text{B}} \mathbb{T}_{\text{z}}(-\chi) \mathbb{T}_{\text{y}}(-\gamma) \Big|_{\text{B}} = \\ &\left[ \begin{array}{ccc} c(-\tau) & s(-\tau) & 0 \\ -s(-\tau) & c(-\tau) & 0 \\ 0 & 0 & 1 \end{array} \right] \left[ \begin{array}{ccc} c\left(\frac{\pi}{2} + \delta\right) & 0 & -s\left(\frac{\pi}{2} + \delta\right) \\ 0 & 1 & 0 \\ s\left(\frac{\pi}{2} + \delta\right) & 0 & c\left(\frac{\pi}{2} + \delta\right) \end{array} \right] \left[ \begin{array}{ccc} c(-\chi) & s(-\chi) & 0 \\ -s(-\chi) & c(-\chi) & 0 \\ 0 & 0 & 1 \end{array} \right] \left[ \begin{array}{ccc} c(-\gamma) & 0 & -s(-\gamma) \\ 0 & 1 & 0 \\ s(-\gamma) & 0 & c(-\gamma) \end{array} \right] = \\ &\left[ \begin{array}{ccc} c(\tau) & -s(\tau) & 0 \\ s(\tau) & c(\tau) & 0 \\ 0 & 0 & 1 \end{array} \right] \left[ \begin{array}{ccc} -s(\delta) & 0 & -c(\delta) \\ 0 & 1 & 0 \\ c(\delta) & 0 & -s(\delta) \end{array} \right] \left[ \begin{array}{ccc} c(\chi) & -s(\chi) & 0 \\ s(\chi) & c(\chi) & 0 \\ 0 & 0 & 1 \end{array} \right] \left[ \begin{array}{ccc} c(\gamma) & 0 & s(\gamma) \\ 0 & 1 & 0 \\ -s(\gamma) & 0 & c(\gamma) \end{array} \right] = \\ &\left[ \begin{array}{ccc} c(\tau) & -s(\tau) & 0 \\ s(\tau) & c(\tau) & 0 \\ 0 & 0 & 1 \end{array} \right] \left[ \begin{array}{ccc} -s(\delta) & 0 & -c(\delta) \\ 0 & 1 & 0 \\ c(\delta) & 0 & -s(\delta) \end{array} \right] \left[ \begin{array}{ccc} c(\chi) c(\gamma) & -s(\chi) & c(\chi) s(\gamma) \\ s(\chi) c(\gamma) & c(\chi) & s(\chi) s(\gamma) \\ -s(\gamma) & 0 & c(\gamma) \end{array} \right] = \\ &\left[ \begin{array}{ccc} c(\tau) & -s(\tau) & 0 \\ s(\tau) & c(\tau) & 0 \\ 0 & 0 & 1 \end{array} \right] \left[ \begin{array}{ccc} -s(\delta) c(\chi) c(\gamma) + c(\delta) s(\gamma) & s(\delta) s(\chi) & -s(\delta) c(\chi) s(\gamma) - c(\delta) c(\gamma) \\ s(\chi) c(\gamma) & c(\chi) & s(\chi) s(\gamma) \\ c(\delta) c(\chi) c(\gamma) - c(\delta) s(\gamma) & -c(\delta) s(\chi) & c(\delta) c(\chi) s(\gamma) - s(\delta) c(\gamma) \end{array} \right] = \\ &\left[ \begin{array}{ccc} c(\tau)(-s(\delta) c(\chi) c(\gamma) + c(\delta) s(\gamma)) - s(\tau) s(\chi) c(\gamma) & c(\tau) s(\delta) s(\chi) - s(\tau) c(\chi) \\ s(\tau)(-s(\delta) c(\chi) c(\gamma) + c(\delta) s(\gamma)) + c(\tau) s(\chi) c(\gamma) & s(\tau) s(\delta) s(\chi) + c(\tau) c(\chi) \\ c(\delta) c(\chi) c(\gamma) - c(\delta) s(\gamma) & -c(\delta) s(\chi) \end{array} \right] \\ &\quad \text{Note: } c(\tau)(-s(\delta) c(\chi) s(\gamma) - c(\delta) c(\gamma)) - s(\tau) s(\chi) s(\gamma) \\ &\quad s(\tau)(-s(\delta) c(\chi) s(\gamma) - c(\delta) c(\gamma)) + c(\tau) s(\chi) s(\gamma) \\ &\quad c(\delta) c(\chi) s(\gamma) - s(\delta) c(\gamma) \quad (8.4) \end{aligned}$$

$$\begin{aligned} \mathbb{T}_{\text{BP}} &= \left| \begin{array}{c} \mathbb{T}_{\text{z}}(-\psi_T) \mathbb{T}_{\text{y}}(-\epsilon_T) \\ \hline \text{P} \end{array} \right| = \left[ \begin{array}{ccc} c(-\psi_T) & s(-\psi_T) & 0 \\ -s(-\psi_T) & c(-\psi_T) & 0 \\ 0 & 0 & 1 \end{array} \right] \left[ \begin{array}{ccc} c(-\epsilon_T) & 0 & -(-\epsilon_T) \\ 0 & 1 & 0 \\ s(-\epsilon_T) & 0 & c(-\epsilon_T) \end{array} \right] = \\ &\left[ \begin{array}{ccc} c(\psi_T) & -s(\psi_T) & 0 \\ s(\psi_T) & c(\psi_T) & 0 \\ 0 & 0 & 1 \end{array} \right] \left[ \begin{array}{ccc} c(\epsilon_T) & 0 & s(\epsilon_T) \\ 0 & 1 & 0 \\ -s(\epsilon_T) & 0 & c(\epsilon_T) \end{array} \right] = \left[ \begin{array}{ccc} c(\psi_T) c(\epsilon_T) & -s(\psi_T) & c(\psi_T) s(\epsilon_T) \\ s(\psi_T) c(\epsilon_T) & c(\psi_T) & s(\psi_T) s(\epsilon_T) \\ -s(\epsilon_T) & 0 & c(\epsilon_T) \end{array} \right] \quad (8.5) \end{aligned}$$

Occasionally transformation matrices can become rather complex and it is easy to make mistakes. Fortunately the motion of the orbiter is already known in Kepler elements. This means that for the gravitational accelerations caused by the Sun described in Equation (7.6), which are in the **MCI RF**, they can be directly transformed to the body fixed  $f_S$ ,  $f_N$  and  $f_W$  **RF**. From now on this **RF** is referred to as the Gaussian frame or  $F_G$ , which can be similar to the  $F_V$  frame but does not have to be. The transformation from  $F_I \rightarrow F_G$  follows from Figure 8.7 and is provided by the transformation convention and matrices described by Equations (8.6) and (8.7). In this case an intermediate reference frame is required which will be called  $F_{I''}$ , because two z-axis rotations are needed, but they are not in the same plane. It can also be seen that the position of the Prime meridian on the 1<sup>st</sup> of January 2000 at 12:00 is not important in this direct transformation and will only have to be taken into account in the transformation from  $F_R \rightarrow F_I$  for the **MAV**.

$$\mathbb{T}_{\text{GI}} = \mathbb{T}_{\text{GI''}} \mathbb{T}_{\text{I''I}} = \left| \begin{array}{c} \mathbb{T}_{\text{z}}(\omega + \theta) \\ \hline \text{G} \end{array} \right|_{\text{I''}} \mathbb{T}_{\text{x}}(i) \mathbb{T}_{\text{z}}(\Omega) \Big|_{\text{I}} \quad (8.6)$$

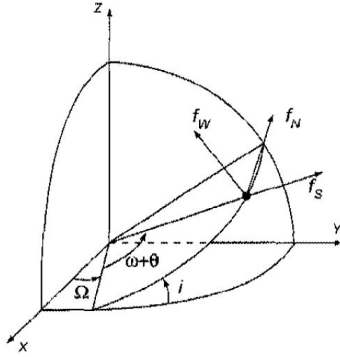


Figure 8.7: Relation between the MCI and the Gaussian body frame [10]

$$\begin{aligned}
 T_{GI} &= \begin{bmatrix} c(\omega + \theta) & s(\omega + \theta) & 0 \\ -s(\omega + \theta) & c(\omega + \theta) & 0 \\ 0 & 0 & 1 \end{bmatrix} \begin{bmatrix} 1 & 0 & 0 \\ 0 & c(i) & s(i) \\ 0 & -s(i) & c(i) \end{bmatrix} \begin{bmatrix} c(\Omega) & s(\Omega) & 0 \\ -s(\Omega) & c(\Omega) & 0 \\ 0 & 0 & 1 \end{bmatrix} \\
 &= \begin{bmatrix} c(\omega + \theta) & s(\omega + \theta) & 0 \\ -s(\omega + \theta) & c(\omega + \theta) & 0 \\ 0 & 0 & 1 \end{bmatrix} \begin{bmatrix} c(\Omega) & s(\Omega) & 0 \\ -c(i)s(\Omega) & c(i)c(\Omega) & s(i) \\ s(i)s(\Omega) & -s(i)c(\Omega) & c(i) \end{bmatrix} \\
 &= \begin{bmatrix} c(\omega + \theta)c(\Omega) - s(\omega + \theta)c(i)s(\Omega) & c(\omega + \theta)s(\Omega) + s(\omega + \theta)c(i)c(\Omega) & s(\omega + \theta)s(i) \\ -s(\omega + \theta)c(\Omega) - c(\omega + \theta)c(i)s(\Omega) & c(\omega + \theta)c(i)c(\Omega) - s(\omega + \theta)s(\Omega) & c(\omega + \theta)s(i) \\ s(i)s(\Omega) & -s(i)c(\Omega) & c(i) \end{bmatrix} \quad (8.7)
 \end{aligned}$$

### 8.3. TRANSFORMATION BETWEEN DIFFERENT COORDINATE SYSTEMS

In the previous sections the different RF and transformations were expressed using x, y and z-axes. These x, y and z-coordinates belong to the Cartesian coordinate system. However, during an integration, simulation or analysis it might be more useful and meaningful to express the position (and velocity) in a different coordinate system. Two other systems are the Spherical and Keplerian coordinate systems. How to transform back and forth from the Cartesian system to these other two systems will be explained in Sections 8.3.1 and 8.3.2 respectively and are based on [12]. The transformation from the Spherical coordinate system to Kepler elements is described in Section 8.3.3. Kepler elements are very useful for orbit computations, unfortunately singularities can occur if this coordinate system is used for certain equations. Therefore Section 8.3.4 will discuss a Non-singular form of the Kepler elements.

#### 8.3.1. SPHERICAL AND CARTESIAN

Spherical coordinates can be useful to determine the location of a satellite above Mars assuming that Mars is a perfect sphere. In this thesis problem, however, spherical coordinates are used during the MAV ascent simulation. The coordinate relation between spherical and Cartesian coordinates is shown in Figure 8.8. Based on this diagram, the relations to go from the spherical system to the Cartesian system are derived and are provided in Equation (8.8).

$$\begin{aligned}
 x &= r \cos(\delta) \cos(\lambda) \\
 y &= r \cos(\delta) \sin(\lambda) \\
 z &= r \sin(\delta)
 \end{aligned} \quad (8.8)$$

The velocities can be obtained by taking the time derivatives of these functions, resulting in the velocity expressions in x, y and z direction given by Equation (8.9). Differentiating those expressions again will result in the accelerations.

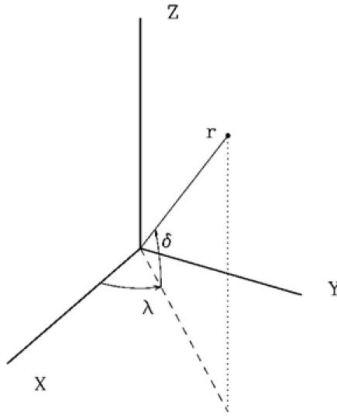


Figure 8.8: Relation between spherical position coordinates and Cartesian position coordinates [12]

$$\begin{aligned}\dot{x} &= \dot{r} \cos(\delta) \cos(\lambda) - r\dot{\delta} \sin(\delta) \cos(\lambda) - r\dot{\lambda} \cos(\delta) \sin(\lambda) \\ \dot{y} &= \dot{r} \cos(\delta) \sin(\lambda) - r\dot{\delta} \sin(\delta) \sin(\lambda) + r\dot{\lambda} \cos(\delta) \cos(\lambda) \\ \dot{z} &= \dot{r} \sin(\delta) + r\dot{\delta} \cos(\delta)\end{aligned}\quad (8.9)$$

The transformation from Cartesian coordinates to spherical coordinates can again be derived from Figure 8.8, resulting in the expressions presented in Equation (8.10).

$$\begin{aligned}r &= \sqrt{x^2 + y^2 + z^2} \\ \delta &= \arcsin\left(\frac{z}{r}\right) \\ \lambda &= \arctan\left(\frac{y}{x}\right)\end{aligned}\quad (8.10)$$

However, the expression for  $\lambda$  only results in a value between  $-\pi/2$  and  $\pi/2$ . Also, if  $x = 0$ , a singularity occurs. In order to solve this issue, the so-called 'atan2' function can be used. This function incorporates both sin and cosine values to provide a value for  $\lambda$  between 0 and  $2\pi$  [12].  $\lambda$  can then be expressed by Equation (8.11) where atan2 is defined by Figure 8.9<sup>4</sup>.

$$\lambda = \text{atan2}(y, x) \quad (8.11)$$

$$\text{atan2}(y, x) = \begin{cases} \text{atan}\left(\frac{y}{x}\right) & x > 0 \\ \pi + \text{atan}\left(\frac{y}{x}\right) & y \geq 0, x < 0 \\ -\pi + \text{atan}\left(\frac{y}{x}\right) & y < 0, x < 0 \\ \frac{\pi}{2} & y > 0, x = 0 \\ -\frac{\pi}{2} & y < 0, x = 0 \\ \text{Undefined} & y = 0, x = 0 \end{cases}$$

Figure 8.9: atan2 function evaluation conditions adapted from

<sup>4</sup>Online blog: <http://guihaire.com/code/?p=1168>

The time derivatives of these function can be taken to find the velocity expressions. The resulting velocity expressions are shown in Equation (8.12). The left expressions in this equation define the velocity characteristics as often expressed in the spherical coordinate system required for transformations.

$$\begin{aligned}\dot{r} &= \frac{x\dot{x} + y\dot{y} + z\dot{z}}{\sqrt{x^2 + y^2 + z^2}} & V &= \sqrt{\dot{x}^2 + \dot{y}^2 + \dot{z}^2} \\ \dot{\delta} &= \frac{x\dot{y} - y\dot{x}}{x^2 + y^2} & \gamma &= \arcsin \left[ \frac{\dot{r}}{V} \right] \\ \dot{\lambda} &= \frac{r\dot{z} - z\dot{r}}{r^2 \sqrt{1 - \left( \frac{z}{r} \right)^2}} & \chi &= \arccos \left[ \frac{r\dot{\delta}}{V \cos(\gamma)} \right]\end{aligned}\quad (8.12)$$

### 8.3.2. KEPLERIAN AND CARTESIAN

The relation between the Keplerian and Cartesian systems is slightly more complex. Figure 8.10 shows the Kepler elements:  $a$  (semi-major axis),  $e$  (eccentricity, not shown but is a ratio that determines the elliptic properties of an orbit),  $i$  (inclination),  $\omega$  (argument of perigee),  $\Omega$  (right ascension of the ascending node) and  $\theta$  (True anomaly). Often, however, the mean anomaly  $M$  is used instead of the true anomaly. The mean anomaly is defined to be the angle between the semi-major axis and line between the centre of the orbit and the mean position of the orbiting body in the auxiliary circle that can be drawn around the orbit. The mean position of the orbiting body is determined by assuming a constant rotational speed in this circular orbit with the same orbital time as the actual orbit.

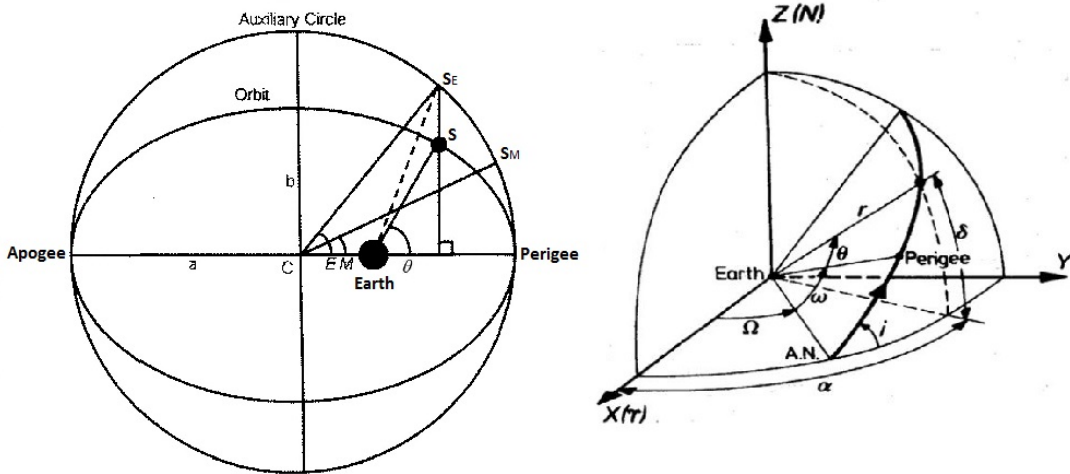


Figure 8.10: Definition of the Kepler elements in 2D (left) and 3D (right) [12, 13]

The transformation from Kepler to Cartesian consists of a number of steps starting with the mean anomaly and eccentricity. Both these values have to be used to determine the eccentric anomaly  $E$  and in turn the true anomaly  $\theta$ . The eccentric anomaly is computed by rewriting the first expression of Equation (8.13) into the second expression [12].

$$\begin{aligned}M &= E - e \cdot \sin E \\ E_{i+1} &= E_i + \frac{M - E_i - e \cdot \sin E_i}{1 - e \cdot \cos(E_i)}\end{aligned}\quad (8.13)$$

The determination of  $E$  is an iterative process. First a decent estimate of  $E$  has to be provided (it is best to use the value for  $M$  for this) and then a new  $E$  can be computed. This has to be done until the desired level of precision is reached. Then the true anomaly can be computed using this  $E$  as shown by Equation (8.14).

$$\theta = 2 \cdot \arctan \left[ \tan \left( \frac{E}{2} \right) \sqrt{\frac{1+e}{1-e}} \right]\quad (8.14)$$

With the true anomaly known, the radial distance from the orbiting body to the centre of Mars  $r$  can be determined using Equation (8.15)

$$r = \frac{a \cdot (1 - e^2)}{1 + e \cos(\theta)} \quad (8.15)$$

The Cartesian coordinates can now be computed using the expression in Equation (8.18) with the matrix entries provided by Equation (8.17)[12].

$$\begin{pmatrix} x \\ y \\ z \end{pmatrix} = \begin{bmatrix} l_1 & l_2 \\ m_1 & m_2 \\ n_1 & n_2 \end{bmatrix} \begin{pmatrix} r \cos(\theta) \\ r \sin(\theta) \end{pmatrix} \quad (8.16)$$

$$\begin{aligned} l_1 &= \cos(\Omega) \cos(\omega) - \sin(\Omega) \sin(\omega) \cos(i) \\ l_2 &= -\cos(\Omega) \sin(\omega) - \sin(\Omega) \cos(\omega) \cos(i) \\ m_1 &= \sin(\Omega) \cos(\omega) + \cos(\Omega) \sin(\omega) \cos(i) \\ m_2 &= -\sin(\Omega) \sin(\omega) + \cos(\Omega) \cos(\omega) \cos(i) \\ n_1 &= \sin(\omega) \sin(i) \\ n_2 &= \cos(\Omega) \sin(i) \end{aligned} \quad (8.17)$$

Equation (8.18) then provides the expressions for  $x$ ,  $y$  and  $z$ .

$$\begin{aligned} x &= r \cdot [\cos(\Omega) \cos(\omega + \theta) - \sin(\Omega) \sin(\omega + \theta) \cos(i)] \\ y &= r \cdot [\sin(\Omega) \cos(\omega + \theta) - \cos(\Omega) \sin(\omega + \theta) \cos(i)] \\ z &= r \sin(i) \sin(\omega + \theta) \end{aligned} \quad (8.18)$$

For the velocity values, an extra parameter is required. This parameter is called the specific relative angular momentum  $h$ . Assuming that the mass of the orbiting body can be neglected with respect to the planet (or other celestial body) it is orbiting,  $h$  can be expressed as a function of the standard gravitational parameter of that planet  $\mu$ ,  $a$  and  $e$  as shown by Equation (8.19).

$$h = \sqrt{\mu a \cdot (1 - e^2)} \quad (8.19)$$

Then with  $h$  and the expression from Equation (8.17), the velocities can be expressed by Equation (8.20).

$$\begin{aligned} \dot{x} &= \frac{\mu}{h} [-l_1 \sin(\theta) + l_2 \cdot (e + \cos(\theta))] \\ \dot{y} &= \frac{\mu}{h} [-m_1 \sin(\theta) + m_2 \cdot (e + \cos(\theta))] \\ \dot{z} &= \frac{\mu}{h} [-n_1 \sin(\theta) + n_2 \cdot (e + \cos(\theta))] \end{aligned} \quad (8.20)$$

It is also possible to convert from the Cartesian system back to the Kepler system, however, this requires more steps and intermediate expressions. First, it is convenient to express the position and velocity both in one vector each as shown by Equation (8.21).

$$\begin{aligned} \mathbf{R} &= [x \quad y \quad z] \\ \mathbf{V} &= [\dot{x} \quad \dot{y} \quad \dot{z}] \end{aligned} \quad (8.21)$$

The cross product of these two ( $\mathbf{R} \times \mathbf{V}$ ) will result in the specific relative angular momentum vector  $\mathbf{H}$  and the scalar values, or lengths, can then be represented by  $r = \|\mathbf{R}\|$ ,  $V = \|\mathbf{V}\|$  and  $h = \|\mathbf{H}\|$ . Also, a vector  $\mathbf{N}$  can be defined as shown by Equation (8.22)[12].

$$\mathbf{N} = \begin{pmatrix} 0 \\ 0 \\ 1 \end{pmatrix} \times \mathbf{H} \quad (8.22)$$

With these parameters set, the first four Kepler elements ( $a$ ,  $e$ ,  $i$  and  $\Omega$ ) can be computed as shown by Equation (8.23). Here, the value for the eccentricity can be obtained by taking the length of the vector:  $e = \|\mathbf{e}\|$ . Also,  $\mathbf{H}(3)$  is the third value of the specific relative angular momentum vector, so the value in the z-direction. The same principle holds for the values from  $\mathbf{N}$ .

$$\begin{aligned} a &= \left( \frac{2}{r} - \frac{V^2}{\mu} \right)^{-1} \\ \mathbf{e} &= \frac{\mathbf{V} \times \mathbf{H}}{\mu} - \frac{\mathbf{R}}{r} \\ i &= \arccos \left( \frac{\mathbf{H}(3)}{h} \right) \\ \Omega &= \text{atan2}(\mathbf{N}(2), \mathbf{N}(1)) \end{aligned} \quad (8.23)$$

For the computation of the values for  $\omega$  and  $\theta$ , three unit vectors are needed:  $\hat{\mathbf{N}} = \frac{\mathbf{N}}{\|\mathbf{N}\|}$ ,  $\hat{\mathbf{e}} = \frac{\mathbf{e}}{\|\mathbf{e}\|}$  and  $\hat{\mathbf{R}} = \frac{\mathbf{R}}{\|\mathbf{R}\|}$ . This leads to the conditional expressions seen in Equation (8.24).

$$\begin{aligned} \omega &= \begin{cases} \arccos(\hat{\mathbf{e}} \cdot \hat{\mathbf{N}}), & \text{if } (\hat{\mathbf{N}} \times \mathbf{e}) \cdot \mathbf{H} > 0 \\ -\arccos(\hat{\mathbf{e}} \cdot \hat{\mathbf{N}}), & \text{otherwise} \end{cases} \\ \theta &= \begin{cases} \arccos(\hat{\mathbf{R}} \cdot \hat{\mathbf{e}}), & \text{if } (\mathbf{e} \times \mathbf{R}) \cdot \mathbf{H} > 0 \\ -\arccos(\hat{\mathbf{R}} \cdot \hat{\mathbf{e}}), & \text{otherwise} \end{cases} \end{aligned} \quad (8.24)$$

The eccentric anomaly can now be computed using  $\theta$  and  $e$  as shown by Equation (8.25), which is the rewritten form of Equation (8.14).

$$E = 2 \cdot \arctan \left[ \tan \left( \frac{\theta}{2} \right) \sqrt{\frac{1-e}{1+e}} \right] \quad (8.25)$$

And finally, the mean anomaly can be found using Equation (8.13)[12].

### 8.3.3. SPHERICAL AND KEPLERIAN

Often it is required to transform the spherical coordinates into Kepler elements. Wakker [108] provides this direct transformation through the relations provided in Equation (8.26). In this case the expressions are written explicitly for Mars by using  $\mu_M$ .

$$\begin{aligned} a &= \frac{r}{2 - \frac{rV^2}{\mu_M}} \\ e &= \sqrt{1 - \frac{rV^2}{\mu_M} \left( 2 - \frac{rV^2}{\mu_M} \right) \cos^2(\gamma)} \\ i &= \arccos(\cos(\delta) \sin(\chi)) \\ \theta &= 2 \arctan \left[ \sqrt{\frac{1+e}{1-e}} \tan \left( \frac{E}{2} \right) \right], \quad \text{where} \quad E = \arctan \left[ \sqrt{\frac{a}{\mu_M}} \frac{rV \sin(\gamma)}{a-r} \right] \\ \omega &= \frac{\sin(\delta)}{\sin(i)} - \theta \\ \Omega &= \lambda - \arccos \left[ \frac{\cos(\chi)}{\sin(i)} \right] \end{aligned} \quad (8.26)$$

Then the spherical coordinates can be computed by rewriting the expressions provided in Equation (8.26) to the spherical coordinates. These rewritten expressions are shown in Equation (8.27).

$$\begin{aligned}
r &= a(1 - e \cos(E)), \quad \text{where} \quad E = 2 \arctan \left[ \sqrt{\frac{1-e}{1+e}} \tan \left( \frac{\theta}{2} \right) \right] \\
V &= \sqrt{\mu_M \left( \frac{2}{r} - \frac{1}{a} \right)} \\
\gamma &= \arcsin \left[ e \sin(E) \frac{\sqrt{\mu_M a}}{r V} \right] \\
\delta &= \arcsin [\sin(\omega + \theta) \sin(i)] \\
\lambda &= \arcsin \left[ \frac{\tan(\delta)}{\tan(i)} \right] - \Omega \\
\chi &= \arccos \left[ \cos(\omega + \theta) - \frac{\sin(i)}{\cos(\delta)} \right]
\end{aligned} \tag{8.27}$$

### 8.3.4. NON-SINGULAR KEPLER ELEMENTS (MEE)

As mentioned in Chapter 7, during the calculation of the change in orbital elements some of the Kepler elements cannot assume every possible value. Singularities occur when  $e = 0$ , and/or  $i = 0^\circ$  or  $180^\circ$ . In Section 7.3 it was mentioned that MEE are chosen in order to avoid these singularities. The transformation from the ordinary Kepler elements to the MEE was already provided in Equation (7.2) and is repeated here once more as shown in Equation (8.28). This equation also includes the expressions to revert back to normal Kepler elements (see left equations). Here  $I$  is the retrograde factor and has a value of +1 for posigrade orbits and -1 for retrograde orbits. This is done to avoid singularities when  $i = 180^\circ$  and thus making the set non-singular.

$$\begin{aligned}
p &= a(1 - e^2) & a &= \frac{p}{1 - (f^2 + g^2)} \\
f &= e \cos(\omega + I\Omega) & e &= \sqrt{f^2 + g^2} \\
g &= e \sin(\omega + I\Omega) & i &= 2 \tan^{-1} \left[ \sqrt{h^2 + k^2} \right] \\
h &= \tan^I \left( \frac{i}{2} \right) \cos(\Omega) & \omega &= L - \theta - I\Omega \\
k &= \tan^I \left( \frac{i}{2} \right) \sin(\Omega) & \Omega &= a \tan 2(k, h) \\
L &= \omega + \theta + I\Omega & \theta &= L - \arccos \left[ \frac{f}{e} \right]
\end{aligned} \tag{8.28}$$

# 9

## MARS ATMOSPHERIC MODEL

During the ascent the MAV will pass through the Martian atmosphere, which will result in a drag force opposite to the velocity direction. This drag force  $D = f(\rho, \mathcal{A})$  where  $\rho$  is the air density and  $\mathcal{A}$  is the speed of sound ( $D = f(C_D)$ ,  $C_D = f(\mathcal{M})$  and  $\mathcal{M} = f(\mathcal{A})$ ). The speed of sound can be written as Equation (9.1) for an ideal gas, where  $\gamma_{\mathcal{A}}$  is the adiabatic index (or isentropic expansion factor) of the Martian atmosphere,  $R_{\mathcal{A}}$  is the molar gas constant,  $T_{\mathcal{A}}$  is the absolute temperature and  $M_{\mathcal{A}}$  is the molar mass of the Martian atmosphere.

$$\mathcal{A} = \sqrt{\frac{\gamma_{\mathcal{A}} R_{\mathcal{A}} T_{\mathcal{A}}}{M_{\mathcal{A}}}} \quad (9.1)$$

The temperature depends on the altitude and should be provided by the atmospheric model. Both  $\gamma_{\mathcal{A}}$  and  $M_{\mathcal{A}}$  depend on the gas composition of the atmosphere. According to [107] the atmosphere has a volumetric composition of 95.32% Carbon dioxide, 2.7% Nitrogen, 1.6% Argon, 0.13% Oxygen and 0.08% Carbon monoxide. This results in a mean molecular weight of 0.04334 kg/mol for the Martian atmosphere. Also, in [128] the adiabatic index  $\gamma_{\mathcal{A}}$  is assumed to have a value of  $\sim 1.35$  for Mars.

Now the only two variables that are required from the atmospheric model are the density  $\rho$  and the absolute temperature  $T_{\mathcal{A}}$  at a certain point in the atmosphere. Another method would be to write the speed of sound as a function of the air density and the pressure  $p_{\mathcal{A}}$  (instead of absolute temperature). In this case the expression for  $\mathcal{A}$  is provided by Equation (9.2).

$$\mathcal{A} = \sqrt{\frac{\gamma_{\mathcal{A}} p_{\mathcal{A}}}{\rho}} \quad (9.2)$$

It would be an asset if the speed of sound can be provided directly, because this alleviates the uncertainty caused by the adiabatic index  $\gamma_{\mathcal{A}}$ . In this chapter the atmospheric models that were used in reference research will be described in Section 9.1 and the preferred atmospheric model will be determined Section 9.2.

### 9.1. REFERENCE ATMOSPHERIC MODELS

During the simulation of the MAV launch, the reference research mentioned in Chapter 3 used different models and assumptions. It is useful to understand which atmospheric model was used and why. It is also important to determine why a certain model would be appropriate to use in this thesis problem. The reference research and their models are provided in Table 9.1. It is interesting to see that either an exponential density model was used, or a model called Mars-GRAM.

The exponential density model is based on the assumption that the density decreases exponentially with increased altitude. For a given altitude  $h$  the local density can be directly computed using Equation (9.3) [8]. Here,  $\rho_0$  is the atmospheric density at zero elevation and  $H_s$  is the scale-height.

$$\rho = \rho_0 \exp\left(-\frac{h}{H_s}\right) \quad (9.3)$$

Table 9.1: Mars atmospheric models used in reference research

Person	Year of research/publication	Atmospheric model used
Fanning and Pierson [8]	1996	Exponential density model (scale-height 11.17 km) and constant $C_D$ ( $\approx 0.88$ )
Desai et al. [18]	1998	Mars-GRAM
Whitehead [9, 19]	2004	Exponential fit to Viking density data (scale-height 8.3 km) and constant $\mathcal{A}$ (250 m/s)
Trinidad et al. [3]	2012	2010 Mars-GRAM

Similarly, the pressure can be assumed to decrease exponentially with increased altitude as well as shown by Equation (9.4). Here  $p_0$  is the atmospheric pressure at zero elevation.

$$p = p_0 \exp\left(-\frac{h}{H_s}\right) \quad (9.4)$$

In Equations (9.1) to (9.4) the same  $H_s$  is used, which means that a constant temperature is assumed and also results in a constant speed of sound ([107] mentions a scale-height of 11.1 km). However, a range of temperatures can be taken into account by selecting different scale-heights for both density and pressure. The scale-height can also be used to simulate different seasons. For each season a different scale-height can be selected to simulate the change in atmospheric conditions. Using this method, both pressure and density can be evaluated directly for every point in the trajectory, however some accuracy is lost due to all the assumptions.

Mars-GRAM is a more sophisticated model that can be used for high-fidelity simulations [129]<sup>1</sup>. It can provide density, temperature and pressure data (among other data). However, since it is such a detailed model, each evaluation requires considerable cpu time and also computes unnecessary data, or overhead, but it is very accurate. The model can even simulate different seasons by itself. One option to reduce the cpu time would be to only evaluate Mars-GRAM every so often. Another option would be to use a hybrid form of both the exponential atmosphere model and Mars-GRAM. Mars-GRAM could for instance be used to determine the scale-height and then the exponential model could determine the density and pressure at each path point.

## 9.2. CHOSEN ATMOSPHERIC MODEL

It was already mentioned that the two main output requirements are either  $\mathcal{A}$  and  $\rho$ , or  $T_{\mathcal{A}}$  and  $\rho$ , or  $p_{\mathcal{A}}$  and  $\rho$ . Two other requirements are the speed at which the model can be evaluated for the current path point and the accuracy at which this is done. Finally, the model should be available to use in the thesis problem. With these requirements, a trade-off table was created to compare both models and determine the most appropriate one, see Table 9.2. Every requirement is assigned a weight depending on how important the requirement is. Then the different models are either green (1), yellow (0.5) or red (0) for every requirement. This results in a final score. It can be seen that the limited Mars-GRAM model fits best with the set requirements and is therefore the preferred model to be used in the thesis problem.

Table 9.2: Atmospheric model trade-off table

	$\rho$	$p_{\mathcal{A}}$	$T_{\mathcal{A}}$	$\mathcal{A}$	Evaluation speed	Accuracy	Availability	Score
Weight	5	2	4	1	3	4	5	
Exponential	Green	Green	Red	Red	Green	Red	Green	15
Mars-GRAM	Green	Green	Green	Red	Red	Green	Green	20
Limited Mars-GRAM	Green	Green	Red	Red	Yellow	Green	Green	21.5
Hybrid	Green	Green	Red	Red	Green	Yellow	Green	17

<sup>1</sup>NASA website: <https://see.msfc.nasa.gov/model-Marsgram>

# 10

## PROPOSED SOFTWARE

Time can be saved by using already written and validated software. Many of the software packages that are used at [JPL](#) fall under the International Traffic in Arms Regulations ([ITAR](#)). This means that the software cannot be used directly by foreign nationals, however some of the tools that are used in those software packages are commercially available. The [JPL](#) software can however still be used as a validation tool for the software that will be written during the course of this thesis project. In that case, a [JPL](#) employee will simulate the trajectory with the same conditions as the written software and the results can be compared to each other. For the optimisation and the Q-law, there is software available that can be integrated into the newly written software. In Section 10.1 the different existing software packages that will be used are described and any adjustments that will have to be made to the software is described in Section 10.2.

### 10.1. EXISTING SOFTWARE PACKAGES

As was discussed in Section 4.6.2 there is already software available for the local optimisation of the [MBH](#) method. Also, for the implementation of the non-singular form of the Q-law, software written by Warren Gebbett [116] will be used. During the ascent, Mars-[GRAM](#) 2010 (originally developed in the '90s) will be used to simulate the Martian atmospheric conditions. In order to determine the influence of perturbations and shadowing by the Sun, information on the relative position of the Sun with respect to Mars is required as well [116]. This information (Ephemeris) is provided by Spacecraft Planet Instrument C-Matrix Events ([SPICE](#)) (created by the Navigation and Ancillary Information Facility ([NAIF](#)) in the '80s [130]). More information on the software packages is provided in Table 10.1.

Table 10.1: Required existing software

Subject	Software	Developer	Year	Language	Provided by
Optimisation	<a href="#">SNOPT</a>	Gill et al. [84]	2002	Fortran 77	TU Delft and <a href="#">JPL</a>
Q-law	Non-singular simplified Q-law	Gebbett [116]	2013	C++	Gebbett
Ascent	Mars- <a href="#">GRAM</a> 2010	Justus [131]	2010	Fortran 90/95 <sup>1</sup>	<a href="#">JPL</a>
Q-law	<a href="#">SPICE</a>	<a href="#">NAIF</a> <sup>2</sup>	2014	Matlab	<a href="#">JPL</a>

The first three programs can be called by Matlab, which makes it possible to incorporate them into the software that will be written and [SPICE](#) is already available in a Matlab format.

### 10.2. ADJUSTMENTS TO THE SOFTWARE

[SNOPT](#) will be used in the [MBH](#) optimisation method and will probably not require any adjustments. Also, both [SPICE](#) and Mars-[GRAM](#) 2010 will solely be used for their outputs, which means that they can be run separately from the optimiser and also will not need to be changed. The only software that will have to be

<sup>1</sup>NASA website: <https://see.msfc.nasa.gov/model-Marsgram>

<sup>2</sup>NASA website: <https://naif.jpl.nasa.gov/naif/spicehistory.html>

updated for this particular thesis problem is the non-singular simplified Q-law program written by Gebbett. The (possible) changes and additions are listed.

**Integrator** In the current version, an Adams-Moulton multi-step integrator is used for the integration of the [MEEs](#) [116], however, this integrator could be replaced by either the simpler [RK4](#), or the more complex [TSI](#) integrator to observe the effects and efficiency.

**Planet** The thesis problem will be situated around Mars, however Gebbett performed his research around the Earth. This is why the software will have to be changed to a Mars setting.

**Penalty function** In the original Q-law a penalty function for the minimum periapsis was used to prevent the [s/c](#) from flying too close to the planet during the trajectory simulation. Gebbett's simplified version does not include this penalty function. But since the Mars 2022 orbiter will be in a low Mars orbit, it might be useful to add this penalty function to the non-singular Q-law to improve the behaviour of the trajectory simulation.

**Language** Currently the non-singular simplified Q-law is written in C++. However, it has been suggested by Gebbett (and it is preferred) to write the tool in Matlab, which will make it easier to call upon the other required functions and change it when necessary.

It could be that more changes are required when actually using the software, but these are the (possible) required changes envisioned at this time.

# 11

## FINAL SUBJECT DEFINITION AND THESIS PROPOSAL

The final subject definition is based on the work performed in this literature study and the early proposal provided in Chapter 2. The updated version of this proposal is provided in Section 11.1. Also, in order to prepare for the thesis, an initial schedule is provided which spans the 7 months that are available for the thesis work. This schedule is based on the updated research questions and is shown in Section 11.2.

### 11.1. FINAL REFINED THESIS TOPIC AND RESEARCH QUESTIONS

In this section the final proposal is discussed. The final working title is "**MSR MAV ascent and Mars 2022 orbiter optimised single-revolution rendezvous in Mars orbit.**"

#### 11.1.1. RESEARCH OBJECTIVE

The objective of this research is to find the optimum combination of the high-thrust MAV launch trajectory and the low-thrust Mars 2022 orbiter trajectory to be able to perform a single-revolution rendezvous in Mars orbit and returning the orbiter to a safe distance from Mars by using Q-law for the low-thrust trajectory propagation and optimising the entire process, using DE combined with and compared to MBH, for both mass and ToF.

#### 11.1.2. RESEARCH PERSPECTIVE

It will be both Theory-testing research (Q-law, DE and MBH) and Problem-analysis research (optimum problem). The problem will be solved through the writing and validation of an optimisation program based on orbital mechanics and from a(n) (initial) mission design standpoint. It is therefore an engineering problem, and was drawn up through discussions between researcher, supervisors and stakeholders.

#### 11.1.3. RESEARCH FRAMEWORK

The framework has been set-up based on the guidelines provided in Research Methodologies and the corresponding literature [16] and is visualized in Figure 11.1. This new framework is slightly different from the previous one in that the research (a) has already been performed in this literature study and the objectives have changed slightly.

*Formulation:* (a) the study of the different theories and the preliminary research will result in a model (b) that can be used to write and validate an optimisation program to optimise for the different parameters and assess the application of Q-law in a Mars problem. (c) A comparison of the different optimisation results will help (d) establish the recommendations for the optimum MAV and orbiter rendezvous above Mars.

#### 11.1.4. RESEARCH QUESTIONS

The corresponding research questions are split up into primary and secondary research questions. The primary research questions have to be answered during the thesis work, the secondary research questions can be answered provided there is enough time. The primary research questions are listed here:

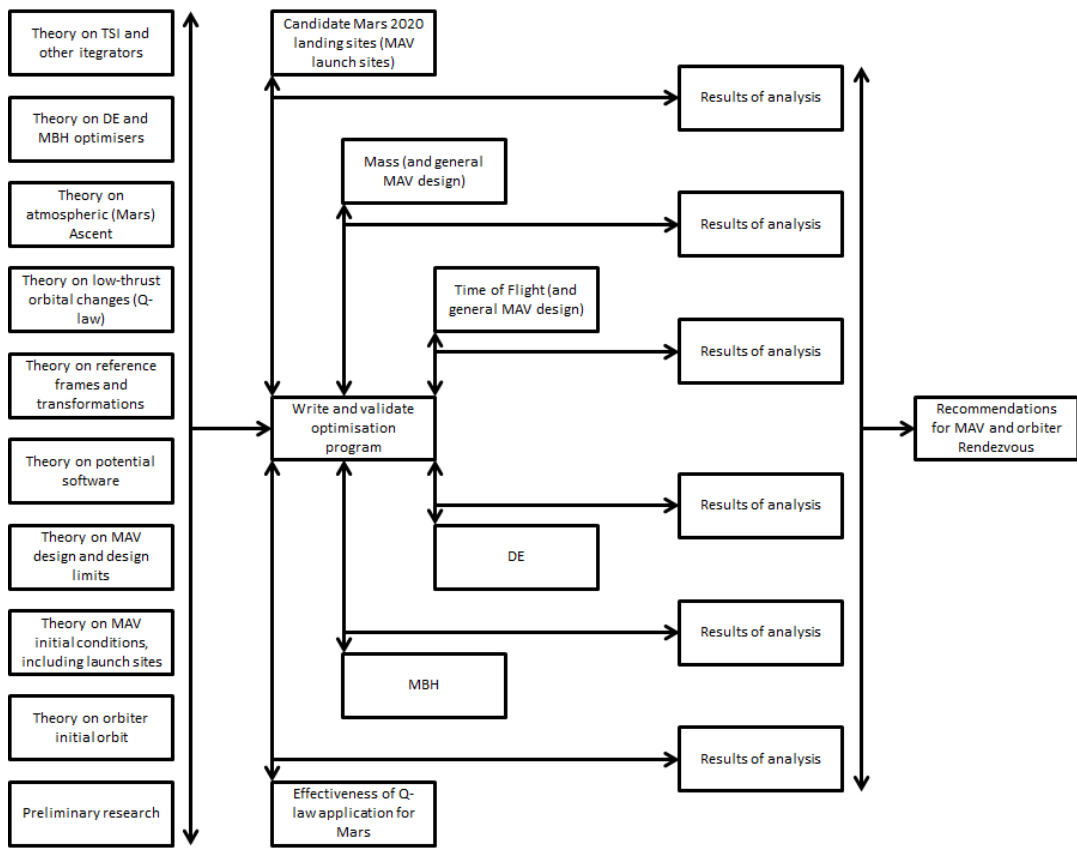


Figure 11.1: Research framework for the literature study (a) and the thesis work (b, c &amp; d)

- Does the single-revolution strategy improve the mass and ToF characteristics of the MSR mission?
  - What is the lowest mass and corresponding ToF using the single-revolution strategy?
  - What is the lowest mass and corresponding ToF using the multi-revolution strategy?
- Which of the current proposed Mars 2020 landing sites would be best considering the MSR mission.
  - Which proposed landing sites provide the best optimum solution for the thesis problem?
  - Which proposed landing sites provide the worst optimum solution for the thesis problem?
- What are the different optimal rendezvous situations given different design choices?
  - In what way does the orbit of the orbiter have to change in order to reach the desired rendezvous point based on the design choices?
  - What is the best MAV configuration and launch parameters in order to reach the desired rendezvous point based on the design choices?
  - Which rendezvous point and combination of parameters results in the lowest mass requirements and fits within the design space.
  - Which rendezvous point and combination of parameters results in the lowest ToF and fits within the design space.
- Which of the two (or what kind of combination of the two) optimisation methods works best in this kind of trajectory optimisation problem?
  - What are the advantages and disadvantages of DE in this particular problem?
  - What are the advantages and disadvantages of MBH in this particular problem?

- Which of the two (or what kind of combination of the two) optimisation methods provides the best combination of accuracy and speed for the ascent trajectory?
- Which of the two (or what kind of combination of the two) optimisation methods provides the best combination of accuracy and speed for the orbiter trajectory?
- Which of the two (or what kind of combination of the two) optimisation methods provides the best combination of accuracy and speed for the combined problem?
- What is the performance of the non-singular Q-law in a Mars environment?
  - Which set of weights produce the best results considering the mass and [ToF](#) for a Mars problem?
  - How does the introduction of the penalty function in the non-singular Q-law effect the optimal condition?

The secondary research questions are listed here:

- Would [TSI](#) be a good alternative for use in future optimisation programs?
  - How much more (or less) accurate is [TSI](#) compared to the other chosen integration methods?
  - How much faster (or slower) is [TSI](#) compared to the other chosen integration methods?
  - What are the advantages and disadvantages (besides the first two sub-questions) when using [TSI](#) in this kind of trajectory optimisation problem?

### 11.1.5. RESEARCH STRATEGY

The first step will be to design the optimisation program architecture, which will include both [DE](#) and [MBH](#) and combinations of the two. Initially the complete architecture to solve the thesis problem will be designed. Once this architecture is known, it will be split up into two sub-architectures: Mars ascent and orbiter manoeuvres. This is done such that both these aspects can first be tested separately. When all architectures have been completed, the Mars ascent simulation program will be written and validated. First for the Moon using Apollo reference data reaching a specific orbit, then the same is done for Mars neglecting the atmosphere and validating it using the same conditions in [JPL](#) software and finally the atmosphere is added and again validated with the [JPL](#) software. This is initially written in order to reach one specific orbit without optimisation, after which the optimisation is included. The optimisers are then validated separately from the simulator as well. Once the program works for a specific orbit, the precise point in that orbit at a certain point in time is also added. After this, the orbiter simulation program will be written and validated. First it is validated for the Earth and then the parameters are changed to the Martian system. Again this first only includes a target orbit and specified weights and afterwards the optimisation is included. Finally, both programs will be combined to create the final simulation and optimisation program. At this time it will be important to identify the different possible combinations of the optimisers and program the different options into the simulation program as well. During the entire process, everything will be documented. Once the simulation program has been completely validated, the initial conditions are set and the optimisation process is started. For one of the candidate landing sites, and each of the optimisers and combination of optimisers, the lowest mass condition and the lowest [ToF](#) condition can be found. Both these processes will be used to determine the best optimiser or combination of optimisers. Once the final optimiser is chosen all intermediate conditions, for mass versus [ToF](#), can be found creating a range of options for each landing site, which will then be used to provide recommendations.

### 11.1.6. RESEARCH METHOD

The research will be performed using a self-written simulation program and validated with Apollo flight data and programs used by [JPL](#).

## 11.2. PROPOSED TIME SCHEDULE

The proposed time schedule is based on the research strategy described in Section 11.1.5. The total time that has to be spent on the thesis project is 1176 hours, or approximately 30 weeks. This schedule does not include any specific dates yet but describes the work that will have to be done per week up to the 30th week of the thesis project. It also includes the different official meetings. The schedule is presented in Table 11.1.

Table 11.1: Proposed time schedule thesis project

Task	Task description	Weeks required	Week number
Architecture	Design the optimisation program architectures	2	1-2
Kick-off	Kick-off session with supervisors	0 (1 day)	2
Mars ascent programming phase 1	Writing the initial Mars ascent simulation program and validating it for the moon (specific orbit)	2	3-4
Mars ascent programming phase 2	Validating against <a href="#">JPL</a> software, first without and then including the atmosphere (specific orbit)	2	5-6
Mars ascent programming phase 3	Including the optimisation (specific orbit) and validation of the optimisers	2	7-8
Mars ascent programming phase 4	Including the specific point and time and validation using <a href="#">JPL</a> software	1	9
Documenting	Finish documentation on the Mars ascent simulation program	1	10
Orbiter trajectory programming phase 1	Writing the initial Mars orbiter trajectory simulation program (non-singular Q-law) and validation of Q-law for Earth using <a href="#">JPL</a> software	2	11-12
Orbiter trajectory programming phase 2	Include the option for a penalty function and validate using <a href="#">JPL</a> software	2	13-14
Orbiter trajectory programming phase 3	Changing all parameters to a Mars system and validating against <a href="#">JPL</a> software	1	15
Orbiter trajectory programming phase 4	Including the optimisation for the weights	1	16
Documenting	Finish documentation on the Mars orbiter trajectory simulation program	1	17
Mid-term review	Mid-term review with supervisors	0 (1 day)	17
Combining both programs	Combine the two programs to create the full simulation and optimisation program	1	18
Different optimiser combinations	Identify the different possible combinations of the optimisers and program them as options into the simulation program	1	19
Documenting	Finish documentation on the complete program	1	20
Simulation and optimisation phase 1	Optimising for lowest mass	1	21
Simulation and optimisation phase 2	Optimising for lowest <a href="#">ToF</a>	1	22
Best optimiser	Determine the best optimiser or best combination of optimisers for the thesis problem	1	23
Documenting	Finish documentation on the initial simulations and the best optimiser	1	24
Simulation and optimisation phase 3	Complete all simulations and find optimal conditions for all mass versus <a href="#">ToF</a> for every landing site	2	25-26
Green light review	Green light review with supervisors	0 (1 day)	26
Documenting	Finish documentation on all results	2	27-28
Conclusions and rec.	Draw conclusions and write recommendations	1	29
Documenting	Finish the complete thesis report	1	30
Thesis hand-in	Hand in of the complete thesis report	0 (1 day)	30

# BIBLIOGRAPHY

- [1] D. Stephenson, *Mars ascent vehicle - concept development*, in *38th Joint Propulsion Conference and Exhibit, Indianapolis, Indiana*, Vol. 4318 (AIAA, 2002).
- [2] G. Mungas, D. Fisher, J. Vozoff, and M. Villa, *Nofbx single stage to orbit mars ascent vehicle*, in *Aerospace Conference, 2012 IEEE* (IEEE, 2012) pp. 1–11.
- [3] M. Trinidad, E. Zabrensky, and A. Sengupta, *Mars ascent vehicle system studies and baseline conceptual design*, in *Aerospace Conference, 2012 IEEE* (IEEE, 2012) pp. 1–13.
- [4] R. Storn and K. Price, *Differential evolution - a simple and efficient heuristic for global optimization over continuous spaces*, in *Journal of global optimization*, Vol. 11 (Springer, 1997) pp. 341–359.
- [5] O. Montenbruck, *Numerical integration methods for orbital motion*, in *Celestial Mechanics and Dynamical Astronomy*, Vol. 53 (1992) pp. 59–69.
- [6] R. Noomen, *ae4-878.integrators.v4-3*, Lecture slides, Delft University of Technology (2013), [Internal publication] Course: Mission Geometry and Orbit Design.
- [7] E. Mooij, *The motion of a vehicle in a planetary atmosphere* (Delft University Press, Delft, 1994).
- [8] J. Fanning and B. Pierson, *A model comparison for optimal mars ascent trajectories*, in *Engineering Optimization+ A35*, Vol. 26 (1996) pp. 271–285.
- [9] J. C. Whitehead, *Mars ascent propulsion trades with trajectory analysis*, in *40th AIAA/ASME/SAE/ASEE Joint Propulsion Conference and Exhibit* (American Institute of Aeronautics and Astronautics, 2004).
- [10] K. Wakker, *Astrodynamic-II course ae4874, part 2*, Reader, Delft University of Technology (2010), [Internal publication] Course: Astrodynamics-II.
- [11] J. Wertz, *Orbit & Constellation Design & Management*, 2nd ed. (Microcosm Press and Springer, USA, 2009).
- [12] R. Noomen, *ae4-878.basics.v4-14*, Lecture slides, Delft University of Technology (2013), [Internal publication] Course: Mission Geometry and Orbit Design.
- [13] O. E. Akcasu and I. Akcay, *Solar time using gps technology*, Lonestar Inventions, L.P., Austin, TX, U.S. Patent (2013), patent application, Docket No. WO 2013070518 A1, filed 2 Nov. 2012.
- [14] J. Mulder, W. van Staveren, J. van der Vaart, E. de Weerdt, A. in 't Veld, and E. Mooij, *Flight dynamics, lecture notes*, Reader, Delft University of Technology (2013), [Internal publication] Course: Flight Dynamics.
- [15] E. Mooij, *Ae3202-week1-lecture1b-frames*, Lecture slides, Delft University of Technology (2013), [Internal publication] Course: Flight Dynamics.
- [16] P. Verschuren and H. Doorewaard, *Designing a research project*, 2nd ed. (Eleven International Publishing, The Hague, 2010).
- [17] Mars Program Planning Group, *Summary of the final report*, (2012), [online database], URL: <http://www.nasa.gov/sites/default/files/files/> [cited 14 October 2015].
- [18] P. Desai, R. Braun, W. Engelund, F. Cheatwood, and J. Kangas, *Mars ascent vehicle flight analysis*, in *7th AIAA/ASME Joint Thermophysics and Heat Transfer Conference* (1998).
- [19] J. C. Whitehead, *Trajectory analysis and staging trades for smaller mars ascent vehicles*, in *Journal of spacecraft and rockets*, Vol. 42 (2005) pp. 1039–1046.

- [20] E. Di Sotto, J. C. Bastante, and R. Drai, *System and gnc concept for rendezvous into elliptical orbit for mars sample return mission*, in *AIAA Guidance, Navigation, and Control Conference and Exhibit, Colorado* (2007).
- [21] E. Dumont, *Design of a modular transportation system for future lunar robotic missions*, in *30th ISTS/34th IEPC/6th NSAT Joint Conference, Kobe, Japan* (2015).
- [22] Mission Evaluation Team, *Apollo 11 mission report*, (1971), [online database], URL: <http://history.nasa.gov/alsj/a11/> [cited 15 October 2015].
- [23] C. A. Brooks and S. Prasad, *Apollo program summary report*, website (2011), [online database], URL: <http://history.nasa.gov/apsr/apsr.htm> [cited 15 October 2015].
- [24] R. R. Sostaric and R. S. Merriam, *Lunar ascent and rendezvous trajectory design*, in *31st Annual AAS Guidance and Control Conference, Breckenridge, Colorado* (2008).
- [25] A. Dietrich, K. Davis, and J. Parker, *Ascent trajectories from the lunar far-side to earth-moon l2 halo orbits*, in *Advances in Space Research*, Vol. 56, University of Colorado (Elsevier, 2015) pp. 2595–2611.
- [26] L. Alkalai, B. Solish, J. Elliott, T. McElrath, J. Mueller, and J. Parker, *Orion/moonrise: A proposed human and robotic sample return mission from the lunar south pole-aitken basin*, in *Aerospace Conference, 2013 IEEE* (IEEE, 2013) pp. 1–10.
- [27] M. Martinez-Sanchez and J. E. Pollard, *Spacecraft electric propulsion—an overview*, in *Journal of Propulsion and Power*, Vol. 14 (1998) pp. 688–699.
- [28] S. Schaeff and S. Erb, *Low thrust trajectory optimization for orbit raising applications*, Presentation, Second U.K. Workshop on Optimisation in Space Engineering (2014), [online database], URL: <http://www.turing-gateway.cam.ac.uk/documents/> [cited 18 October 2015].
- [29] S. Geffroy and R. Epenoy, *Optimal low-thrust transfers with constraints—generalization of averaging techniques*, in *Acta Astronautica*, Vol. 41 (1997) pp. 133–149.
- [30] C. A. Kluever and S. R. Oleson, *Direct approach for computing near-optimal low-thrust earth-orbit transfers*, in *Journal of Spacecraft and Rockets*, Vol. 35 (1998) pp. 509–515.
- [31] R. Bertrand, J. Bernussou, S. Geffroy, and R. Epenoy, *Electric transfer optimization for mars sample return mission*, in *Acta Astronautica*, Vol. 48 (2001) pp. 651–660.
- [32] G. J. Whiffen, *Mystic: Implementation of the static dynamic optimal control algorithm for high-fidelity, low-thrust trajectory design*, in *AIAA/AAS Astrodynamics Specialist Conference and Exhibit, Keystone, Colorado* (NASA Jet Propulsion Laboratory, 2006).
- [33] J. A. Sims, P. A. Finlayson, E. A. Rinderle, M. A. Vavrina, and T. D. Kowalkowski, *Implementation of a low-thrust trajectory optimization algorithm for preliminary design*, in *AIAA/AAS Astrodynamics Specialist Conference and Exhibit, Keystone, Colorado* (NASA Jet Propulsion Laboratory, 2006).
- [34] L. D. Kos, T. Polsgrove, R. Hopkins, D. Thomas, and J. A. Sims, *Overview of the development for a suite of low-thrust trajectory analysis tools*, in *AIAA/AAS Astrodynamics Specialist Conference and Exhibit* (NASA Jet Propulsion Laboratory, 2006).
- [35] U. Derz and W. Seboldt, *Mars sample return mission architectures utilizing low thrust propulsion*, in *Acta Astronautica*, Vol. 77 (2012) pp. 83–96.
- [36] E. Grayzeck, *Gemini 6a*, Website (2014), [online database], URL: <http://nssdc.gsfc.nasa.gov/nmc/spacecraftDisplay.do?id=1965-104A> [cited 20 October 2015].
- [37] J. Mayer and R. Parten, *Development of the gemini operational rendezvous plan*, in *Journal of spacecraft and rockets*, Vol. 5 (NASA Manned Spacecraft Center, 1968) pp. 1023–1028.
- [38] E. Ezell and L. Ezell, *The partnership: A history of the apollo-soyuz test project*, website (1978), [online database], URL: <http://www.hq.nasa.gov/pao/History/SP-4209/ch3-8.htm> [cited 20 October 2015].

- [39] R. Murtazin and N. Petrov, *Usage of pre-flight data in short rendezvous mission of soyuz-tma spacecrafts*, in *Acta Astronautica*, Vol. 93 (2014) pp. 71–76.
- [40] A. F de Almeida Prado, *Optimal rendezvous maneuvers for space vehicles*, in *Revista Brasileira de Ciencias Mecanicas/Journal of the Brazilian Society of Mechanical Sciences*, Vol. 18 (1996) pp. 297–301.
- [41] R. C. Woolley, R. L. Mattingly, J. E. Riedel, and E. J. Sturm, *Mars sample return - launch and detection strategies for orbital rendezvous*, in *AAS/AIAA Astrodynamics Specialist Conference*, Vol. 142 (Univelt, Inc., 2011).
- [42] J. Whitehead, *Mars ascent propulsion options for small sample return vehicles*, in *33rd AIAA/ASME/SAE/ASEE Joint Propulsion Conference and Exhibit* (AIAA Joint Propulsion Conference and Exhibit, 1997).
- [43] C. S. Guernsey, *Mars ascent propulsion system (maps) technology program: Plans and progress*, in *34th AIAA/ASME/SAE/ASEE Joint Propulsion Conference and Exhibit* (1998).
- [44] C. Stone, *Rice mars*, presentation/website (1999), [online database], URL: <http://www.slideshare.net/cliffordstone/rice-mars-nov99> [cited 25 October 2015].
- [45] D. D. Stephenson and H. J. Willenberg, *Mars ascent vehicle key elements of a mars sample return mission*, in *Aerospace Conference, 2006 IEEE* (IEEE, 2006) p. 11.
- [46] A. Sengupta, A. Kennett, M. Pauken, M. Trinidad, and E. Zabrensky, *Systems engineering and technology considerations of a mars ascent vehicle*, in *2011 IEEE Aerospace Conference* (2012).
- [47] A. J. Colozza, *Comparison of Mars Aircraft Propulsion Systems*, Tech. Rep. (NASA Glenn Research Center, 2003) : NASA/CR-2003-212350.
- [48] D. J. Anderson, E. Pencil, D. Vento, J. Dankanich, M. Munk, and D. Hahne, *Propulsion technology development for sample return missions under nasas ispt program*, in *47th AIAA/ASME/SAE/ASEE Joint Propulsion Conference & Exhibit* (2011).
- [49] H. Visser, *Aircraft performance optimization course ae4447*, Reader, Delft University of Technology (2014), [Internal publication].
- [50] R. Noomen, *ae4-878.optimistion.v4-7*, Lecture slides, Delft University of Technology (2013), [Internal publication] Course: Mission Geometry and Orbit Design.
- [51] P. Musegaas, *Optimization of Space Trajectories Including Multiple Gravity Assists and Deep Space Maneuvers*, *Master's thesis*, Delft University of Technology (2012).
- [52] S. Boyd and L. Vandenberghe, *Convex Optimization*, 1st ed. (Cambridge University Press, New York, 2004).
- [53] I. Sobol, *On quasi-monte carlo integrations*, in *Mathematics and Computers in Simulation*, Vol. 47 (Elsevier, 1998) pp. 103–112.
- [54] P. Boggs and J. Tolle, *Sequential quadratic programming*, in *Acta Numerica*, Vol. 4 (Cambridge University Press, 1995) pp. 1–51.
- [55] M. Iwamatsu and Y. Okabe, *Basin hopping with occasional jumping*, in *Chemical Physics Letters*, Vol. 339 (Elsevier, 2004) pp. 396–400.
- [56] C. C. Coello, G. Lamont, and D. V. Veldhuizen, *Evolutionary Algorithms for solving multi-objective problems*, 2nd ed., edited by D. Goldberg and J. Koza (Springer Science+Business Media, New York, 2007).
- [57] V. Selvi and R. Umarani, *Comparative analysis of ant colony and particle swarm optimization techniques*, in *International Journal of Computer Applications*, Vol. 5 (2010).
- [58] B. Bhowmik, *Dynamic programming—its principles, applications, strengths, and limitations*, in *International Journal of Engineering Science and Technology*, Vol. 2 (2010) pp. 4822–4826.

- [59] R. Horst and P. Pardalos, *Handbook of Global Optimization*, Vol. 1 (Kluwer Academic Publishers, Boston, 1995) available at JPL library.
- [60] P. Gage, R. Braun, and I. Kroo, *Interplanetary trajectory optimization using a genetic algorithm*, in *Journal of Astronautical Sciences*, Vol. 43 (1995) pp. 59–76.
- [61] G. A. Rauwolf and V. L. Coverstone-Carroll, *Near-optimal low-thrust orbit transfers generated by a genetic algorithm*, in *Journal of Spacecraft and Rockets*, Vol. 33 (1996) pp. 859–862.
- [62] Y. H. Kim and D. B. Spencer, *Optimal spacecraft rendezvous using genetic algorithms*, in *Journal of Spacecraft and Rockets*, Vol. 39 (2002) pp. 859–865.
- [63] D. Myatt, V. M. Becerra, S. J. Nasuto, and J. Bishop, *Advanced global optimisation for mission analysis and design*, Tech. Rep. (University of Reading, 2004) ariadna id 03/4101.
- [64] S. Lee, P. von Ailmen, W. Fink, A. E. Petropoulos, and R. J. Terr, *Design and optimization of low-thrust orbit transfers*, in *Aerospace Conference, 2005 IEEE* (IEEE, 2005) pp. 855–869.
- [65] O. Abdelkhalik and D. Mortari, *N-impulse orbit transfer using genetic algorithms*, in *Journal of Spacecraft and Rockets*, Vol. 44 (2007) pp. 456–460.
- [66] M. Vasile, E. Minisci, and M. Locatelli, *On testing global optimization algorithms for space trajectory design*, in *AIAA/AAS Astrodynamics Specialist Conference and Exhibit, Honolulu, Hawaii* (2008).
- [67] J. A. Garcia, J. L. Brown, D. J. Kinney, J. V. Bowles, L. C. Huynh, X. J. Jiang, E. Lau, and I. C. Dupzyk, *Co-optimization of mid lift to drag vehicle concepts for mars atmospheric entry*, in *10th AIAA/ASME Joint Thermophysics and Heat Transfer Conference, Chicago, Illinois* (2010).
- [68] S. Li and Y. Peng, *Mars entry trajectory optimization using doc and dcnlp*, in *Advances in Space Research*, Vol. 47 (Elsevier, 2011) pp. 440–452.
- [69] B. Addis, A. Cassioli, M. Locatelli, and F. Schoen, *A global optimization method for the design of space trajectories*, in *Computational Optimization and Applications*, Vol. 48 (Springer, 2011) pp. 635–652.
- [70] E. Boudestijn, *Development of a low-thrust earth-centred transfer optimizer for the preliminary mission design phase*, Master's thesis, Delft University of Technology (2014).
- [71] F. Miranda, *Design Optimization of Ground and Air-Launched Hybrid Rockets*, Master's thesis, Delft University of Technology (2015).
- [72] R. Storn and K. Price, *Differential Evolution - A simple and efficient adaptive scheme for global optimization over continuous spaces*, Tech. Rep. (ICSI, USA, 1995) tR-95-012.
- [73] K. V. Price, R. M. Storn, and J. A. Lampinen, *Differential evolution: a practical approach to global optimization*, edited by G. Rozenberg (Springer, Berlin, 2005).
- [74] V. Feoktistov, *Differential Evolution, In Search of Solutions*, edited by D. Du, Vol. 5 (Springer, New York, 2006).
- [75] A. Qing, *Differential evolution: fundamentals and applications in electrical engineering* (John Wiley & Sons, Singapore, 2009).
- [76] R. H. Leary, *Global optimization on funneling landscapes*, in *Journal of Global Optimization*, Vol. 18 (2000) pp. 367–383.
- [77] D. J. Wales and J. P. Doye, *Global optimization by basin-hopping and the lowest energy structures of lennard-jones clusters containing up to 110 atoms*, in *The Journal of Physical Chemistry A*, Vol. 101 (1997) pp. 5111–5116.
- [78] J. A. Englander and A. C. Englander, *Tuning monotonic basin hopping: Improving the efficiency of stochastic search as applied to low-thrust trajectory optimization*, in *24th International Symposium on Space Flight Dynamics, Laurel, MD* (2014).

- [79] B. Addis, A. Cassioli, M. Locatelli, and F. Schoen, *Global optimization for the design of space trajectories*, DB FILE 2008/11/2150 (2008), [online database], URL: <http://www.optimization-online.org/> [cited 23 October 2015].
- [80] C. Yam, D. Lorenzo, and D. Izzo, *Low-thrust trajectory design as a constrained global optimization problem*, in *Proceedings of the Institution of Mechanical Engineers, Part G: Journal of Aerospace Engineering*, Vol. 225 (2011) pp. 1243–1251.
- [81] J. A. Englander, B. A. Conway, and T. Williams, *Automated interplanetary trajectory planning*, in *AAS/AIAA Astrodynamics Specialist Conference, Minneapolis, Minnesota* (2012) pp. 4517–4537.
- [82] J. A. Englander, M. A. Vavrina, B. Naasz, R. G. Merill, and M. Qu, *Mars, phobos, and deimos sample return enabled by arrm alternative trade study spacecraft*, in *AIAA/AAS Astrodynamics Specialist Conference, San Diego, CA* (2014).
- [83] A. Jalal Uddin Jamali, A. Grossi, M. Locatelli, and F. Schoen, *Packing identical circles in a minimized circular container by monotonic basin hopping heuristic approach*, in *ICCIT'09. 12th International Conference on Computers and Information Technology, Dhaka* (2009) pp. 1–6.
- [84] P. E. Gill, W. Murray, and M. A. Saunders, *Snopt: An sqp algorithm for large-scale constrained optimization*, in *SIAM journal on optimization*, Vol. 12 (2002) pp. 979–1006.
- [85] P. E. Gill, W. Murray, and M. A. Saunders, *Users guide for snopt version 7 - software for large-scale nonlinear programming*, (2008), [online database], URL: <http://web.stanford.edu/group/SOL/guides/> [cited 23 October 2015].
- [86] R. Hofsteenge, *Computational Methods for the Long-Term Propagation of Space Debris Orbits*, Master's thesis, Delft University of Technology (2013).
- [87] A. Milani and A. M. Nobili, *Integration error over very long time spans*, in *Celestial mechanics*, Vol. 43 (Springer, 1987) pp. 1–34.
- [88] P. Deuflhard, U. Nowak, and U. Poehle, *Program descriptions of elib*, (1994), [online database], URL: <http://elib.zib.de/pub/elib/codelib/difex2/readme> [cited 30 October 2015].
- [89] H. Ramos and J. Vigo-Aguiar, *Variable stepsize störmer-cowell methods*, in *Mathematical and Computer Modelling*, Vol. 42 (2005) pp. 837–846.
- [90] E. Fehlberg, *Low order classical Runge-Kutta formulas with stepwise control*, Tech. Rep. (Marschall Space Flight Center, NASA, 1969) : NASA TR R-316.
- [91] E. Fehlberg, *Classical fifth-, sixth-, seventh-, and eighth-order Runge-Kutta formulas with stepsize control*, Tech. Rep. (Marschall Space Flight Center, NASA, 1968) : NASA TR R-287.
- [92] J. R. Scott and M. C. Martini, *High speed solution of spacecraft trajectory problems using taylor series integration*, in *AIAA/AAS Astrodynamics Specialist Conference and Exhibit, Honolulu, Hawaii* (2008).
- [93] M. M. Berry, *A variable-step double-integration multi-step integrator*, Ph.D. thesis, Virginia Polytechnic Institute and State University (2004).
- [94] J. Meijaard, *A comparison of numerical integration methods with a view to fast simulation of mechanical dynamical systems*, in *Real-Time Integration Methods for Mechanical System Simulation*, Vol. 69 (Springer, 1991) pp. 329–343.
- [95] J. Dormand, M. El-Mikkawy, and P. Prince, *Families of runge-kutta-nystrom formulae*, in *IMA Journal of Numerical Analysis*, Vol. 7 (1987) pp. 235–250.
- [96] T. R. Quinn, S. Tremaine, and M. Duncan, *A three million year integration of the earth's orbit*, in *The Astronomical Journal*, Vol. 101 (1991) pp. 2287–2305.
- [97] P. J. van der Houwen, E. Messina, and J. J. de Swart, *Parallel Stormer-Cowell methods for high-precision orbit computations*, Tech. Rep. 12 (Centrum voor Wiskunde en Informatica, 1998) : MAS-R9812.

- [98] A. B. Gonzalez, P. Martin, and D. J. Lopex, *On the numerical integration of orbital problems with high order runge–kutta–nystrom methods*, in *Applied numerical mathematics*, Vol. 35 (Elsevier, 2000) pp. 1–10.
- [99] D. Gondelach, *A hodographic-shaping method for low-thrust trajectory design*, Master's thesis, Delft University of Technology (2012).
- [100] B. A. Romgens, E. Mooij, and M. C. Naeije, *Verified interval orbit propagation in satellite collision avoidance*, in *AIAA Guidance, Navigation, and Control, Portland, OR* (2011).
- [101] O. Montenbruck, *Numerical integration of orbital motion using taylor series*, in *Spaceflight mechanics* (1992) pp. 1217–1231, available at JPL library.
- [102] J. R. Scott and M. C. Martini, *High-speed solution of spacecraft trajectory problems using taylor series integration*, in *Journal of Spacecraft and Rockets*, Vol. 47 (2010) pp. 199–202.
- [103] A. Pagano, *Global Launcher Trajectory Optimization for Lunar Base Settlement*, Master's thesis, Delft University of Technology (2010).
- [104] M. Balesdent, *Multidisciplinary design optimization of launch vehicles*, Ph.D. thesis, Ecole Centrale de Nantes (2011).
- [105] M. van Kesteren, *Air Launch versus Ground launch: a multidisciplinary design optimization study of expendable launch vehicle on cost and performance*, Master's thesis, Delft University of Technology (2013).
- [106] H. Wittenberg, B. Ambrosius, M. Naeije, and E. Mooij, *Ae4-870a: Rocket motion*, Lecture Notes (2014), course: Rocket Motion.
- [107] D. Williams, *Mars fact sheet*, website (2015), [online database], URL: <http://nssdc.gsfc.nasa.gov/planetary/factsheet/marsfact.html> [cited 1 November 2015].
- [108] K. Wakker, *Astrodynamic-i course ae4874, part 1*, Reader, Delft University of Technology (2010), [Internal publication] Course: Astrodynamics I.
- [109] D. Smith and M. Zuber, *The relationship between mola northern hemisphere topography and the 6.1-mbar atmospheric pressure surface of mars*, in *Geophysical research letters*, Vol. 25 (1998) pp. 4397–4400.
- [110] D. E. Smith, M. T. Zuber, H. V. Frey, J. B. Garvin, J. W. Head, D. O. Muhleman, G. H. Pettengill, R. J. Phillips, S. C. Solomon, H. J. Zwally, et al., *Mars orbiter laser altimeter: Experiment summary after the first year of global mapping of mars*, in *Journal of Geophysical Research*, Vol. 106 (2001) pp. 23689–23722.
- [111] N. Barlow, *Mars: An introduction to its interior, surface and atmosphere*, Vol. 8 (Cambridge University Press, Cambridge, 2008).
- [112] R. Noomen, *ae4-878.orbit-design.v4-7*, Lecture slides, Delft University of Technology (2013), [Internal publication] Course: Mission Geometry and Orbit Design.
- [113] J. Polk, R. Kakuda, J. Anderson, J. Brophy, V. Rawlin, M. Patterson, J. Sovey, and J. Hamley, *Validation of the nstar ion propulsion system on the deep space one mission: overview and initial results*, in *35th AIAA/ASME/SAE/ASEE Joint Propulsion Conference and Exhibit*, Vol. 99 (1999) p. 2274.
- [114] R. Killinger, R. Kukies, M. Surauer, A. Tomasetto, and L. van Holtz, *Artemis orbit raising inflight experience with ion propulsion*, in *Acta Astronautica*, Vol. 53 (Elsevier, 2003) pp. 607–621.
- [115] ESA, *All-electric propulsion and multi-satellite launch system for communication satellites*, Website (2015), [online directory], URL: <https://directory.eoportal.org/web/eoportal/satellite-missions/a/all-electric> [cited 25 November 2015].
- [116] W. Gebbett, *Multi-revolution, low-thrust trajectory design using Lyapunov feedback control*, Master's thesis, Delft University of Technology (2014).
- [117] A. E. Petropoulos, *Refinements to the q-law for low-thrust orbit transfers*, in *Advances in the Astronautical Sciences*, Vol. 120 (2005) pp. 963–983, available at JPL library.

- [118] G. R. Hintz, *Survey of orbit element sets*, in *Journal of guidance, control, and dynamics*, Vol. 31 (2008) pp. 785–790.
- [119] R. Noomen, *Ae2-104, lecture hours 15+16: Kepler orbit, specialized orbits*, Lecture slides, Delft University of Technology (2011), [Internal publication] Course: Flight and Orbital Mechanics.
- [120] J. A. Kechichian, *Minimum-time constant acceleration orbit transfer with first-order oblateness effect*, *Journal of Guidance, Control, and Dynamics* **23**, 595 (2000).
- [121] R. Battin, *An introduction to the mathematics and methods of Astrodynamics* (AIAA, 1999) revised version, available at JPL library.
- [122] A. E. Petropoulos, *Simple control laws for low-thrust orbit transfers*, in *AAS/AIAA Astrodynamics Specialists Conference, Big Sky, MT* (2003) available at JPL library.
- [123] A. E. Petropoulos, *Low-thrust orbit transfers using candidate lyapunov functions with a mechanism for coasting*, in *AIAA/AAS Astrodynamics Specialist Conference and Exhibit, Providence, Rhode Island* (2004).
- [124] N. Bachman, *Naif spice toolkit hypertext documentation, required reading documents, reference frames*, website (2014), [online database], URL: <http://naif.jpl.nasa.gov/pub/naif/> [cited 18 December 2015].
- [125] J. D. del Rio, *Generic frame definition kernel file for esa planetary missions*, (2008), [online database], URL: <http://naif.jpl.nasa.gov/pub/naif/VEX/kernels/fk/RSSD0002.TF> [cited 8 December 2015].
- [126] B. A. Archinal, M. Ahearn, E. Bowell, A. Conrad, G. J. Consolmagno, R. Courtin, T. Fukushima, D. Hestroffer, J. L. Hilton, G. A. Krasinsky, *et al.*, *Report of the iau working group on cartographic coordinates and rotational elements: 2009*, in *Celestial Mechanics and Dynamical Astronomy*, Vol. 109 (2011) pp. 101–135.
- [127] T. Duxbury, P. Christensen, D. Smith, G. Neumann, R. Kirk, M. Caplinger, A. Albee, N. Seregina, G. Neukum, and B. Archinal, *The location of airy-0, the mars prime meridian reference, from stereo photogrammetric processing of themis ir imaging and digital elevation data*, in *Journal of Geophysical Research: Planets*, Vol. 119 (John Wiley & Sons, 2014) pp. 2471–2486.
- [128] C. Ho, N. Golshan, and A. Kliore, *Radio Wave Propagation Handbook for Communication on and Around Mars*, 1st ed. (NASA Jet Propulsion Laboratory, Pasadena, CA, 2002) handbook JPL Publication 02-5.
- [129] H. L. Justh and C. G. Justus, *Utilizing mars global reference atmospheric model (mars-gram 2005) to evaluate entry probe mission sites*, Presentation (2008), [online database], URL: <https://smartech.gatech.edu/bitstream/handle/1853/26375/34-186-1-PB.pdf?sequence=1> [cited 10 December 2015].
- [130] W. Knopf, *Spice history*, Website (2015).
- [131] C. Justus, *A mars global reference atmospheric model (mars-gram) for mission planning and analysis*, in *28th Aerospace Sciences Meeting, Reno, Nevada* (1990).